Pharmacological and Chemogenetic Characterization and Modulation of the Brain Neuropeptide S and Oxytocin

Dissertation zur Erlangung des Doktorgrades

der Naturwissenschaften (Dr. rer. nat.)

an der Fakultät für Biologie und Vorklinische Medizin

der Universität Regensburg

vorgelegt von

Thomas Grund

aus Arnstadt

im Jahr 2017

Summary

Anxiety is a natural response to a real or perceived threat that has been conserved throughout evolution. From this perspective, sensation of anxiety is viewed as an adaptive behavioral state, which occurs in response to signals of danger. However, excessive or inappropriate anxiety can become pathological. Anxiety disorders represent one major burden of our modern society, and the available treatment options are limited by adverse side effects. During the last decades, research centered on anxiety disorders has focused on neuropeptides. Neuropeptide S (NPS) and oxytocin (OXT) represent potential neuropeptide candidates for the treatment of various psychopathologies, including anxiety disorders due to their potent anxiolytic profile. Both signal through G protein-coupled receptors and thereby regulate complex neuronal signaling pathways. How these pathways contribute to behavioral and physiological effects of NPS and OXT remains to be elucidated. Therefore, in the present thesis I aimed to reveal, (i) whether NPS acts on the brain OXT system to exert its anxiolytic properties, (ii) whether the anxiolytic profile of NPS is mediated in a Gq pathway-dependent manner, and (iii) to characterize the spatiotemporal characteristics of chemogenetically induced OXT neurons activation.

NPS receptors (NPSR) are found within the hypothalamic paraventricular nucleus (PVN), where OXT is synthesized besides the supraoptic and accessory nuclei. Besides anxiolysis, NPS and OXT share other effects, such as the reversal of social fear, the attenuation of aggressive-like behavior as well as the inhibition of food-intake and anti-nociceptive properties as demonstrated in rodents. These behavioral similarities, together with the neuroanatomical overlapping of the NPSR and OXT expression within the PVN, led me to hypothesize that NPS effects are mediated by acting on the OXT system within the PVN. Herein, I present a chain of evidence that the effects of NPS within the PVN are mediated via actions on local OXT neurons

in male Wistar rats. Retrograde tracing revealed that NPS-immunoreactive neurons originating within the Locus coeruleus innervate the PVN. Moreover, fluorescence-activated cell sorting identified NPSR expression in PVN-OXT neurons. NPS reliably induced transient Ca^{2+}-influx in a subpopulation of OXT neurons - an effect mediated via the NPSR. Moreover, intracerebroventricular (icv) NPS evoked a significant release of OXT within the PVN as assessed by microdialysis in combination with a highly sensitive radioimmunoassay. Both, chemogenetic silencing of the endogenous OXT system using designer receptors exclusively activated by designer drugs (DREADD) as well as pharmacological blockade of brain OXT receptors (OXTR) abolished the anxiolytic effect of NPS infused icv. These findings provide the first evidence for an intra-hypothalamic mechanism involving NPSR-expressing OXT neurons in the potent anxiolytic profile of NPS, and fill an important gap in our neurophysiological understanding of brain neuropeptide interactions in the context of regulation of emotional behaviour within the hypothalamus.

Next, I performed studies in order to extend our knowledge on the intraneuronal mechanisms underlying the anxiolytic profile of NPS by studying signaling pathways downstream of NPSR activation. Here, bilateral microinfusion of NPS into the medial amygdala (MeA) of male adult Wistar rats reduced anxiety-related behavior on the elevated plus maze and the open field. Moreover, icv infusion of NPS evoked expression as well as increased phosphorylation of Ca^{2+}/calmodulin-dependent kinase II in the amygdala, and subsequent phosphorylation of the mitogen-activated protein kinase ERK1/2. Importantly, NPS-induced anxiolysis in the MeA was prevented by local inhibition of phospholipase C using the specific inhibitor U73122. In contrast, local pharmacological blockade of adenylyl cyclase signaling using the specific inhibitor 2',5'-dideoxyadenosine failed to inhibit the anxiolytic effect of NPS infused into the MeA. Hence, NPS promotes acute anxiolysis within the MeA dependent on NPSR-mediated phospholipase C signaling.

Finally, in order to validate an innovative and highly specific tool for activating OXT neurons

within the PVN in a behavioral context, I performed a series of experiment using the DREADD technique. Acute chemogenetic activation of PVN-OXT neurons resulted in enhanced release of OXT within the PVN within one hour as assessed using intracerebral microdialysis. Further, DREADD activation reduced anxiety-related behavior in the light/dark box, and increased self-grooming behavior in the home cage. In addition, chemogenetic activation of PVN-OXT neurons marginally improved ethanol-induced locomotor deficits.

In summary, my experimental data advance our understanding of the mechanisms by which NPS promotes anxiolysis and the temporal release patterns of OXT following chemogenetic activation and its behavioral relevance.

Zusammenfassung

Aus evolutionsbiologischer Sicht ist Angst eine konservierte, natürliche Reaktion auf eine reale oder gefühlte Bedrohung. Allerdings können exzessive bzw. unangepasste Angstzustände ein pathologisches Ausmaß annehmen. Angsterkrankungen repräsentieren daher eine der Hauptbelastungen unserer modernen Gesellschaft. Da die derzeitigen Behandlungsmethoden limitiert und von Nebenwirkungen geprägt sind, rückten Neuropeptide in den letzten Jahrzehnten mehr und mehr in den Fokus der Wissenschaft. Aufgrund ihrer potenten, angstlösenden Wirkung repräsentieren Neuropeptid S (NPS) und Oxytocin (OXT) zwei mögliche Kandidaten zur Behandlung von Angsterkrankungen. Beide Neuropeptide binden an G-Protein-gekoppelte Rezeptoren und regulieren dadurch komplexe neuronale Signalwege. Daher war das Ziel meiner Doktorarbeit zu erforschen (i) welchen Einfluss OXT-Neurone im Hypothalamus auf die angstlösende Wirkung von NPS haben, (ii) welche intrazellulären Signalkaskaden der anxiolytischen Wirkung von NPS zugrunde liegen, und (iii) den zeitlichen Ablauf einer chemogenetischen Aktivierung der OXT-Neurone zu charakterisieren.

NPS-Rezeptoren (NPSR) werden im hypothalamischen Nucleus paraventricularis (PVN) exprimiert und zeigen eine morphologische Überlappung mit OXT-Neuronen, die sowohl im PVN also auch dem Nucleus supraopticus und den Nucleus accessorius lokalisiert wurden. Neben ihrer angstlösenden Wirkung reduzieren sowohl NPS als auch OXT soziale Angst und aggressives Verhalten in Ratten und Mäusen. Darüber hinaus mindern beide Neuropeptide die Nahrungsaufnahme und hemmen die Schmerzwahrnehmung in Ratten. Aufgrund der ähnlichen Verhaltenseffekte beider Neuropeptide sowie der neuroanatomischen Überlappung der neuronalen NPSR- und OXT-Expression untersuchte ich die Fragestellung, ob NPS-induzierte Effekte über das Oxytocin-System im PVN vermittelt werden. Mittels einer retrograden Markierung konnte ich zeigen, dass NPS-immunoreaktive Neurone aus dem Locus

coeruleus zum PVN projizieren. Darüber hinaus bewies Fluoreszenz-aktivierte Zellsortierung, dass der NPSR in OXT-Neuronen des PVN exprimiert wird. In einer Subpopulation von OXT-Neuronen induzierte NPS durch die Bindung an seinen Rezeptor einen Anstieg des intrazellulären Calcium-Spiegels. Durch intrazerebrale Mikrodialyse in Verbindung mit einem hochsensitiven Radioimmunoassay für OXT konnte ich zeigen, dass NPS die somato-dendritische Freisetzung von OXT im PVN erhöht. Um einen kausalen Zusammenhang zwischen der NPS-induzierten Stimulation der OXT-Neurone und deren Effekt auf die angstlösende Wirkung von NPS zu untersuchen, habe ich eine chemogenetische Inhibierung der OXT-Neurone sowie eine pharmakologische Blockade der OXT-Rezeptoren (OXTR) durchgeführt. Meine Ergebnisse demonstrieren, dass das OXT-System im PVN eine essentielle Rolle für die angstlösende Wirkung von NPS spielt.

Um das Wissen über die intraneuronalen Wirkmechanismen von NPS zu erweitern, habe ich die NPSR-gekoppelten Signalwege untersucht. Meine Experimente zeigten, dass eine bilaterale Mikroinfusion von NPS in den Nucleus amygdalae medialis (MeA) das Angstverhalten männlicher Wistar-Ratten sowohl auf der *elevated plus maze* als auch in der *open field box* reduziert. Zusätzlich demonstrierten die Untersuchungen, dass icv infundiertes NPS zur Expression und Phosphorylierung der Calcium/Calmodulin-abhängigen Kinase II und zur Phosphorylierung der Mitogen-aktivierten Proteinkinase ERK1/2 in der Amygdala führt. Durch die Inhibierung der Phospholipase C mittels des spezifischen Blockers U73122 wurde die NPS-induzierte Anxiolyse gehemmt. Im Gegensatz dazu verhinderte die pharmakologische Blockade der Adenylatcyclase nicht die angstlösende Wirkung von NPS. Daher kann geschlussfolgert werden, dass die akute NPS-induzierte Anxiolyse von einem Phospholipase C-gekoppelten Signalweg in der MeA abhängig ist.

Im Hinblick auf die Validierung einer innovativen und hoch spezifischen Methode zur Aktivierung der OXT-Neurone im PVN und den damit verbundenen Verhaltenskontext, habe ich die zeitliche Abfolge einer chemogenetischen Stimulation der OXT-Neurone untersucht.

Dadurch konnte ich zeigen, dass die chemogenetische Aktivierung innerhalb einer Stunde zum Höhepunkt der OXT-Freisetzung führt, das Angstverhalten in der Light/Dark Box mindert und zu einer Zunahme des Putzverhaltens führt. Darüber hinaus untersuchte ich den Einfluss der chemogenetisch aktivierten OXT-Neurone auf die Bewegungsaktivität während eines Alkohol-induzierten Rauschzustandes. Hierbei hatte die endogene OXT-Freisetzung allerdings nur einen marginal förderlichen Effekt auf den Bewegungsablauf.

Zusammengefasst erweitern meine experimentellen Ergebnisse unser Verständnis im Hinblick auf den zugrundliegenden Mechanismus, der zur NPS-induzierten Anxiolyse führt, und den zeitlichen Verlauf der chemogenetisch induzierten Aktivierung von OXT-Neuronen im PVN sowie deren Einfluss auf definierte Verhaltensweisen.

Table of contents

List of abbreviations

AAV	adeno-associated virus
rAAV	recombinant AAV
AC	adenylyl cyclase
AN	accessory nuclei
ANOVA	analysis of variance
AP	anteroposterior axis
BAPTA	1,2-bis(o-aminophenoxy)ethane-N,N,N’,N’-tetraacetic acid
CaMK	Ca^{2+}/calmodulin-dependent kinase
cAMP	cyclic adenosine monophosphate
cDNA	complementary DNA
CHO	Chinese hamster ovary (cell line)
CNO	clozapine N-oxide
CRF	corticotropin-releasing factor
CRF-R	CRF receptor
CTB-488	Cholera toxin subunit B coupled to Alexa Fluor 488
DAG	1,2-diacylglygerol
DDA	2',2'-dideoxyadenosine
DEPC-H2O	diethylpyrocarbonate-treated water
DMSO	dimethylsulfoxide
DREADD	designer receptor exclusively activated by designer drugs
DV	dorsoventral axis
EPM	elevated plus maze
ER	endoplasmic reticulum
ERK1/2	extracellular signal-regulated kinase 1/2
EtOH	ethanol
FACS	fluorescence-activated cell sorting
GABA	gamma-aminobutyric acid

GAD	generalized anxiety disorder
GCaMP	genetically encoded Ca2+ indicator
GFP	green fluorescent protein
GIRK	G protein-coupled inwardly rectifying potassium channel
GPCR	G protein-coupled receptor
HEK293T	Human embryonic kidney 293 T (cell line)
hM3Dq	G_q protein-coupled DREADD
hM4Di	G_i protein-coupled DREADD
icv	intracerebroventricular
ID	inner diameter
Ile	isoleucine
ip	intraperitoneal
IP_3	inositol-1,4,5-triphosphate
KOR	kappa opioid receptor
KORD	KOR designer receptor
LC	locus coeruleus
LDB	light/dark box
LDCV	large-dense core vesicle
MAOI	monoamine oxidase inhibitor
MAPK	mitogen-activated protein kinase
MeA	medial nucleus of the amygdala
MEK1/2	mitogen-activated protein kinase kinase
ML	mediolateral axis
mRNA	messenger RNA
NPS	neuropeptide S
NPSR	neuropeptide S receptor
OD	outer diameter
OF	open field
OXT	oxytocin
OXTR	oxytocin receptor
OXTR-A	OXTR antagonist

PBS	phosphate-buffered saline
PCR	polymerase-chain reaction
PFA	paraformaldehyde
PI3K	phosphoinositide 3-kinase
PLC	phospholipase C
PVN	paraventricular nucleus
rAAV	recombinant AAV
RNA	ribonucleic acid
RPL13a	ribosomal protein L13a
rpm	rounds per minute
RT	room temperature
RT-PCR	reverse transcription PCR
SALB	Salvinorin B
SEM	standard error of the mean
SNP	single nucleotide polymorphism
SNRI	selective serotonin/noradrenalin reuptake inhibitor
SOCE	store operated Ca^{2+} entry
SON	supraoptic nucleus
SSRI	selective serotonin reuptake inhibitor
TBS	tris(hydroxymethyl)aminoethane-buffered saline
TBS-T	TBS supplemented with 0.1 % Tween-20
TCA	tricyclic antidepressants
TRPV2	transient receptor potential vanilloid type 2
Veh	vehicle
YFP	yellow fluorescent protein

1 Introduction

1.1 Definition of an emotion termed anxiety

Anxiety is a psychological and physiological state characterized by emotional, somatic, and behavioral imbalances (Seligman *et al.*, 2000). It is a state characterized by dreaded feelings about something that appears intimidating an individual. In the actual or imaginary presence of psychological stress, anxiety can create feelings of fear, worry, and uneasiness (Bouras & Holt, 2007). The main function of anxiety is to act as a signal of danger, threat, or motivational conflict, and to trigger appropriate adaptive responses (Steimer, 2002). Activation of the sympathetic nervous system resulting in increased heart rate, elevated blood pressure, enhanced vigilance, and increased autonomic and neuroendocrine activation may enable individuals to cope with a precarious situation (Steimer, 2002). These physiological adaptations are important and lead to fight-or-flight responses. Therefore, anxiety is considered to be a natural reaction to a stressor (Sokolowska & Hovatta, 2013), which enhances an individual's lifespan especially in the case of the presence of predators and risky situations (Price, 2003). However, when anxiety becomes pathological and interfere with the ability to cope successfully with various challenges and stressful events, it may fall under the classification of an anxiety disorder (Lewis *et al.*, 2010).

1.2 Categories and comorbidity of anxiety disorders

The term anxiety disorder refers to panic disorders, post-traumatic stress disorders, agoraphobia, social anxiety disorders, obsessive-compulsive disorders, specific phobias and generalized anxiety disorders (GAD) with a lifetime prevalence of about 28 % (Kessler *et al.*, 2005). These anxiety disorders have specific symptoms, but all of them are dealing with

excessive, irrational fear and dread (Nutt & Ballenger, 2003). Unlike the relatively mild, brief anxiety caused by a stressful event (such as speaking in public or a first date), anxiety disorders last at least six months (Kessler *et al.*, 2005; Kessler & Wang, 2008). Anxiety disorders commonly occur along with other mental or physical illnesses making the diagnosis of anxiety disorders difficult (Nutt & Ballenger, 2003). This is for instance exemplified by comorbid alcohol or substance abuse, which may mask anxiety symptoms or make them worse (Merikangas *et al.*, 1998; Grant *et al.*, 2004; Luthi & Luscher, 2014). Furthermore depressive-like behavior, psychosomatic discomfort, eating disorders, as well as suicidal thoughts accompany anxiety disorders (Steimer, 2002). A reinforcing factor is that impaired social interactions lead to isolating oneself from one´s social environment, which results in social isolation and enhance the side effects mentioned above (Teo *et al.*, 2013). Moreover, anxiety disorders require increased rates of chronic medical conditions (Scott *et al.*, 2007).

Steinhausen and colleagues report alarming figures: 14 % of the European population suffers from anxiety disorders, which constitute the second leading cause of mental illness after depression (Wittchen *et al.*, 2011). In 2010, mental illnesses have caused costs around 74.4 billion Euro in the health system of the European Union (Gustavsson *et al.*, 2011). To reduce these costs, and to improve the quality of life of those suffering from anxiety disorders, several research groups are working to develop appropriate therapeutic approaches.

1.3 Drug treatment of anxiety disorders

In December 1951, Paul Charpentier synthetized the tricyclic antidepressant (TCA) chlorpromazine from synthetic histamines (Ban, 2007). The psychiatric effects were first noticed in a hospital in Paris in 1952 and, then, widely used as an antipsychotic drug all over the world. The TCAs with their 3-ring molecular structure are primarily used in the clinical treatment of mood disorders such as major depression and anxiety disorders by inhibiting

both serotonin and norepinephrine reuptake from the synaptic cleft primarily by binding to and modulating serotonin and norepinephrine transporters (Feighner, 1999). With respect to GAD, imipramine was found to exert anxiolytic-like effects (Rickels *et al.*, 1993) and to decrease the risk of relapse (Mavissakalian & Perel, 1999). The major limiting factor to the more widespread use of TCAs are their side effects, which includes anti-cholinergic and anti-adrenergic effects such as sedation, sexual dysfunction, dry mouth, constipation and their well-documented toxicity in overdose (Ravindran & Stein, 2009).

Based on the knowledge that an imbalanced serotonin and norepinephrine system play a crucial role in the development of psychiatric disorders, monoamine oxidase inhibitors (MAOI), selective serotonin reuptake inhibitors (SSRI), and serotonin/norepinephrine reuptake inhibitors (SNRI) were developed (Ravindran & Stein, 2009). MAOIs are another class of older antidepressants that has been investigated for anxiety disorders (Ravindran & Stein, 2009). The enzyme monoamine oxidase is irreversibly inhibited and thereby blocks the degradation of monoamines such as serotonin and norepinephrine in the synaptic cleft. This results in an overall increased availability of these brain neurotransmitters. However, the efficacy and potency of MAOI is controversially discussed in the literature, since the effectiveness is limited to a subpopulation of patients suffering from anxiety disorders (Frank *et al.*, 1988; Shestatzky *et al.*, 1988; Kosten *et al.*, 1991).

More specifically, SSRIs and SNRIs inhibit the reuptake of the neurotransmitters via the presynaptic serotonin/norepinephrine transporter pump, resulting in increased levels of brain serotonin and norepinephrine. Currently, six SSRIs are available for clinical use including fluoxetine and, most recently, escitalopram. Due to their tolerability, efficacy and safety they became the gold standard for the treatment of GAD. Moreover, escitalopram is effective for both acute and long-term treatment for GAD (Davidson *et al.*, 2004; Goodman *et al.*, 2005; Allgulander *et al.*, 2006). The most prominent SNRI available for clinical use is venlafaxine, which is considered as alternative first-line agent for the treatment of anxiety disorders. Tzanis

and colleagues demonstrated that venlafaxine was effective to prevent relapse during a six-month follow-up (Ferguson *et al.*, 2007). However, it points out that drugs targeting the serotonin and/or norepinephrine system demonstrate a slow onset of actions and thereby require a constant drug intake over months.

In 1955, Leo Sternbach discovered an antipsychotic drug by chance which core structure is based on a benzene ring and a diazepine ring. A few years later, benzodiazepines were made available as diazepam (also called Valium; Hoffmann-LaRoche)(Wick, 2013). Benzodiazepines enhance signaling of the neurotransmitter *gamma*-aminobutyric acid (GABA) by binding to the $GABA_A$ receptor resulting in increased total conductance of chloride ions. From this follows a decreased excitability of neurons that brings about sedative, muscle relaxant, anxiolytic and hypnotic properties. Based on their fast onset of action and tolerability, benzodiazepines are commonly used. On the other side, benzodiazepine treatment is dangerous in overdose (due to oversedation, cognitive impairment, loss of locomotor coordination), comprises a risk of tolerance and dependence in long-term use. Moreover, individuals discontinuing benzodiazepine use may experience uncomfortable withdrawal symptoms. Thus, benzodiazepines and SSRIs are prescribed simultaneously to treat anxiety disorders. Once the major symptoms are attenuated by fast-acting benzodiazepines, SSRIs stabilize patient's mood for a longer period (Gross & Hen, 2004).

So far, the development of therapeutics for anxiety disorders has generally focused on the improvement of acute symptoms and relapse prevention with little discussion of primary prevention (Mathew *et al.*, 2008). Therefore, it is important to investigate neuropeptide systems and their involvement in anxiety disorders as this might help in the quest to i) understand the underlying mechanisms, which are responsible for the emergence of an anxiety disorder and ii) to develop new pharmacological tools to treat anxiety disorders.

1.4 Neuropeptides

Neurons use many chemical signals to convey information, including more than 100 different neuropeptides (Hokfelt *et al.*, 2003). The human genome contains 90 genes that encode precursors of neuropeptides. Neuropeptides are small protein-like molecules composed of 3-100 amino acids, which are synthesized at ribosomes in the perikaryon (Hokfelt *et al.*, 2003). The peptides are stored in vesicles and released either autocrine, paracrine or neuroendocrine by various stimuli at axon collaterals and dendrites and then bind to G protein-coupled receptors (GPCR) presented at plasma membrane of the target cell.

Neuropeptides also function as neuromodulators: These neuronal signaling molecules exert influence on the activity of the brain in specific ways and are thus involved in particular brain functions, like analgesia, reward, food intake, and learning and memory (Strand, 1999).

Due to the multifactorial etiology of anxiety disorders, neuropeptides have been recognized to play a crucial role in the development of an anxiety-like phenotype, the onset of an anxiety disorder and their potential as a pharmacological tool. Thus, neuropeptides are a “hot spot” in research for which reason a growing number of publications over the last decades focus on orexin, galanin, vasopressin, corticotropin releasing hormone, neuropeptide Y, substance P, prolactin, oxytocin (OXT) and neuropeptide S (NPS) (Mathew *et al.*, 2008). Understanding the underlying mechanisms resulting in a more or less anxious phenotype may lead to discover the causes of anxiety disorders and open up the possibility to develop new therapies and drugs.

1.5 The brain neuropeptide S system

1.5.1 Discovery of Neuropeptide S receptor and its endogenous ligand by GPCR deorphanization

GPCRs are a main component in the regulation of cellular homeostasis. Activated by natural ligands, they induce the activation of various signaling cascades. At least 800 seven-transmembrane receptors participate in diverse physiological and pathological functions (Tang *et al.*, 2012). Historically, ligands were discovered first, but the advent of molecular biology reversed this trend (Civelli, 2012). Bioinformatics of DNA sequences gave rise to about 140 GPCRs whose natural ligands remain unknown. Thus, these GPCRs are called “orphan receptors”. The natural ligand is discovered by so-called “deorphanization”, a process that is based on reverse pharmacology (Pausch, 1997; Chung & Civelli, 2006; Civelli *et al.*, 2006; Suga & Haga, 2007).

GPR154 (also known as GPRA, PGR14, ASRT2 and VRR1) and its ligand were first reported in the patent literature (Sato *et al.*, 2002). Searching public DNA databases, Reinscheid and colleagues identified a genomic sequence encoding for the GPR154 ligand, which was highly conserved among various species including humans, rats and mice (Xu *et al.*, 2004). The precursor protein contains a hydrophobic signal peptide that is immediately followed by the initiator methionine. Moreover, a pair lysine/arginine motif might serve for proteolytic cleavage to process the peptide (Reinscheid & Xu, 2005b). The mature ligand consists of 20 amino acids (N-SFRNGVGSGVKKTSFRRAKQ-C), whereas the amino-terminal residue is a serine. According to the nomenclature that has been used earlier (Shimomura *et al.*, 2002), the ligand was named NPS.

1.5.2 Expression patterns of Neuropeptide S

NPS is expressed in all vertebrates with the exception of fish (Reinscheid, 2007). In the rat brain, NPS mRNA expression was examined using *in situ* hybridization. NPS mRNA is expressed discretely in a few brain areas with strongest expression in the locus coeruleus (LC), principle sensory 5 nucleus and the lateral parabrachial nucleus (Xu *et al.*, 2004). Moderate NPS expression is present in the dorsomedial hypothalamic nucleus and the amygdala (Xu *et al.*, 2004). Moreover, double *in situ* hybridization revealed that NPS mRNA colocalizes predominantly with vesicular glutamate transporter (VGLUT) mRNA, indicating that these cells are glutamatergic (Xu *et al.*, 2007). A small number of NPS neurons coexpresses choline acetyltransferase mRNA, suggesting presence of acetylcholine (Xu *et al.*, 2007). However, NPS mRNA expression does not colocalize with tyrosine hydroxylase or glutamate decarboxylase 67 (GAD67, marker for GABAergic neurons) mRNA. Moreover, a colocalization of NPS mRNA and corticotropin-releasing factor (CRF) mRNA is present in the lateral parabrachial nucleus. Densitometry analysis of rat NPS-immunoreactive fibers revealed that NPS-positive nerve endings innervate the thalamus, hypothalamus, septal nuclei and septal border zone as well as amygdala (Adori *et al.*, 2015).

In mice, Pape and colleagues showed that NPS neurons coexpress the CRF receptor 1 (CRF-R1) and are in close proximity to CRF-containing fibers (Jungling *et al.*, 2012). They demonstrated that CRF depolarizes NPS neurons through activation of CRF-R1. *In vivo*, acute immobilization stress leads to an activation of NPS neurons indicated by increased expression of the immediate early gene cFos (Jungling *et al.*, 2012). Their data provide evidence for a direct interaction between the CRF and NPS system. In accordance, forced swim stress increases the expression of cFos in NPS-immunoreactive neurons suggesting a role for NPS and its involvement in stress system (Liu *et al.*, 2011). In 2011, Singewald and colleagues measured *in vivo* release of NPS following stress exposure. Microdialysis performed within the basolateral amygdala in male Sprague-Dawley rats revealed increased NPS-release during and after forced

swim stress suggesting that NPS might play a regulatory role in stress responsiveness (Ebner *et al.*, 2011).

1.5.3 NPS receptor distribution and intracellular signaling

The NPS receptor (NPSR) is a typical GPCR composed of a 7-transmembrane domain. The highest degree of similarity with respect to homology is found with vasopressin and OXT receptors (OXTR) (Reinscheid & Xu, 2005b). Using *in situ* hybridization, Reinscheid and colleagues demonstrated NPSR mRNA expression widely throughout the central nervous system with moderate to high levels of NPSR expression found in thalamus and several nuclei of the hypothalamus, including the paraventricular hypothalamic nucleus as well as cortex and amygdala (Xu *et al.*, 2004; Reinscheid & Xu, 2005b). Contrary, within the brainstem the NPSR mRNA was detected at low levels. Similar expression patterns have been demonstrated at mRNA levels in mouse brain (Clark *et al.*, 2011). Thus, the expression of NPSR mRNA in anxiety-associated neurocircuits of the limbic system indicates that the NPS system may interact with other neurotransmitter and neuropeptide systems.

The pharmacological characteristics of NPSR activation were examined in both, Chinese hamster ovary (CHO) cells and human embryonic kidney 293 T (HEK293T) cells (Reinscheid *et al.*, 2005; Camarda *et al.*, 2009; Liao *et al.*, 2016). *In vitro*, cells stably transfected with NPSR construct demonstrate reliable increases in intracellular Ca^{2+} levels and cyclic adenosine monophosphate (cAMP) levels at low nanomolar concentrations of NPS (Reinscheid *et al.*, 2005). This suggests that the NPSR is coupled to both G_q and G_s proteins (Xu *et al.*, 2004; Reinscheid *et al.*, 2005). In hippocampal NPSR-transfected neurons, researchers detected a biphasic time course of NPSR-mediated Ca^{2+} influx with a fast and slow component suggesting two major Ca^{2+} routes via intracellular stores and extracellular space (Erdmann *et al.*, 2015). In Ca^{2+}-free solution the slow component was drastically reduced suggesting Ca^{2+} influx from the extracellular space. However, it is not known which Ca^{2+} channel(s) manage(s) the entry of the

divalent ion upon NPS administration. Moreover, NPS induces phosphorylation and thereby an activation of the mitogen-activated protein kinase (MAPK) pathway (Reinscheid *et al.*, 2005).

1.5.4 Single nucleotide polymorphism in NPSR gene

Two studies identified a possible panic disorder susceptibility locus on human chromosome 7p15 (Knowles *et al.*, 1998; Logue *et al.*, 2003). In 2004, Kere and collogues described a number of single nucleotide polymorphisms (SNP) in the NPSR gene that is located on chromosome 7p14-15 (Laitinen *et al.*, 2004). Analysis of genomic DNA from blood samples of a Japanese cohort revealed that the functional NPSR A/T polymorphism (SNP database accession number rs324981), which leads to an amino acid exchange of asparagine into isoleucine (Ile) at position 107, is associated with panic disorders in male patients (Okamura *et al.*, 2007). Paradoxically, this SNP leads to a gain-of-function in NPSR functioning by increasing its sensitivity to NPS about tenfold (Reinscheid & Xu, 2005a). Moreover, Therien and colleagues demonstrated an increased expression of Ile107 allele that caused an increased cell surface expression *in vitro* (Bernier *et al.*, 2006). This effect was recently confirmed by Neumann and colleagues using a rat model selectively bred for high anxiety-related behavior; here a synonymous SNP was found (Slattery *et al.*, 2015). It is speculated that the Ile107 allele characterized by increased agonist sensitivity might lead to an overstimulation of neuronal circuits that are modulated by NPS (Okamura *et al.*, 2007; Raczka *et al.*, 2010). A second population-based study of NPSR SNPs in a Swedish cohort confirmed a correlation between NPSR polymorphisms and anxiety disorders (Donner *et al.*, 2010). Moreover, a multilevel approach was applied to further elucidate the role of NPS/NPSR system in the etiology of human anxiety (Domschke *et al.*, 2011). Herein, the A/T polymorphism was found to be associated with panic disorders, too. Moreover, the T risk allele was related to increased anxiety sensitivity. As the amygdala has a pivotal role in transforming stressful events into anxiety (Roozendaal *et al.*, 2009), Domschke and colleagues found the above-mentioned

functional SNP in the human NPSR gene to be associated with altered amygdala responsiveness to aversive stimuli in healthy European participants free from any life-time history of psychiatric disorders (Dannlowski *et al.*, 2011). Hence, this might contribute to the development of an anxiety disorders (Dannlowski *et al.*, 2011).

1.5.5 Neurobiological actions of NPS

Neurons from lateral parabrachial nucleus (which amongst others harbors a cluster of NPS-immunoreactive cells) project to ventromedial and paraventricular hypothalamic nuclei, amygdala and periaqueductal gray (Gauriau & Bernard, 2002). Since the NPSR is highly abundant in limbic brain regions such as amygdala, hypothalamus, bed nucleus of the stria terminalis, raphe nucleus and ventral tegmental area, NPS might influence emotional behaviors and body homeostasis (Reinscheid & Xu, 2005a).

Reinscheid and colleagues demonstrated strong anxiolytic-like activity of intracerebroventricularly (icv) infused NPS in mice subjected to elevated plus maze (EPM), light/dark box (LDB) and open field (OF) (Xu *et al.*, 2004). Moreover, the anxiolytic activity was confirmed by a marble-burying test, a model that is not biased by locomotor activity (Xu *et al.*, 2004; Paneda *et al.*, 2009). Since 2006, the anxiolytic action of NPS was confirmed using various tests in mice and rats following icv (Leonard *et al.*, 2008; Rizzi *et al.*, 2008; Vitale *et al.*, 2008; Wegener *et al.*, 2011; Slattery *et al.*, 2015) and local infusions (Smith *et al.*, 2006) as well as intranasal applications (Ionescu *et al.*, 2012; Lukas & Neumann, 2012; Dine *et al.*, 2015).

Based on Pavlovian conditioning, an aversive stimulus such as an electric foot shock is associated with a neutral stimulus (e.g. tone), a process termed acquisition phase. This cued fear conditioning paradigm is based on associative fear memory that is tested by presentation of conditioned stimulus alone. The freezing behavior during extinction phase indicates fear response of an animal. However, repeated presentation of the conditioned stimulus without

aversive stimulus leads to gradual extinction of fear response. NPS was found to reliably reverse cued fear in both mice and rats (Jungling *et al.*, 2008; Slattery *et al.*, 2015; Zoicas *et al.*, 2016). This effect is mediated by NPS-evoked increase in glutamatergic transmission to intercalated GABAergic neurons in the amygdala (Jungling *et al.*, 2008; Pape *et al.*, 2010). More specifically, NPS blocked the expression of fear-potentiated startle (Fendt *et al.*, 2010). In addition, NPS facilitates extinction of social fear and reduces avoidance behavior in a social defeat model in mice (Zoicas *et al.*, 2016). Although NPS enhances object recognition (Okamura *et al.*, 2011), it failed to prolong social memory in rats suggesting that NPS has memory-enhancing effects in a non-social context (Lukas & Neumann, 2012). Reinscheid and colleagues demonstrated an attenuation of NPS-induced memory enhancement by blocking the adrenergic signaling, suggesting an interaction between NPS system and the brain noradrenergic system to promote arousal (Okamura *et al.*, 2011).

NPS effects were also investigated in the context of aggressive-like behavior. Neumann and colleagues demonstrated anti-aggressive effects of icv infused NPS in rats selectively bred for low anxiety-like behavior (Beiderbeck *et al.*, 2014). This effect was confirmed in mice subjected to the resident/intruder test (Ruzza *et al.*, 2015). Herein, NPS facilitated anti-aggressive effects that were abolished in the presence of the non-peptidergic NPSR antagonist SHA-68.

In 2005, Sticker-Krongrad and colleagues described an anorexigenic effect of NPS. In Long-Evans rats, *icv* infused NPS strongly inhibited chow intake in overnight fasted rats (Beck *et al.*, 2005). Moreover, they demonstrate that this effect is independent of neuropeptide Y, ghrelin and leptin pathways. A second study confirms the findings as both *icv* and intra-PVN infusion of NPS reduced food intake, too (Smith *et al.*, 2006). In 2009, Ciccocioppo and colleagues identified the hypothalamic PVN as an important site of NPS' anorexic effect. Moreover, the NPS effects on reduction of food intake were completely blocked in the presence of a NPSR antagonist (Fedeli *et al.*, 2009). In addition, it was demonstrated that the NPS-induced decrease of food intake were not modified by CRF-R antagonists indicating that NPS' effects

are independent of the hypothalamic CRF system (Fedeli *et al.*, 2009; Peng *et al.*, 2010).

Patients suffering from chronic pain have an increased prevalence to develop an anxiety disorder (Hasnie *et al.*, 2007; Kroenke *et al.*, 2009; Newcomer *et al.*, 2010; Reme *et al.*, 2011). The periaqueductal gray is an important component of pain system (Fields *et al.*, 1991). Moreover, this brain region has been demonstrated to express high levels of NPSR mRNA (Xu *et al.*, 2007). In 2009, Wang and colleagues demonstrated an anti-nociceptive effect of NPS in a dose-dependent manner using hot-plate test and a formalin test, an effect that was prevented in the presence of a NPSR antagonist (Li *et al.*, 2009; Peng *et al.*, 2010). In 2014, Mao and colleagues demonstrated that sciatic nerve injury increases anxiety-like behavior, a condition that was accompanied by a decreased NPS expression (Zhang *et al.*, 2014). However, exogenously applied NPS reversed pain-induced anxiety. Herein, they argue that NPS enhances GABAergic transmission in the amygdala and thus reduces anxiety-like behavior.

In summary, the brain NPS/NPSR system promotes anxiolysis, reverses cued and social fear, enhances memory, facilitates anti-aggressive effects, reduces food intake and has anti-nociceptive properties. Thus, the NPS/NPSR system is a strong regulator of both emotional behaviors and body homeostasis.

1.6 The brain oxytocin system

1.6.1 Synthesis and release of oxytocin

In 1906, Sir Henry Dale discovered that extracts from the posterior pituitary stimulated uterus contractions of a cat. It was also Henry Dale who coined out the name oxytocin (OXT) from the Greek words “ὀξύς τόκος”, meaning swift birth. Accordant to the Greek name, the most prominent peripheral effect of OXT is the induction of uterine contractions facilitating birth (Fuchs & Poblete, 1970) and, moreover, maintaining well-known neuroendocrine effects such

as milk ejection and orgasm (Rhodes *et al.*, 1981; Gimpl & Fahrenholz, 2001).

The nonapeptide OXT is synthetized by neurons located in the hypothalamic PVN, the supraoptic nucleus (SON), and accessory nuclei (AN) of the hypothalamus (Fig. 1) (Rhodes *et al.*, 1981; Swanson & Sawchenko, 1983). Stored in large-dense core vesicles (LDCV) along with their respective carrier proteins called neurophysins, OXT is released from magnocellular neurons with a diameter of 20-30 µm into the periphery via axons forming neurohemal contacts within the neurohypophysis (Gimpl & Fahrenholz, 2001; Meyer-Lindenberg *et al.*, 2011).

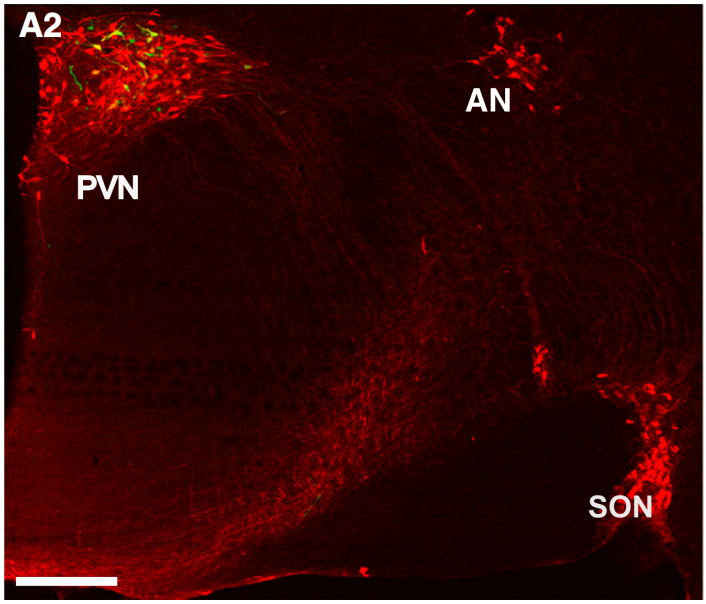

Figure 1: OXT neurons located within hypothalamic PVN, SON and AN. Scale bar represents 500 µm. Adapted from Eliava *et al.,* 2016.

Moreover, magnocellular PVN-OXT neurons innervate forebrain structures such as the nucleus accumbens (Dolen *et al.*, 2013) and the central nucleus of the amygdala (CeA). Within the CeA, Grinevich and colleagues demonstrated that OXT release from local axonal endings specifically controls region-associated behaviors such as decreased freezing responses in fear-conditioned

rats (Knobloch *et al.*, 2012).

Electron microscopic profiles demonstrated that dendrites of magnocellular OXT neurons have a strong peptide immunoreactivity (Armstrong, 1995) revealing abundant LDCV in somatodendritic structures (Pow & Morris, 1989). The first evidence that dendrites could be a substantial source of peptide release came from studies of the magnocellular neurons of the supraoptic nucleus demonstrating that central and peripheral release of vasopressin and OXT differ in temporal dynamics and do not necessarily act in a linear fashion (Neumann *et al.*, 1993a; Ludwig, 1998; Ludwig & Leng, 2006).

In contrast to magnocellular neurons, parvocellular OXT neurons terminate mainly in spinal chord and brainstem (Swanson & Sawchenko, 1983). It has been proposed that OXT from parvocellular OXT axonal terminals contributes to the modulation of cardiovascular functions, breathing, and feeding behavior (Mack *et al.*, 2002; Petersson, 2002; Atasoy *et al.*, 2012). Recently, a subpopulation of parvocellular OXT neurons located within the PVN has been demonstrated to control the activity of magnocellular OXT neurons within the SON and to suppress nociception in order to facilitate analgesia (Eliava *et al.*, 2016).

The release of LDCVs is evoked by a rise in intracellular Ca^{2+} levels (Hokfelt, 1991). Magnocellular neurons synthesizing OXT are densely filled with LDCV, representing 85% of the total volume of the neuron and thus contain very large amounts of OXT (Stoop, 2012; Stoop *et al.*, 2015). Under physiological conditions, OXT-filled LDCVs are bound to F-actin (Ludwig *et al.*, 2016). Once OXT neurons are activated (e.g. by transient Ca^{2+} influx), F-actin is rapidly and reversibly depolymerized to G-actin, the OXT-filled vesicle is transported to the membrane, and following binding of a SNARE complex, the vesicle fuses with the plasma membrane resulting in the release of OXT into the extracellular space (Ludwig *et al.*, 2016). The Ca^{2+} that triggers release of OXT can originate from extracellular and intracellular sources such as N-type voltage-gated Ca^{2+} channels which appeared to be particularly important for dendritic OXT-

release (Fisher & Bourque, 1996), N-methyl-D-aspartate receptors that influence burst firing of OXT neurons (Hu & Bourque, 1992), and intracellular Ca^{2+} stores like the endoplasmic reticulum (Lambert *et al.*, 1994). Similarly, dendritic release of OXT also depends on the increase in intracellular Ca^{2+} (Neumann *et al.*, 1993b; Lambert *et al.*, 1994; Ludwig *et al.*, 2002; Landgraf & Neumann, 2004; Ludwig & Leng, 2006). Moreover, dendritic release is accompanied by "priming", an effect facilitated by internal Ca^{2+} mobilization which makes secretory vesicles available for release in response to electrical stimuli (Ludwig & Leng, 2006). Once released within the brain, OXT has a half-life time of 20 min in the cerebrospinal fluid (Ludwig & Leng, 2006); the half-life in blood was assessed to be about 1.5 min (Higuchi *et al.*, 1986). Its degradation is mainly operated by aminopeptidases (Stoop, 2012).

Altogether, these studies demonstrate that OXT neurons show widespread central projections of hypothalamic OXT neurons, underlining the evolution of a fine-tuned network composed of various projections originating from hypothalamic areas (Viviani *et al.*, 2011; Stoop, 2012).

1.6.2 Brain OXTR distribution and intracellular signaling

The OXTR is a GPCR composed of a 7-transmembrane domain. Most notably, the OXTR expression is located in cortical areas, the olfactory system, the basal ganglia, the limbic system (e.g. lateral septum, amygdala, subiculum), the thalamus and hypothalamus, the brain stem and the spinal cord (Gimpl & Fahrenholz, 2001). The OXTR is functionally coupled to a G_q protein that stimulates the activity of phospholipase C (PLC). Consequently, PLC cleaves inositol-4,5-bis-phosphate (PIP_2) into 1,2-diacylglycerol (DAG) and inositol-1,4,5-triphosphate (IP_3), whereas DAG stimulates protein kinase C, and IP_3 increases intracellular Ca^{2+} levels (Gimpl & Fahrenholz, 2001; van den Burg & Neumann, 2011). The latter is of great importance in the regulation of firing patterns and excitability and, consequently, neurosecretion, gene transcription, and protein synthesis. In most cellular systems, the OXT-induced rise in intracellular Ca^{2+} levels is more prominent in the presence of extracellular Ca^{2+} (Clapham,

2007). This suggests that OXT might increase intracellular Ca^{2+} levels via receptor- or voltage-gated channels (Zhong *et al.*, 2008). Recently, it has been shown that OXT stimulation promotes Ca^{2+} influx via transient receptor potential vanilloid type 2 (TRPV2) channels in a phosphoinositide 3-kinase (PI3K)-dependent manner (van den Burg *et al.*, 2015). Moreover, Ca^{2+} influx from extracellular space is necessary for MAPK kinase (MEK1/2) phosphorylation and the anxiolytic effect of OXT within the PVN. In addition, Neumann and colleagues demonstrated that an OXT-induced phosphorylation of MEK1/2 is necessary to promote anxiolysis in male (Blume *et al.*, 2008) as well as in female virgin and lactating rats (Jurek *et al.*, 2012).

1.6.3 Central effects of OXT

Local infusion of synthetic OXT into the hypothalamic PVN and the central amygdala promotes acute anxiolytic activity in both males and females (Neumann *et al.*, 2000; Bale *et al.*, 2001; Blume *et al.*, 2008; Neumann, 2008; van den Burg & Neumann, 2011; Jurek *et al.*, 2012; van den Burg *et al.*, 2015). Besides induction of lordosis behavior in females and erectile effect of OXT in males in response to the expectation of copulation (McCarthy *et al.*, 1994; Argiolas & Melis, 2004), mating-induced release of endogenous OXT similarly reduces the state of anxiety-related behavior (Waldherr & Neumann, 2007).

Furthermore, OXT has been demonstrated to reduce pain perception (Juif *et al.*, 2013; Juif & Poisbeau, 2013), which is maintained by a population of parvocellular OXT neurons that prevent inflammatory pain processing by inhibition of sensory spinal cord neurons (Eliava *et al.*, 2016).

In 1991, Verbalis and colleagues discovered an anorexic effect following central OXT infusion. This effect was confirmed using a specific OXTR agonist, whereas an OXTR antagonist (OXTR-A) blocked the anorexic effect in food-deprived rats (Olson *et al.*, 1991a; Olson *et al.*, 1991b).

Moreover, OXT was found to attenuate ethanol-induced motor impairments in rats by preventing ethanol actions at *delta*-subunit of the $GABA_A$ receptor (Bowen *et al.*, 2015). In addition, central OXT infusion inhibits ethanol-induced dopamine release in the nucleus accumbens and reduces ethanol consumption after long-term voluntary ethanol intake (Peters *et al.*, 2016).

Besides OXT's non-social effects, Kelsch and colleagues demonstrated that OXT enhances social recognition by modulating cortical control of early olfactory processing (Oettl *et al.*, 2016). Moreover, social fear represents a main symptom of social anxiety disorder that can be mimicked in the social fear-conditioning paradigm (Toth *et al.*, 2012; Toth & Neumann, 2013). Fittingly, synthetic OXT promotes extinction of social fear (Zoicas *et al.*, 2014). In extension, OXT has been shown to facilitate pro-social behavior and it prevents social avoidance in both rats and mice (Lukas *et al.*, 2013). In addition, OXT increases social investigation and mediates rodent social memory in regions of the limbic system, namely lateral septum and medial amygdala (Lukas & Neumann, 2013). Furthermore, OXT has been shown to be a crucial regulator of pair bonding (Insel & Shapiro, 1992; Carter *et al.*, 1995; Insel & Hulihan, 1995; Cho *et al.*, 1999) and maternal behavior (Pedersen & Prange, 1979; Neumann *et al.*, 2000; Bosch *et al.*, 2004; Bosch *et al.*, 2005; Pedersen *et al.*, 2006). Lastly, OXT has been demonstrated to play a major role in the regulation of stress responsiveness and the regulation of hypothalamic-pituitary-adrenal axis in response to a variety of emotional, but also physical and pharmacological stressors (Neumann, 2008; Neumann & Slattery, 2016).

Taking into account that OXT release is maintained by magnocellular and parvocellular neurons, by axonal and/or somatodendritic release, the regulatory role of Ca^{2+} influx and its influence on OXT release and the numerous cell types expressing OXTRs might explain the distinct impact of OXT in brain-region specific behaviors (Lee *et al.*, 2009).

1.7 Characterization of distinct cellular populations by fluorescent signals

In 2008, the Nobel Prize in Chemistry was awarded to Osamu Shimomura, Martin Chalfie and Roger Y. Tsien “for the discovery and development of the green fluorescent protein (GFP)” (Figure 2). Originally derived from jellyfish *Aequorea victoria*, GFP is frequently used as a reporter gene and redefined fluorescent microscopy (Arun *et al.*, 2005; Yuste, 2005).

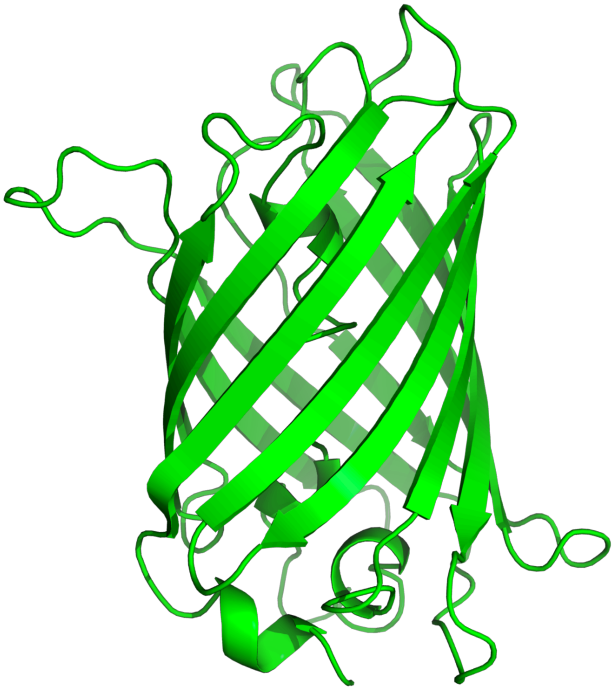

Figure 2: **Green fluorescent protein (GFP).** Typical *beta*-barrel structure of the green-light emiting protein originally derived from *Aequorea victoria*.

Based on the properties of GFP, genetic mutants have been examined for their fluorescent activity such as the yellow fluorescent protein (YFP). To date, improved versions of YFP are Citrine, Ypet and Venus. The latter contains a novel amino acid substitution transforming the protein to the most powerful fluorescent protein to date (Miyawaki *et al.*, 1997). Tagging proteins of interest with Venus allows identification of a specific cell population with highest precision.

1.7.1 Fluorescence-activated cell sorting

Recently, Grinevich and colleagues constructed an adeno-associated virus (AAV) expressing Venus under the control of an OXT promoter fragment and infused it into the PVN, SON and AN of female Wistar rats. More than 97 % colocalization of OXT and Venus has been observed (Knobloch *et al.*, 2012) underlying the high specificity of this construct. Thus, Venus-labeling of OXT-immunoreactive neurons provides the basis for precise cell sorting.

Fluorescence-activated cell sorting (FACS) is a specialized form of flow cytometry. Hereby, a heterogeneous cell population is sorted cell-by-cell. First, each cell enters a single droplet as soon it leaves the nozzle tip. Since each fluorophore has a characteristic peak excitation and emission wavelength following excitation by laser, a detector characterizes each single cell. Depending on the fluorescent signal of the cell, the drop is electronically charged. Next, drops containing a single cell pass two deflection plates that either attract or repel the cells accordant to their charge into collection tubes. Following FACS, cells can be cultured or analyzed further for specific expression patterns, thereby allowing characterization of a distinct cellular population.

1.7.2 Measuring Ca^{2+} dynamics in living cells by genetically encodable Ca^{2+} indicators

Ca^{2+} is one of the most abundant mineral compounds of the vertebrate body. In form of hydroxyapatite, Ca^{2+} is stored in bones and teeth and thus gives stability and strength. Outside of bones Ca^{2+} acts as a versatile second messenger. It is involved in muscle contraction, exocytosis, gene expression, proliferation, differentiation, blood clotting and apoptosis (Krebs, 1998; Clapham, 2007).

The Ca^{2+} concentration within a non-stimulated cell is low. A reason for this phenomenon is that this divalent ion precipitates with phosphate. Thus, cells have to compartmentalize,

chelate, or extrude it (Clapham, 2007). Concentrations of free intracellular Ca^{2+} are regulated by a large variety of channels, exchangers and pumps on both the plasma membrane and intracellular storage organelles such as endoplasmic as well as sarcoplasmic reticula or mitochondria (Berridge *et al.*, 2000). However, about 0.1 % of the Ca^{2+} are located in the extracellular space and available as free, biologically active ions. Ca^{2+} enters the cell via diverse set of Ca^{2+}-permeable channels and thus regulates intracellular signaling cascades and cellular activity. Differences in the amplitude, frequency and location of Ca^{2+} can encode a variety of messages that are decoded by a number of Ca^{2+} binding proteins.

In order to measure cellular activity, enormous effort has been devoted to develop tools for Ca^{2+} imaging in living cells. Such indicators allow dissecting spatial and temporal Ca^{2+} signaling processes. Small molecule Ca^{2+} indicators based on the chelating character of 1,2-bis(*o*-aminophenoxy)ethane-*N,N,N',N'*-tetraacetic acid (BAPTA) are frequently used to measure changes in intracellular Ca^{2+} levels. However, loading cells *in vivo* with these Ca^{2+} indicators is invasive and does not allow chronic timescales. Thus, genetically encoded Ca^{2+} indicators (GCaMP) have been developed based on the most prominent representative of intracellular Ca^{2+}-binding proteins named calmodulin (Cheung, 1980). Calmodulin is a small, ubiquitous adaptor protein, which is evolutionary highly conserved and expressed in all eukaryotes (Clapham, 2007). The Ca^{2+}-binding EF-hand has a typical helix-loop-helix structure. Its affinity for Ca^{2+} is increased by interaction with target proteins. When Ca^{2+} binds, the shape of the calmodulin domains changes, thus triggering the ability to remodel active sites (Hoeflich & Ikura, 2002). Based on this knowledge, Ca^{2+} indicators are composed of calmodulin, an *alpha*-helix of M13 protein and a circularly permutated GFP (fusion of N- and C-terminus). Once Ca^{2+} is chelated by calmodulin, the latter undergoes a conformational change leading to a deprotonation of GFP. Hence, the chromophore changes its spectral properties and thus emits light (Figure 3) (Wang *et al.*, 2008; Akerboom *et al.*, 2009).

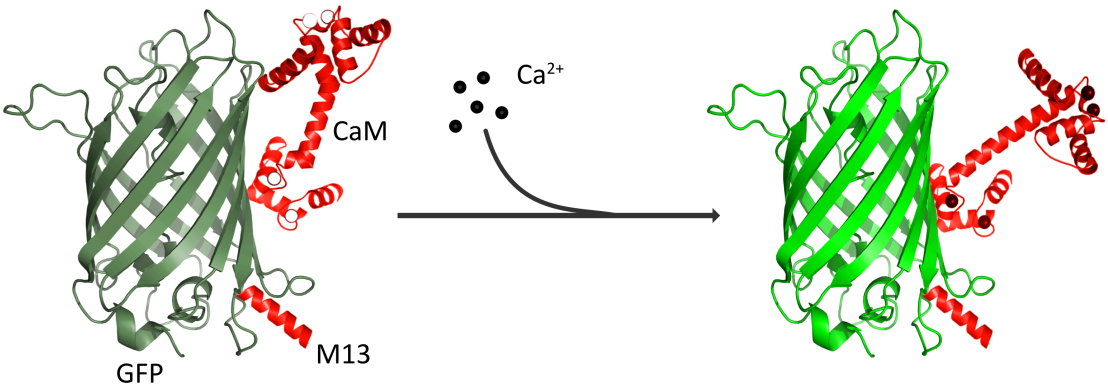

Figure 3: **Principle of GCaMP.** Following Ca^{2+} binding, calmodulin (CaM) undergoes a conformational change and thereby deprotonates green fluorescent protein (GFP). Hence, its spectral properties are changed and GFP emits light.

GCaMP expression is introduced into living cells using AAVs that allow genetically specified expression under the control of a promoter fragment. In 2004, the first transgenic mouse expressing GCaMP was reported (Ji *et al.*, 2004). However, the sensitivity, thermostability and response kinetics were slow in comparison to BAPTA-based indicators (McCombs & Palmer, 2008). Since neural activity evokes fast changes in intracellular Ca^{2+} levels (Tank *et al.*, 1988; Kerr *et al.*, 2000; Sabatini *et al.*, 2002), efforts have been made to optimize GCaMP system. Using structure-based mutagenesis and neuron-based screening, Kim and colleagues developed a family of ultrasensitive fluorescent Ca^{2+} sensors (GCaMP6) that outperformed other sensors in cultured neurons and in zebrafish, flies and mice *in vivo* (Chen *et al.*, 2013). GCaMP6 reliably detects single action potentials in neuronal somata and, hence, provides a new window into the organization and dynamics of neural circuits over multiple spatial and temporal scales.

In conclusion, rapid intracellular Ca^{2+} dynamics can be monitored using genetically engineered ultrasensitive fluorescent proteins and thus allow imaging of neuronal activity *in* and *ex vivo* over a large timescale.

1.8 Recent technologies to selectively regulate cellular activity

In 1979, Francis Crick predicted that in order to elucidate neuronal codes that specify behavior and perception ‘‘a method (is needed) by which all neurons of just one type could be inactivated, leaving the others more or less unaltered’’ (Crick, 1979). In the past decade, emerging synthetic biology technologies have been developed and thereby revolutionized selective targeting of specific neuronal populations similar like a remote control (Rogan & Roth, 2011). The most prominent techniques are optogenetics, which is based on the activation of light-sensitive channels using an optrode, and chemogenetics, which uses engineered GPCRs that are activated by biologically inert drugs (Boyden *et al.*, 2005; Armbruster *et al.*, 2007).

The term chemogenetics refers to a designer receptor exclusively activated by designer drugs (DREADD). In 2007, Roth and colleagues created a mutated human muscarinic acetylcholine receptor, which lost its affinity for its natural ligand (Armbruster *et al.*, 2007), but has an increased affinity towards clozapine *N*-oxide (CNO), an otherwise chemically inert drug. Usually, DREADDs are introduced into cells using viral vectors such as AAV. The selective targeting is achieved by cell type-specific promoter fragment to drive DREADD expression (Fig. 4). In order to verify successful transfection and expression of DREADD *in vivo*, the construct encodes for a reporter gene (such as mCherry, GFP, tdTomato, mCitrine or Venus). Moreover, the expression can further be controlled using recombinase-based system (CRE recombinase-dependent manner), which allows DREADD expression in a subpopulation of a certain cell type (Boender *et al.*, 2014). Once CNO is applied intraperitoneally via osmotic minipumps, chow pellets, or drinking water, it crosses the blood-brain barrier and binds with low nanomolar affinity to its receptor (Armbruster *et al.*, 2007; Dong *et al.*, 2010; Urban & Roth, 2015; Urban *et al.*, 2016).

DREADDs, much like endogenous GPCRs, are either coupled to inhibitory (G_i) or excitatory (G_q, G_s) signaling cascades (Whissell *et al.*, 2016). CNO-evoked activation of the modified human M4 class muscarinic DREADD via G_i-signaling (hM4Di receptor) induces neuronal silencing by transactivation of G protein-coupled inwardly rectifying potassium channels (GIRK). Thus, the efflux of K^+ induces hyperpolarization resulting in decreased neuronal firing. Conversely, CNO-induced activation of the modified human M3 class muscarinic DREADD via G_q-signaling (hM3Dq receptor) induces neuronal activation characterized by increased PLC activity, elevated IP_3 and DAG levels, and a rise in intracellular Ca^{2+} concentration (Whissell *et al.*, 2016).

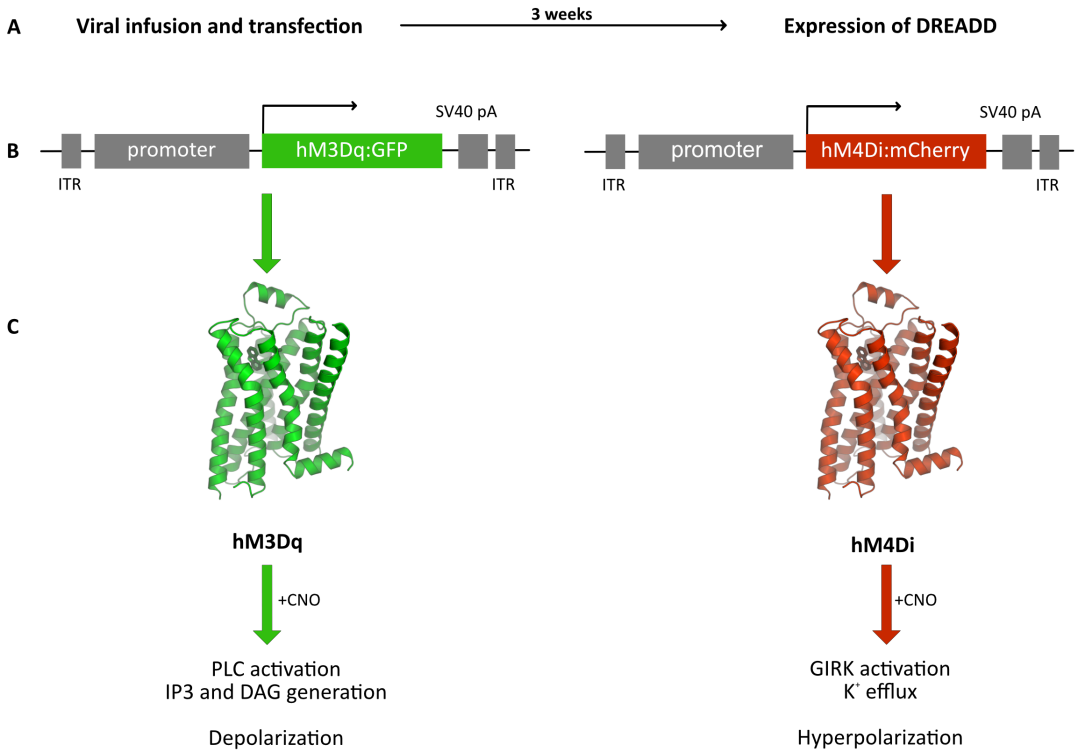

Figure 4: **Theory of designer receptors exclusively activated by designer drugs (DREADD).** (A) Following cellular transfection, DREADDs are expressed within three weeks. (B) Cell type-specific promoter fragments achieve selective targeting and expression of hM3Dq or hM4Di in combination with a reporter gene (GFP, mCherry). (C) Both receptor types are activated by clozapine N-oxide (CNO) resulting in altered intracellular signaling and cellular activity inducing depolarization in a G_q- and hyperpolarization in a G_i-dependent manner.

While CNO plasma levels following ip injection peak within 30 min and sharply decline within two hours (Guettier *et al.*, 2009), the amount of bioavailable CNO within the brain is currently not known. Various reports controversially describe the duration of CNO-induced activation of DREADD-expressing cell-types ranging from 30 min up to six hours (Alexander *et al.*, 2009).

Since CNO-dependent DREADDs appeared to be very useful for manipulating cell activity, there is a strong interest to develop new DREADD systems. Based on mutated *kappa*-opioid receptors (KOR) coupled to G_i-signaling cascade, so-called KOR DREADDs (KORD) have been developed (Vardy *et al.*, 2015). Based on the principle of chemogenetics, KORDs are exclusively activated by Salvinorin B (SALB). In a recent study, Roth and colleagues performed a bidirectional chemogenetic manipulation using two DREADDs, an excitatory hM3Dq and an inhibitory KORD within the same animal (Vardy *et al.*, 2015). Thereby, they facilitated the multiplexed dissection of neural circuits and behavior in mice. Moreover, they demonstrate differences in pharmacokinetics between CNO and SALB. SALB was shown to have rapid short-lasting effects, whereas CNO mediates delayed long-lasting effects (Whissell *et al.*, 2016).

In conclusion, DREADDs represent a powerful technique allowing spatiotemporal control in a cell type-specific manner. Thus, this method allows activation or inhibition of specific neuropeptidergic neurons (Burnett & Krashes, 2016), and was used in this thesis for modulating OXT neurons. Predominantly used in rodents, a first study has recently been published, where researchers introduced the DREADD system in rhesus monkeys (Grayson *et al.*, 2016). Due to unlimited DREADD construct designs relating to promoter fragment, the potential combination in a CRE-dependent manner, and the acute, remote and reversible modulation of cellular activity open doors to new and enriching possibilities to study behavioral relevance of a defined cellular population. Thus, using this technique has the potential to map brain circuits and their possible interactions with other systems, and to bridge the gap between an anatomical structure and its behavioral relevance. This will give rise

to fundamental knowledge in neuroscience to develop pharmacogenetic tools to treat mood and anxiety disorders.

1.9 Aims and outline of the present study

Psychopathologies associated with socio-emotional dysfunctions such as anxiety disorders have 28% lifetime prevalence (Gross & Hen, 2004; Kessler *et al.*, 2005). Altogether, they decrease the quality of life, may induce social isolation and substance abuse. Both, OXT and the recently discovered NPS represent putative treatment options due to their potent anxiolytic activity described in pre-clinical studies. Although the knowledge about these neuropeptides increases continuously, many aspects of the underlying mechanisms at molecular, cellular and tissue-wide levels remain elusive. Therefore, three hypotheses have been postulated to gather more fundamental knowledge about the neuropeptidergic mechanisms that might influence the behavioral phenotype of an individual. Each of these questions has been addressed in one of the three chapters constituting this thesis.

In chapter 1, I tested the hypothesis that NPS effects are mediated via OXT neurons within the PVN of male Wistar rats. Both, NPS and OXT have been described to exert robust anxiolytic activity (Neumann *et al.*, 2000; Xu *et al.*, 2004; Slattery *et al.*, 2015; van den Burg *et al.*, 2015), to reverse both social (Zoicas *et al.*, 2014; Zoicas *et al.*, 2016) and cued fear (Jungling *et al.*, 2008; Slattery *et al.*, 2015), to decrease aggressive-like behavior (Beiderbeck *et al.*, 2014; de Jong *et al.*, 2014; Ruzza *et al.*, 2015), and to exert anorexic effects (Olson *et al.*, 1991a; Smith *et al.*, 2006). Moreover, *in situ* hybridization data demonstrate a strong overlap of NPSR and OXTR expression in limbic brain regions (Yoshimura *et al.*, 1993; Gimpl & Fahrenholz, 2001; Xu *et al.*, 2007). More precisely, NPSR expression is highly abundant within the PVN (Xu *et al.*, 2007), a brain nucleus that harbors parvo- and magnocellular OXT-immunoreactive neurons (Swanson & Sawchenko, 1980; Gimpl & Fahrenholz, 2001). Taken together, the data suggest a

possible interaction between the NPSR- and OXT system. Specifically, I postulated that NPS evokes activation of PVN-OXT neurons. As the PVN is abundantly innervated by NPS-positive fibers in mice (Clark *et al.*, 2011), I analyzed LC-NPS afferents within the PVN, and I examined NPSR expression in PVN-OXT neurons. Using ultrasensitive fluorescent proteins and intracerebral microdialysis, I investigated potential effects of NPS on the endogenous OXT system. Moreover, I hypothesized that the anxiolytic effect of NPS is mediated via the paraventricular OXT system. In order to directly reveal the involvement of endogenous OXT in the anxiolytic effects of NPS within the PVN I employed two experimental strategies: First, I blocked OXTR-mediated effects using a selective OXT receptor antagonist (OXTR-A), and second I inhibited the activity of OXT neurons within the PVN by chemogenetic silencing using a G_i-coupled DREADD, prior to central NPS infusion. These findings provide the first evidence for an intra-hypothalamic mechanism involving NPSR-expressing OXT neurons in the potent anxiolytic profile of NPS.

In vitro studies in NPSR-transfected HEK293T and CHO cells revealed increased cAMP concentration by adenylyl cyclase (AC) activation and a rise in intracellular Ca^{2+} levels due to phospholipase C (PLC) stimulation suggesting that the NPSR is coupled to both G_s and G_q proteins (Reinscheid & Xu, 2005a; Camarda *et al.*, 2009; Erdmann *et al.*, 2015; Liao *et al.*, 2016), respectively. However, the underlying mechanism(s) mediating the anxiolytic activity following NPSR activation is still unknown. In chapter 2, I hypothesized that the anxiolytic activity of NPS depends on G_q-dependent intracellular signaling. In situ hybridization studies revealed that NPSR mRNA expression within the rat amygdala is restricted to the intercalated and the medial nucleus (MeA) (Xu *et al.*, 2007). As the amygdala regulates fear and anxiety-related behavior (Tovote *et al.*, 2015), I specifically postulated that NPS (i) promotes anxiolysis within the MeA, (ii) activates Ca^{2+}-dependent signaling pathways in the amygdala *in vivo*, and (iii) induces anxiolysis in a PLC-dependent manner. These findings increase our understanding with respect to the intracellular signaling mechanism that might be involved in the

pathophysiology of anxiety disorders.

Since 2007, chemogenetics developed into a frequently used technical tool that allows spatiotemporal control over a distinct cellular population. However, the CNO-dependent potency and the intracerebral dynamics are controversially discussed. While CNO plasma levels peak within 30 min and sharply decline within two hours (Guettier *et al.*, 2009), the amount of bioavailable CNO within the brain is currently not known. Various reports controversially describe the duration of CNO-induced activation of DREADD-expressing cell-types ranging from 30 min up to six hours (Alexander *et al.*, 2009). Although DREADDs allow selective activation (or inhibition) of specific neuronal populations in order to dissect their contribution to complex behaviors and brain circuitries, the spatiotemporal dynamics of DREADD actions with respect to OXT neurons remain unknown. In chapter III, I analyzed the spatiotemporal dynamics of chemogenetic OXT neuron activation within the rat PVN using DREADDs, and its behavioral relevance. After viral vector-based expression of an excitatory DREADD (hM3Dq) specifically in OXT neurons, I monitored the dynamics of OXT release within PVN, lateral septum, and peripheral blood following chemogenetic stimulation initiated by CNO using microdialysis technique and via jugular vein catheter. Altogether, these results narrow down the time window, when chemogenetic stimulation of neuropeptidergic neurons can be efficiently applied for studying behavioral changes. Furthermore, my findings demonstrate that chemogenetic manipulation of OXT neurons is a powerful tool for dissection of novel functional OXT brain circuits and hence various OXT-dependent behaviors under normal and psychopathological conditions.

2 Materials and methods

2.1 Animals and husbandry

Male Wistar rats (230-250 g; Charles River Laboratories, Bad Sulzfeld, Germany) were housed in groups of 3-4 under standard laboratory conditions with access to food and water *ad libitum*. Rats were maintained on a 12:12 h light/dark cycle with lights on at 07.00 a.m. in a temperature- and humidity-controlled room (21 – 23 °C, 55 % humidity). All experiments were performed between 08:00 a.m. – 01:00 p.m. in accordance with the Guide for the Care and Use of Laboratory Animals by the NIH, and were approved by the government of the Oberpfalz.

2.2 Surgical procedures

The animals were allowed at least one week of habituation before they were used for surgical procedures. Rats received a subcutaneous injection of the antibiotic Baytril (Baxter, 10 mg/kg Enrofloxacin) and an intraperitoneal (ip) injection of the analgesic Buprenovet (Bayer, 0.05 mg/kg Buprenorphine) 30 min before the start of the surgery. All stereotaxic procedures were performed under isofluran anesthesia and semi-sterile conditions. All coordinates used are based on the rat brain atlas (Paxinos & Watson, 1998) and summarized below (table 1).

Stereotaxic coordinates	AP	ML	DV	angle	Vol
Intra-PVN infusion					
$AAV_{1/2}$ OXTpr-Venus, $AAV_{1/2}$ OXTpr-GCaMP6s $AAV_{1/2}$ OXTpr-hM3Dq:mCherry, $AAV_{1/2}$ OXTpr-hM4Di:mCherry	-1.8	±0.3	-8.0	0°	280 nl
Intra-SON infusion					
$AAV_{1/2}$ OXTpr-Venus, $AAV_{1/2}$ OXTpr-hM3Dq:mCherry	-1.4	±1.7	-9.0	0°	280 nl
Intra-AN infusion					
$AAV_{1/2}$ OXTpr-hM3Dq:mCherry	-1.9	±1.2	-8.5	0°	280 nl
Microdialysis probe implantation					
PVN	-1.4	+1.8	-8.3	10°	
Septum	+0.5	+0.7	-6.2	0°	
Guide cannula implantation					
icv (12 mm, 21G)	-1.0	-1.6	-2.0	0°	
Above PVN (12 mm, 23 G)	-1.4	+1.8 / -2.1	-6.3	10°	
Above MeA (12 mm, 23 G)	-2.3	±3.2	-7.5	0°	

Table 1: Stereotaxic coordinates (in mm) used for viral infusions and implantation of microdialysis probes and guide cannulas accordant to bregma (AP: anteroposterior axis; ML: mediolateral axis; DV: dorsoventral axis).

2.2.1 Intracerebral infusion of recombinant adeno-associated virus

Either $AAV_{1/2}$(OXTpr-Venus), $AAV_{1/2}$(OXTpr-GCaMP6s), $AAV_{1/2}$(OXTpr-hM3Dq:mCherry), or $AAV_{1/2}$(OXTpr-hM4Di:mCherry) was bilaterally microinfused using a 5-µl calibrated micropipette (VWR, inner diameter: 0.3 mm), which was pulled to create a long narrow shank. The micropipette shaft was marked with a 1-mm scale that corresponds to a volume of ~70 nl.

In total, 280 nl of cell-type specific recombinant adeno-associated viral vectors (rAAV) were infused slowly by pressure infusion into each PVN or PVN, SON and AN, respectively. After the infusion, the micropipette was kept in place for 3 min to ensure adequate rAAV diffusion. The drill hole in the skull was closed using bone wax (Ethicon, Somerville, New Jersey, USA), and the wound was sutured using sterile nylon material. After the surgery, animals were single-housed for 48 h to recover from anesthesia and then group-housed for 16 days.

2.2.2 Implantation of guide cannulas

For icv infusions, a 12 mm long 21-G guide cannula was stereotaxically placed 2 mm above the lateral ventricle. For local infusions, 12-mm long 23-G guide cannulas were implanted bilaterally 2 mm above the left and right MeA or the PVN. The cannulas were fixed to two stainless steel screws using dental cement. Rats were housed singly after surgery, allowed to recover for at least 5 days and handled daily to habituate them to the infusion procedures and to minimize non-specific stress responses at the day of experiment. All guide cannulas were closed using a stylet, which was cleaned daily during the handling procedure with 70 % ethanol.

2.2.3 Implantation of a microdialysis probe

A U-shaped microdialysis probe (self-made, for details see (Neumann *et al.*, 1993b; Horn & Engelmann, 2001)) with a molecular cut-off of 18 kDa was implanted unilaterally into the PVN. The implant was anchored to two stainless steel screws using dental cement. Following surgery, animals were single-housed and allowed to recover for 48 h and handled trice the day after surgery to habituate to the microdialysis procedure.

2.2.4 Implantation of jugular vein catheter

Under urethane anesthesia and using sterile procedures, rats expressing hM3Dq-mCherry selectively under the control of the OXT promoter within the hypothalamic PVN, SON and AN were implanted with a jugular vein catheter 19 days following viral infusion as previously described (Neumann *et al.*, 1998; Nyuyki *et al.*, 2012). Briefly, the jugular vein catheter consisted of a 13-cm piece of PE-20 tubing (ID: 0.58 mm, OD: 0.96 mm) and a 4.3-cm piece of silicone tubing (ID: 0.64 mm, OD: 1.19 mm). One end of the silicone tubing was expanded by dipping in chloroform for 15 s to facilitate insertion of the PE-20 tubing with an overlap of 1 cm. The free end of the silicone tubing was cut to an angle of 45° to allow easy insertion into the jugular vein. The catheter was stored under aseptic conditions in 70% ethanol. Before surgery, catheters were repeatedly flushed with sterile saline to remove remaining ethanol and were filled with heparinized saline. Next, a longitudinal skin incision of about 1 cm was made above the right clavicle and the jugular vein was exposed. Then, two nylon sutures were placed underneath the vein. One suture was tightly knotted cranially to occlude the vein and interrupt blood flow, while the caudal suture remained untied. Following V-like incision into the wall of the vein between both ligatures, the catheter with silicone tubing first was inserted 3.3 cm into the vessel in order to reach the right atrium. Subsequently, the catheter was filled with sterile saline and the caudal suture was repeatedly knotted on top of the silicone-PE-20 tubing overlap and the free ends of the sutures were cut off. Then, the catheter was exteriorized in the neck and the wound was sutured using sterile nylon material.

2.3 Drug infusion in conscious rats

For icv or intra-PVN infusions, the dummy cannula was replaced by the infusion cannula (icv: 25 G, 14.7 mm, intra-PVN: 27 G, 14 mm). All intracerebrally infused drugs were diluted in Ringer's solution (B. BRAUN Melsungen AG) from highly concentrated stock solutions on the

day of experiment. Sterile Ringer's solution was infused as control (vehicle, Veh). After each infusion, the cannula was kept in place for 10 s to allow local substance diffusion. None of the drug-infused rats showed any signs of tremor, convulsions, or wet-dog shakes in their homecage.

2.4 Experimental design - Chapter I

Retrograde tracing of NPS-immunoreactive neurons

In order to test whether LC-NPS neurons project towards the hypothalamic PVN, 0.5 µl of Cholera toxin subunit B coupled to Alexa Fluor 488 (CTB-488, ThermoScientific, 5 µg/µl PBS, pH 7.4) were infused bilaterally into the PVN under isofluran anesthesia via 30-G infusion cannula, which was connected via polyethylene tubing to a 5-µl Hamilton microsyringe. Following infusion, infusion system was kept in place for 3 min to ensure adequate tracer diffusion from the infusion tip. Next, animals were housed singly in observation cages. Five days later, animals were transcardially perfused and neurons immunoreactive for CTB-488, OXT, and NPS were analyzed (for details see 2.9 Immunofluorescent staining).

Fluorescence-activated cell sorting

In order to examine NPSR expression in OXT neurons, fluorescence-activated cell sorting (FACS) was performed in combination with quantitative RT-PCR. Rats were infused with cell-type specific rAAV into the SON and PVN to express Venus in OXT neurons (Knobloch et al., 2012). Three weeks later, the rats were killed by overdose of halothane, their brains were extracted, sectioned by large pieces, using rat brain matrix (1-mm thick sections). SON and PVN were bilaterally extracted by micro-punch technique.

FACS method of neuronal cells was modified from established protocol (Lobo *et al.*, 2006; Guez-Barber *et al.*, 2012). The tissue was placed in 1 ml of dissection buffer (in mM: sucrose (150), NaCl (125), KCl (3.5), NaH_2PO_4 (1.2), $CaCl_2$ (2.4), $MgCl_2$ (1.3), glucose (6.65 mM), and HEPES (2), pH 6.9, osmolarity (326), all from Sigma) (Li *et al.*, 2015) and minced with razor blades on an ice-cold glass plate. Later, dissection buffer was replaced with 1 ml of Accutase (Sigma-Aldrich, A6964) and tubes were rotated for 30 min at 4°C. Then, tissue pieces were rinsed twice in ice-cold Neurobasal-A complete medium: 50% Neurobasal-A, 50% Leibovitz L-

15 Medium (31415, Gibco), 2% B27 supplement (17504044, Invitrogen), DNase I 0.001%, 0.5% penicillin-streptomycin (15140122, Invitrogen). To dissociate the cells, tissue pieces were triturated in 1 ml Neurobasal-A complete medium with a Pasteur pipette. Supernatant containing cloudy dissociated cells were transferred to a new 15 ml Falcon tube on ice. Cells were filtered with 70-µm cell strainer and centrifuged for 3 min at 430*g* through a three-step density gradient of Percoll (P1644, Sigma). Cells at the bottom layer were collected for later use. For FACS of OT-Venus^{+} cells, propidium iodide (PI; 20 µg ml^{-1}) was used to label dead cells just before sorting. Negative controls were done at the same time. Subsequently, FACS-based purifications of Venus^{+}PI^{-} and Venus^{-}PI^{-} cells were sorted into RNase-free tubes with RNA extraction lysis buffer by BD FACSAria II at Flow Cytometry Core Facility at DKFZ.

Next, total RNAs were extracted and purified from FACS-sorted cells with the RNeasy Mini kit or RNeasy FFPE Kit (Qiagen). RNA was transcribed into cDNA using random primers (dN6, Roche) and M-MLV reverse transcriptase (Promega). cDNA were quantified by using SYBR gene expression assays (Qiagen) or Taqman Probe with Absolute Blue qPCR Rox mix (ThermoFisher Scientific), on the CFX96 Real-time System (Biorad). Primers and Probes used for qRT-PCR are listed below (table 2).

NPSR primer/probe	5' – 3` Sequence
NPSR (forward)	TCCAATGGTGAGGTACAGTGC
NPSR (reverse)	ACACCAGAAAGGCAACGATG
Beta actin (forward)	TCCTGTGGCATCCATGAAAC
Beta actin (reverse)	ACAGCACTGTGTTGGCATAG

Table 2: List of NPSR primers used for mRNA expression studies in rats.

Immunofluorescent staining of NPSR

Localization patterns of NPSR on PVN-OXT neurons was verified in perfused brains of naïve rats by immunofluorescent staining of NPSR and OXT (for detailed immunofluorescent staining see

2.9).

Characterization of NPSR knockout vs. wild type mice

NPSR mRNA expression

In order to characterize the molecular background of transgenic NPSR C57Bl/6 mice, RNA was extracted from wildtype ($NPSR^{+/+}$) and knockout ($NPSR^{-/-}$) mouse tissue micropunches (1 mm in diameter) containing the PVN using the isolation kit peqGOLD TriFast (Peqlab, Erlangen, Germany). First, tissue micropunches were homogenized in 200 µl of TriFast reagent. Next, 40 µl of chloroform were added, vortexed, and then centrifuged (20 min, 12.000 g, 4 °C). During centrifugation three phases develop from top to bottom: A colorless phase containing RNA, a middle white phase containing the DNA (with low amounts of proteins such as histones), and the bottom purple phase containing proteins. The RNA-containing phase was transferred into a new cup and the RNA precipitated with an equal volume of isopropanol overnight at -20 °C.

On the next day the samples were centrifuged (30 min, 17.000 g, 4 °C). The supernatant was discarded and the pellet was washed with ice-cold 80 % ethanol and centrifuged again (15 min, 17.000 g, 4 °C) to extract resting isopropanol, chloroform and phenol-containing TriFast. Next, 15 µl diethylpyrocarbonate-treated water (DEPC-H_2O) (Ambion, Lifetechnologies, Carlsbad, California, USA) was added to the pellet and incubated for 5 min at 70 °C and 1.000 rpm in a heating block (Eppendorf, Hamburg, Germany). Subsequently the sample was spinned down and the RNA concentration was measured using Nanodrop (NanoDrop Technologies Inc., Wilmington, Delaware, USA). For evaluation, the software ND-1000 (NanoDrop Technologies Inc., Wilmington, Delaware, USA) was used. If 260/280- and 260/230-quotients were $1.5 < x < 2$, the sample was used for reverse transcription and PCR of cDNA.

Next, RNA was reversely transcribed into cDNA. Here, 1 µg of RNA was mixed with 1 µl of Random Primers (Invitrogen, Lifetechnologies, Carlsbad, California, USA) and 1 µl of a 10-mM

dNTP mix (Invitrogen, Lifetechnologies, Carlsbad, California, USA). The sample was adjusted to a total volume of 15 µl with DEPC-H_2O. Then, the mixture was incubated for 5 min at 65 °C to guarantee the annealing of the primers. Next, 4 µl of 5x First Strand Buffer, 2 µl of 0.1 M dithiothreitol, and 40 units of RNase OUT (all from Invitrogen, Lifetechnologies, Carlsbad, California, USA) were added and incubated for 2 min at room temperature. To test contamination of genomic DNA, 5 µl of the total volume were separated (-RT sample). To the rest, 1 µl of SuperScript III (Invitrogen, Lifetechnologies, Carlsbad, California, USA) was added and incubated for 10 min at room temperature. This step is followed by an incubation at 42 °C for 50 min, which guarantees the reverse transcription and elongation. To inactivate reverse transcriptase, the sample was incubated for 15 min at 70 °C.

Next, 1 µl of cDNA (or –RT sample, or DEPC-H_2O as negative control) was mixed with 12.5 µl of DreamTAQ (Fermentas, Thermo Scientific, Waltham, MA, USA), 1 µl of 2-µM forward and 1 µl of 2-µM reverse primer (Metabion, Planegg-Martinsried, Germany), and 9.5 µl of DEPC-H_2O. All primers were designed using PerlPrimer (an open source software) and ordered from Metabion (Table 3).

	Forward primer (5'-3')	Reverse primer (5'-3')	Amplicon (bp)
NPSR	CTCTTCACTGAGGTGGGCTC	CCAGTGCTTCAGTGAACGTC	196
RPL13a	CACTCTGGAGGAGAAACGGAAGG	GCAGGCATGAGGCAAACAGTC	182

Table 3: List of primers used for mRNA expression studies in NPSR wild type and knockout mice.

PCR was performed using the ThermoCycler (BIORAD, München, Germany), starting with an initial denaturation step at 95 °C, and followed by 40 cycles consisting of denaturation at 95 °C for 30 s, primer annealing at 60 °C for 1 min, and elongation at 72 °C for 30 s. A final prolongation step at 72 °C for 10 min was added to the end of the 40^{th} cycle to ensure complete prolongation of all cDNA amplicons. Amplification products were separated by agarose gel electrophoresis at 140 V for 1 h, stained with RotiStain (Roth), and then images

were captured using ChemiDoc XRS system (Bio-Rad, München, Germany).

Genotyping of NPSR1 knockout mice

Genomic DNA was prepared from mouse brain tissue micropunches of $NPSR^{+/+}$ and $NPSR^{-/-}$ (kindly provided by Dr. Chiara Ruzza, University of Ferrara, Ferrara, Italy). Tissue was homogenized and incubated overnight in 200 µl of proteinase K lysis buffer containing KCl (50 mM), tris(hydroxymethyl)aminoethane-HCl (10 mM, pH 8.3), $MgCl_2$ (1 mM), 0.45 % Nonidet P-40, 0.45 % Tween 20, gelatin (0.1 mg/ml), and proteinase K (0.5 mg/ml) at 55 °C and 1.000 rpm with horizontal shaking conditions. Thereafter, samples were incubated for 10 min at 95°C and centrifuged for 10 min at 14.000 g, 4 °C. Two microliters of genomic DNA was added to a PCR mix containing DreamTaq PCR Master Mix (Thermo Scientific) and primers in a final concentration of 0.2 µM. The following three oligonucleotide primers were used: the forward primer was specific to the endogenous NPSR locus [5-CCTTATCCTCAAACCACGAAGTAT-3], the second was a common reverse primer [5 -GTGGGTACATGAGAAGGTTAGGAG-3], and the third was a forward primer [5-AAATGCCTGCTCTTTACTGAAGG-3] specific to the targeting plasmid. The reaction mix was placed in a thermal cycler and incubated for 5 min at 95 °C. The PCR proceeded for 40 cycles as follows: 95 °C for 30 s, 55 °C for 30 s, and 72 °C for 1 min. Additionally, samples were incubated at 72 °C for 5 min and was finally stored at 12 °C. Amplification products were separated by agarose gel electrophoresis at 140 V for 1 h, stained with RotiStain (Roth), and then images were captured using ChemiDoc XRS system (Bio-Rad, Munich, Germany).

Specificity of NPSR antibodies

In order to test the specificity of the NPSR antibody Ab2 (Leonard & Ring, 2011) and the commercially available NPSR1 antibody (abcam, ab 92425), proteins from $NPSR^{+/+}$ and $NPSR^{-/-}$ hypothalamic mouse brain tissue micropunches were isolated. Briefly, tissue was homogenized in radioimmunoprecipitation assay buffer (composed of 25 mM tris(hydroxymethyl)-

aminoethane pH 7-8, 150 mM sodium chloride, 0.1 % sodium dodecylsulfate, 0.5 % sodium deoxycholate and 1 % Triton X-100) supplemented with 0.1 M phenylmethylsulfonyl fluoride, 0.1 M sodium orthovanadate, and protease inhibitor, and incubated on ice for 30 min. After centrifugation (15 min, 14.000 g, 4°C), the supernatant was collected. The protein concentration in all samples was determined using the Pierce BCA Protein Assay Kit (Thermo Scientific, Rockford). After a 30-min incubation at 37 °C, the absorbance was measured using the microplate reader FLUOstar OPTIMA (BMG Labtech, Ortenberg, Germany) at a wavelength of 560 nm. For evaluation the software OPTIMA 1.26 (BMG Labtech, Ortenberg, Germany) was used. Next, western blot analysis was carried out in order to test the specificity of the antibodies. Thirty microgram of each protein extract was separated by sodium dodecyl sulfate-polyacrylamide gel electrophoresis. After transfer onto a nitrocellulose membrane, non-specific binding was blocked using tris(hydroxymethyl)aminoethane-buffered saline/0.1 % Tween-20 (TBS-T) supplemented with 2 % non-fat dry milk powder for 1h at room temperature and gently shaking conditions. NPSR protein was visualized by incubation with either Ab2 antibody (Leonard & Ring, 2011) or commercially available NPSR1 antibody (abcam, ab92425) over night at 4°C. Next, membranes were washed 3 x 5 min each in TBS-T, incubated in a 1:1.000 dilution of horse-radish peroxidase-conjugated anti-rabbit antibody (New England Biolabs) in TBS-T for 30 min at room temperature, washed three times, and visualized by chemiluminescence (Western Lighting, PerkinElmer). Images were acquired using ChemiDoc XRS system (Bio-Rad, Munich, Germany).

Ex-vivo Ca^{2+} imaging in PVN-OXT neurons using GCaMP6s

To examine NPS-evoked transient Ca^{2+} increase in PVN-OXT neurons, Ca^{2+} imaging in PVN-OXT neurons was carried out using ultrasensitive fluorescent proteins (GCaMP6s). 300 nl of $AAV_{1/2}$ (OXTpr-GCaMP6s) was infused bilaterally into the PVN. Hence, expression of GCaMP6s indicator was confined to OXT neurons.

Three weeks later, animals were anaesthetized using a ketamine/xylazine (Imalgene 90 mg/kg, Rompun, 10 mg/kg) mixture administered ip. Transcardial perfusion was then performed using one of the following artificial cerebrospinal fluids (ACSFs) dissection solutions. For rats between 20 and 22 weeks old, an ice-cold NMDG-based ACSF was used containing (in mM): NMDG (93), KCl (2.5), NaH_2PO_4 (1.25), $NaHCO_3$ (30), $MgSO_4$ (10), $CaCl_2$ (0.5), HEPES (20), D-Glucose (25), L ascorbic acid (5), Thiourea (2), Sodium pyruvate (3), N-acetyl-L-cysteine (10), Kynurenic acid (2). The pH was adjusted to 7.4 using HCl, after bubbling in 95% O_2-5% CO_2 gas; bubbling was maintained throughout the duration of use of the various ACSFs. Following decapitation, the brain was swiftly transferred into the same ice-cold ACSFs dissection solution as for transcardial perfusion, and 300 µm-thick coronal slices containing the PVN were obtained using a Leica VT1000s vibratome. After slicing, brain slices were placed in 35°C NMDG ACSF for 10 min. Next, brain slices were placed in a room-temperature holding chamber with normal ACSF, for a minimum of 1 hour before the conduction of any experiments. Normal ACSF, also used during experiments, was composed of (in mM): NaCl (124), KCl (2.5), NaH_2PO_4 (1.25), $NaHCO_3$ (26), $MgSO_4$ (2), $CaCl_2$ (2), D-Glucose (15), adjusted for pH values of 7.4 with HCl and continuously bubbled in 95% O_2-5% CO_2 gas. All ACSFs were checked for osmolarity and kept for values between 300-310 mOsm/l. In Ca^{2+} imaging experiments, slices were transferred from the holding chamber to an immersion recording chamber and superfused at a rate of 2 ml/min with normal ACSF unless indicated otherwise.

Spinning disk confocal microscope used to perform OXT neuron Ca^{2+} imaging was composed of a Zeiss Axio examiner microscope with a 20x water immersion objective (numerical aperture of 1.0), mounted with a X-Light Confocal unit – CRESTOPT spinning disk. Images were acquired at 5Hz with an optiMOS sCMOS camera (Qimaging, BC, Canada). Cells within a confocal plane were illuminated for 100 to 150 ms for each wavelength (GCaMP6s: 475 nm) using a Spectra 7 LUMENCOR. The different hardware elements were synchronized through the MetaFluor software, which was also used for online and offline quantitative fluorescence analysis.

OXT neuron calcium levels were measured in hand drawn regions of interest (ROIs) comprising the cell body. $[Ca^{2+}]_i$ variation were estimated as changes in fluorescence signals over the baseline (ΔF/F) after drug applications. NPS (2 µM, Bachem) and SHA-68 (NPSR antagonist, 100 µM, Tocris) were bath applied during 20 s and > 15 min, respectively. Baseline was established for each ROI as the average fluorescence over all pictures. Bleaching was corrected using a linear regression on the overall ΔF/F trace for each OXT neurons, which values were then subtracted to the ΔF/F. Upon extraction of data, calculations and corrections of ΔF/F for each neuron, the area under the curve (AUC) was calculated over a time period of 5 min before and after drug application. An OXT neuron was considered as being responsive if the relative ratio of AUCs after drug/light application over baseline was 20% greater than in baseline conditions. The relative AUCs ratios values were used for quantitative analysis and called "relative AUC ratio". Maximal peak reached after drug application was also measured in responsive cells and used in quantitative analysis. Data were averaged across OXT neurons per slices, which were used as the statistical unit over a minimum of 3 animals per condition. Image J software was also used on GCaMP6s pictures to produce illustrative pictures such as the one in Fig. 2. All calcium imaging experiments were conducted at conditioned room temperature of 22°C.

Monitoring of intra-PVN release of OXT

To analyze NPS-induced OXT release, a microdialysis probe (U-shaped, molecular cut-off of 18 kDa, for details see (Neumann *et al.*, 1993b; Bosch *et al.*, 2005)) was implanted into the right PVN and a guide cannula (21 G, 12 mm) was stereotaxically placed 2 mm above the left lateral ventricle. Following surgery, animals were allowed to recover for 48 h and handled trice a day to habituate to the microdialysis and the infusion procedure. Microdialysis probes were connected to a syringe mounted onto a microinfusion pump via polyethylene tubing and perfused with sterile Ringer's solution (3.3 µl/min) starting at 8:00 a.m. for 2 h before the start of the experiment to establish equilibrium between inside and outside of the microdialysis membrane. Then, five consecutive 30-min dialysates were collected: samples 1 and 2 were

taken under basal conditions and sample 3, 4 and 5 after icv infusion of either NPS (1 or 5 nmol / 5µl) or Veh (5 µl). The outflow of the microdialysis probe was equipped with a tube holder that allowed direct sample collection into a 1.5-ml Eppendorf tube containing 10 µl of 0.1 M HCl. Following this, samples were immediately frozen on dry ice, and subsequently stored at -20 °C until quantification of OXT. OXT content was measured in evaporated dialysates by a highly sensitive and selective radioimmunoassay (detection limit 0.1 pg per sample, cross-reactivity of the antisera with other related peptides was <7%, for details see (Landgraf *et al.*, 1995; de Jong *et al.*, 2015)).

Pharmacological inhibition of the OXTR system

In order to analyze the behavioral importance of the OXT receptor (OXTR) system on NPS-evoked anxiolysis, guide cannulas were implanted 2 mm above the lateral ventricle for icv infusion or the PVN for intra-PVN infusions, respectively. For evaluation of the local effect of the OXT receptor antagonist (OXTR-A) des-Gly-NH_2,d$(CH_2)_5$[Tyr(Me)^2,Thr^4]OVT (Manning *et al.*, 2012) on NPS-induced anxiolysis, four groups of conscious rats were studied, which received either Veh/Veh, Veh/NPS, OXTR-A/Veh or OXTR-A/NPS with a 5-min interval. The infused dose of the OXTR-A (icv: 0.75 µg / 5 µl; intra-PVN: 0.15 µg / 0.5 µl) was selected on the basis of earlier experiments (Lukas *et al.*, 2013). NPS was infused icv (1 nmol / 5 µl) or intra-PVN (0.2 nmol / 0.5 µl); controls were infused with an equal volume of sterile Ringer's solution (Veh). Next, anxiety-related behavior was tested using the LDB and the OF (for details see 2.7) 15 min after last intracerebral infusion.

Chemogenetic silencing of PVN-OXT neurons

To verify the behavioral relevance of NPS-evoked activation of OXT neurons, 0.3 µl of $AAV_{1/2}$ OXTpr-hM4Di:mCherry was bilaterally microinfused into the PVN, and an icv guide cannula was implanted as described above. Three weeks later, the designer receptor hM4Di was activated

by ip injection of CNO (2 mg/kg); controls received 1 ml/kg of sterile phosphate-buffered saline (PBS, pH 7.4). NPS (1 nmol) or Veh (5 µl) were infused icv 40 min later. Testing on the EPM (for details see 2.7.3) was carried out 15 min after intracerebral infusion. Expression of OXTpr-hM4Di:mCherry was verified in perfused brains by immunofluorescent staining of mCherry and OXT (for details see 2.9).

2.5 Experimental design - Chapter II

Bilateral infusion of NPS into the MeA on anxiety-related behavior

To examine the effect of a subsequent intra-MeA infusion of NPS on anxiety-related behavior, adult male Wistar rats were infused with NPS (Bachem, H-6164) at 0.2 nmol / 0.5 µl or 0.5 µl of sterile Ringer's solution as control (Veh) per hemisphere using a 14-mm long 27-G infusion cannula. Behavioral assessment was performed 15 min after the last intracerebral infusion using the EPM and the OF (for details see 2.7).

Effects of icv NPS on Ca^{2+}/calmodulin-dependent kinases and ERK1/2 in the amygdala

In order to assess NPS-induced activation of intracellular signaling pathways, rats were infused icv with either NPS (1 nmol / 5 µl) or Veh (5 µl) using a 14.7-mm long 25-G infusion system. Animals were sacrificed by rapid decapitation 15 min after drug infusion, brains were removed and amygdala tissue was harvested using a 2 mm-wide micropuncher accordant to the brain atlas. The cytoplasmic and nuclear proteins from amygdala tissue micropunches were extracted consecutively using a protein extraction kit (Cat No. 40010, Active Motif, Rixensart, Belgium). In detail, tissue micropunches were homogenized in 1x hypotonic buffer consisting of PBS, hypotonic buffer, phosphatase and protease inhibitors for 15 min on ice. Following centrifugation for 10 min at 3.200 rpm and 4 °C, the supernatant containing cytoplasmic proteins was collected and transferred into a pre-chilled cup. The remaining pellet was washed once with ice-cold PBS to wash away any remaining cytoplasmic proteins. Subsequently the pellet was re-suspended in complete lysis buffer, supplemented with dithiothreitol, and phosphatase and protease inhibitors. The samples were incubated on ice for 30 min, vortexed, and centrifuged for 10 min at 13.000 rpm and 4 °C. Then, the supernatant containing nuclear proteins was collected. The protein concentration was determined using the Pierce BCA Protein Assay Kit (Thermo Scientific, Cat No. 23225). Thirty micrograms of each cytosolic

protein extract were separated by sodium dodecyl sulfate-polyacrylamide gel electrophoresis. After transfer onto a nitrocellulose membrane, non-specific binding was blocked using TBS-T supplemented with non-fat milk powder (2% for (p)CaMKII) or bovine serum albumin (5% for (p)ERK1/2) for 1h at room temperature and gently shaking conditions. (p)CaMKII and (p)ERK1/2 levels were visualized by incubation with respective antibodies against either pCaMKII (1:500, Thr286, Santa Cruz Biotechnology, sc-12886-R) or pERK1/2 (1:1.000, Cell Signaling Technology, #8544S) over night at 4°C. Thereafter, the membranes were washed three times for 5 min each in TBS-T, incubated in a 1:1.000 dilution of horseradish peroxidase-conjugated anti-rabbit antibody (Cell Signaling Technology, #7074) in TBS-T for 30 min at room temperature, washed three times, and visualized by chemiluminescence using ECL Detection Reagent (Amersham Biosciences). Images were acquired using ChemiDoc XRS+ system (BIORAD, Germany) and evaluated using ImageLab software (BIORAD). After imaging, immunocomplexes were removed from the blot with Re-Blot Plus Solution (Millipore), probed with anti-total CaMKII (1:500, Santa Cruz Biotechnology, sc-13082) or ERK1/2 (1:1.000, Cell Signaling Technology, #4695S), and imaged as described above. *beta*-tubulin was used as a loading control (1:1.000, Cell Signaling Technology, #2146).

Effect of simultaneous blockade of both phospholipase C and adenylyl cyclase on NPS-induced anxiolysis

In order to reveal the relevance of the NPSR-mediated phospholipase C (PLC) and adenylyl cyclase (AC) activation on NPS-induced anxiolysis, PLC and AC were blocked simultaneously by infusion of an inhibitor-cocktail (Inh) composed of the AC inhibitor 2',5'-dideoxydenosine (DDA, EnzoLifeScience, BML-CN110) and the PLC inhibitor U73122 (EnzoLifeScience, BML-ST391). The infused dose of DDA (12.5 nmol) and U73122 (0.5 nmol) was selected on the basis of previous *in vitro* studies and their half-maximal inhibitory dose (for details see (Holgate *et al.*, 1980; Smallridge *et al.*, 1992; Ogawa *et al.*, 1995; Feisst *et al.*, 2005)). As DDA and U73122 stocks were diluted in dimethyl sulfoxide (DMSO, Merck), Veh_1 was composed of 20 % DMSO

and 80 % Ringer's solution; Veh_2 was composed of Ringer's solution. Consequently, 4 groups of conscious rats received the following two subsequent intra-MeA infusions of Veh_1/Veh_2, Veh_1/NPS, Inh/Veh_2 or Inh/NPS with a 20-min interval between infusions. Next, anxiety-related behavior was assessed 15 min after the last intracerebral infusion using the EPM and the OF (for details see 2.7).

Specific effects of blockade of either PLC or the AC signaling on NPSR-mediated anxiolysis in the MeA

To assess whether the anxiolytic activity of NPS is mediated via the NPSR-evoked activation of PLC or AC or via both signaling pathways within the MeA, U73122 (0.5 nmol), DDA (12.5 nmol), or Veh_1 were separately infused bilaterally 20 min prior to NPS or Veh_2 infusion into the MeA. Then, anxiety-related behavior was assessed using the EPM and the OF (for details see 2.7) 15 min after the last drug infusion.

2.6 Experimental design - Chapter III

Monitoring of chemogenetically induced intracerebral OXT-release

In order to analyze OXT release as a consequence of chemogenetic activation of OXT neurons, rats were implanted with a U-shaped microdialysis probe into PVN or lateral septum, respectively, 19 days following infusion of $AAV_{1/2}$OXTpr-hM3Dq:mCherry into either PVN or PVN, SON and AN.

To monitor OXT release within the PVN of conscious rats, the microdialysis probes were connected to a syringe mounted onto a microinfusion pump via polyethylene tubing and perfused with sterile Ringer's solution (3.3 µl ⁄ min) starting at 8:00 a.m. for 2 h before the start of the experiment to establish equilibrium between inside and outside of the microdialysis membrane two days after surgery. Five consecutive 30-min dialysates were collected on both experimental day 1 and day 2. On day 1, samples 1 and 2 were taken before, and sample 3, 4 and 5 after ip injection of CNO (2 mg/kg) or sterile PBS as control. On day 2, sample 1 was taken before, and samples 2 and 3 after ip injection of CNO or control. Thereafter, rats were exposed to 5-min forced swim stress (water temperature 22-24°C), and samples 4 and 5 were collected. The outflow of the microdialysis probe was equipped with a tube holder that allowed direct sample collection into a 1.5-ml Eppendorf tube containing 10 µl of 0.1 M HCl.

To monitor OXT release within the lateral septum of urethane-anesthetized rats expressing an excitatory DREADD selectively under the control of an OXT promoter fragment in PVN, SON and AN, the microdialysis procedure was performed as described above. Here, five consecutive 30-min dialysates were collected: samples 1 and 2 were taken before, and sample 3, 4 and 5 after ip injection of CNO (2 mg/kg) or sterile PBS as control.

All dialysates were immediately frozen on dry ice and subsequently stored at -80 °C until

quantification of OXT by radioimmunoassay. Expression of OXTpr-hM3Dq:mCherry was verified in perfused brains by immunofluorescent staining of mCherry and OXT (for details see 2.9).

Monitoring of chemogenetically induced peripheral OXT-release

To monitor peripheral OXT release, blood samples were taken via jugular vein catheter. The catheters were connected to a 1-ml plastic syringe filled with sterile heparinized saline (30 IU/ml, Heparin-Natrium, Ratiopharm, Ulm, Germany), and the rats were then placed on a heating plate to maintain homeostasis of body temperature. 45 min before and after ip injection of CNO or PBS, 500 µl of blood was taken. The same volume of blood was replaced with sterile saline before the PE-20 tubing was filled with heparinized saline again. All blood samples were collected on ice in EDTA-coated tubes (Bayer AG, Leverkusen, Germany) and centrifuged (13.000 rpm, 10 min, 4 °C). 200 µl of plasma samples were separated and stored at -80 °C until quantification of OXT.

Behavioral consequences induced by chemogenetic activation of the endogenous OXT system

In a separate cohort, the consequence of increased intracerebral OXT-release on anxiety-related behavior was tested in the LDB 55 min after CNO injection (for details see 2.7.1). During ongoing microdialysis on day 1, an experimenter blind to treatment analyzed food and water intake, sleep, exploration and self-grooming every fifth minute.

Effects of chemogenetic activation of the PVN-OXT system on ethanol intoxication

Icv infusion of 1 µg of OXT attenuates locomotor impairments induced by ethanol intoxication (Bowen *et al.*, 2015). Herein, I tested whether chemogenetic activation of the endogenous PVN-OXT system inhibits ethanol-induced ataxia. Briefly, to evoke endogenous OXT-release, hM3Dq, an activating designer receptor, was expressed selectively under the control of an OXT

promoter fragment in PVN-OXT neurons. Conscious rats were injected ip with CNO (2 mg/kg) or PBS as control (Veh) 21 days following intra-PVN infusion of $AAV_{1/2}$OXTpr-hM3Dq:mCherry. Thirty minutes later, animals were injected either with ethanol (1.5 g/kg, 15% wt/vol) or PBS. Five minutes after the last drug infusion, animals underwent the wire-hanging test and the rightning-reflex test as described in detail below. Both tests were repeated 30 min later.

Wire-hanging test

The wire-hanging test is sensitive to ethanol-induced locomotor impairments, such as reduced muscle strength (Shukitt-Hale *et al.*, 1998; Crabbe *et al.*, 2003; Boyce-Rustay & Holmes, 2006). First, animals were placed on a standard cage grid. An experimenter softly shakes the platform horizontally for 4 times and then the platform is inverted at a height of 80 cm above a box filled with bedding to avoid injuries to the rat from the fall. The duration the rat spent hanging at the cage grid is indicative for the degree of locomotor impairments due to ethanol intoxication. Each trial was recorded, evaluated using Final Cut Pro (Apple, California, USA) and an average time of the three consecutive trials were used for statistical analysis.

Righting-reflex test

The righting-reflex test is used to investigate motor coordination and sedation in ethanol-intoxicated animals (Little *et al.*, 1996). Briefly, rats were placed on a table and turned on their back by an experimenter. The latency to right all four paws on the ground after release by the experimenter was recorded. The rightning-reflex test was performed immediately after the wire-hanging test on each of the three consecutive trials and evaluated using Final Cut Pro (Apple, California, USA). The average of three trials at each time point was used for statistical analysis.

2.7 Anxiety-related behavior

Following the respective treatment, the anxiety-related behavior was assessed using the LDB, OF, and the EPM. Basically, these tests generate a natural conflict between the explorative drive and the innate fear of open, lit and exposed areas. The more anxious an animal is, the less time it spends in bright, potentially unsecure areas and vice versa.

2.7.1 Light-dark box

In detail, the LDB setup consisted of two compartments (one lit compartment (40 x 50 cm, 100 lux; light box) and one dark compartment (40 x 30 cm, 0 lux)). Each compartment was connected via a small opening (7.5 x 7.5 cm) enabling transition between the two floors. Rats were placed in the light compartment after the last drug infusion for 5 min, and the time spent in the light box and numbers of entries into the light box were taken as measurements for anxiety-related behavior. LDB testing was analyzed using an automated video tracking system (Noldus, EthoVision X7, Netherlands).

2.7.2 Open field

For the OF, rats were placed in the center of the box (80 x 80 x 40 cm, 140 lux) and were allowed to freely explore the arena during a 5-min test. The time the animals spent in the center zone (40 x 40 cm), the number of center zone entries and the travelled distance as an indicator of locomotor activity were assessed on video recordings using EthoVision X7.

2.7.3 Elevated plus maze

Five-minute testing on the EPM was performed on a plus-shaped maze, which was elevated (70 cm) from the floor and consisted of two closed arms (50 x 10 cm, 10 lux) and two open

arms (50 x 10 cm, 40-50 lux) separated by a central neutral zone (10 x 10 cm). A camera above the maze enabled video recordings and subsequent assessment of behavior. The test started by placing the animal in the neutral zone facing a closed arm. The percentage time spent on the open versus all arms, as an indicator of anxiety-related behavior, was determined by an observer blind to treatment. The number of closed arm entries was used as an indicator of locomotor activity.

2.8 Verification of cannula and microdialysis probe placement

After the behavioral experiments, animals were sacrificed by CO_2 and rapidly decapitated, brains were snap-frozen in pre-chilled N-methylbutane on dry ice, and the placement of microdialysis probes and cannulas was verified on 40-µm thick Nissl-stained coronal cryosections according to brain atlas. Only animals with correctly positioned probes and cannulas were included for statistical analyses.

2.9 Immunofluorescent staining

In order to analyze retrogradely labeled neurons, to localize NPSR protein expression in PVN-OXT neurons and to verify successful DREADD expression (hM3Dq or hM4Di, respectively) within the PVN, rats were deeply anesthetized with Xylazin (2%, 0.5 ml/kg, Bernburg) and Ketamine (10%, 1 ml/kg, WDT), and perfused transcardially with 100 ml of 0.01 M PBS (pH 7.4) and 300 ml of PBS supplemented with 4 % paraformaldehyde. Next, brains were removed and post-fixed overnight at 4 °C in paraformaldehyde solution (4 %), cryo-protected in 30 % sucrose for 3 days at 4 °C, and snap-frozen in N-methylbutane cooled by dry ice.

Coronal brain slices (40 µm) containing the PVN or the LC were collected, washed 3 x 5 min in PBS supplemented with 0.3 % Triton-X (PBS-T), and were blocked in PBS-T supplemented with

1 % bovine serum albumine for 1h at room temperature (RT). Brain slices were incubated with primary antibodies (summarized in table 4) overnight at 4 °C, then rinsed 3 x 10 min with PBS-T and incubated with the corresponding AlexaFluor 488- or AlexaFluor 594-coupled secondary antibody (1:1.000, 2h, RT, Lifetechnologies), washed again in PBS-T, and mounted with Vectashield Hard Set Mounting Medium (Vector Labs) onto SuperFrost object slides.

Antibody	Host	Dilution	Origin
mCherry	Rabbit polyclonal	1:1.000	Abcam, ab167453
OXT	Mouse monoclonal	1:500	(Ben-Barak *et al.*, 1985)
NPS	Rabbit polyclonal	1:500	Abcam, ab18252
NPSR	Rabbit polyclonal	1:1.000	(Leonard & Ring, 2011)

Table 4: List of antibodies used for immunofluorescent protein labeling.

Images were acquired using Leica DM5000B and Leica TCS SP8 microscope. Digitized images were analyzed using FIJI (NIMH, Bethesda, MD, USA).

Pre-incubation of the OXT antibody with the sister-nonapeptide vasopressin had no effect on immunoreactivity, further demonstrating the specificity of the antibody (see also (Ben-Barak et al., 1985)).

2.10 Statistical analysis

Two-tailed *t*-test or non-parametric Mann-Whitney U-test was used in order to evaluate FACS analysis, to analyze differences of a single drug treatment on a specific selected behavior according to the experimental protocol, and to evaluate Western blot data.

In experiments designed out of four groups, anxiety-related behavior was analyzed using a two-way analysis of variance (ANOVA, factors treatment 1 x treatment 2). OXT content in microdialysates and plasma, and behavioral evaluation during ongoing microdialysis was analyzed using two-way ANOVA with repeated measures (factor time x treatment). Any overall statistical differences, which were set at $p < 0.05$, were further analyzed using Tukey´s post-hoc test.

Data are expressed as group mean + SEM. Statistical analyses were performed using SigmaPlot 13 (Systat).

3 Results

Chapter I – NPS evokes anxiolysis by acting on paraventricular OXT neurons

The results of Chapter 1 have been submitted to the *Journal of Physiology* on 6th of June 2017.

Grund, T., Goyon, S., Charlet, A., Grinevich, V., Neumann, I.D. (submitted) At the core of neuropeptidergic modulation of anxiety: Activation of oxytocin neurons by neuropeptide S.
Journal of Physiology

1. LC-NPS afferents towards the hypothalamic PVN

To examine whether NPS neurons located in the LC innervate the PVN, the retrograde tracer cholera toxin subunit B conjugated to Alexa Fluor-488 (CTB-488) was infused bilaterally into the PVN of male rats. Five days later, this tracing resulted in dense labeling of NPS-immunoreactive neurons throughout the LC, indicating prominent LC-PVN afferents to the PVN (Fig. 5).

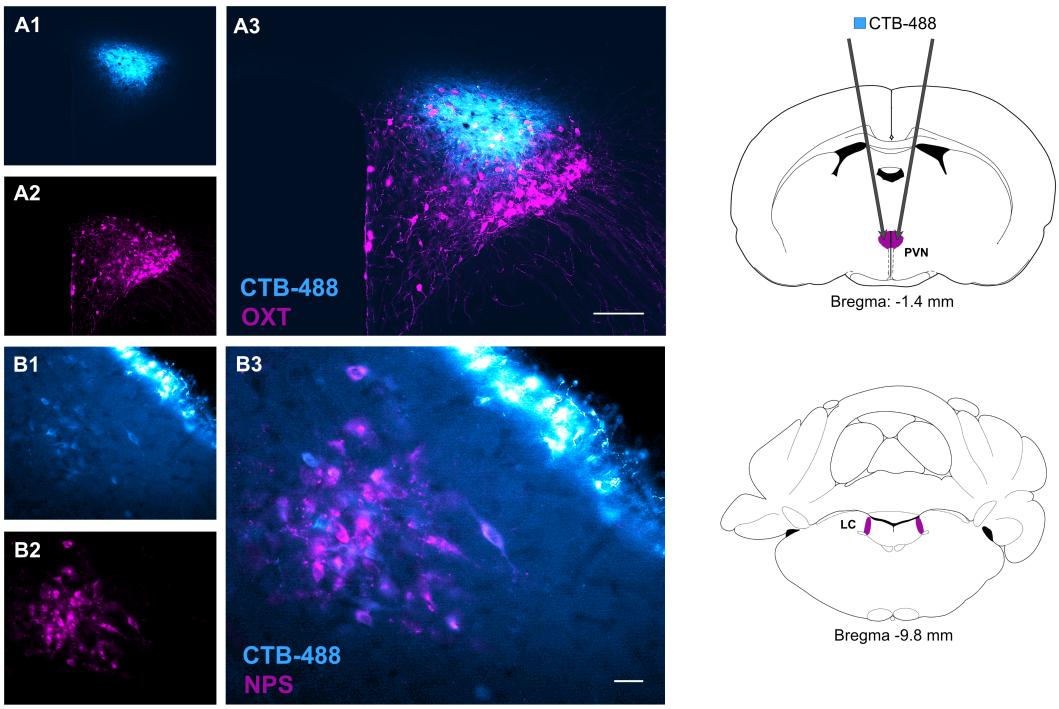

Figure 5: Retrograde tracing of NPS neurons innervating the hypothalamic PVN. A) OXT-immunoreactive neurons demonstrate correct intra-PVN infusion site of cholera toxin subunit B conjugated to Alexa Fluor-488 (CTB-488). B) Five days following intra-PVN infusion of the tracer, retrogradely transported CTB-488 labeled neurons immunoreactive for NPS in the LC. Scale bar: A3=100 µm, B3=30 µm. Right site: Schematic drawing of the bilateral intra-PVN infusion sites of CTB-488 and pericoerulear region harboring NPS-immunoreactive neurons.

2. PVN-OXT neurons express NPSR

Declaration: FACS analysis was performed in collaboration with Valery Grinevich, Marina Eliava, Haikun Liu, and Yuting Li (DKFZ, University of Heidelberg, Germany). Chiara Ruzza and Girolamo Calo (University of Ferrara, Italy) kindly provided frozen brains from wild type and NPSR knockout mice.

NPSR expression has been described in the rat PVN (Xu et al., 2007). Thus, I specifically investigated NPSR expression in PVN-OXT neurons. In the absence of a specific NPSR antibody (Slattery *et al.*, 2015), I performed FACS analysis in extracted PVN samples 3 weeks after

bilateral intra-PVN infusion of a cell-type specific rAAV expressing Venus selectively under the control of an OXT promoter fragment ($AAV_{1/2}$(OXTpr-Venus)). Hence, Venus expression was confined to PVN-OXT neurons (Knobloch *et al.*, 2012). FACS analysis of viable cells in combination with quantitative RT-PCR revealed that NPSR mRNA was predominantly expressed in Venus$^+$ neurons, whereas NPSR expression in Venus$^-$ cells was almost negligible (Fig. 6).

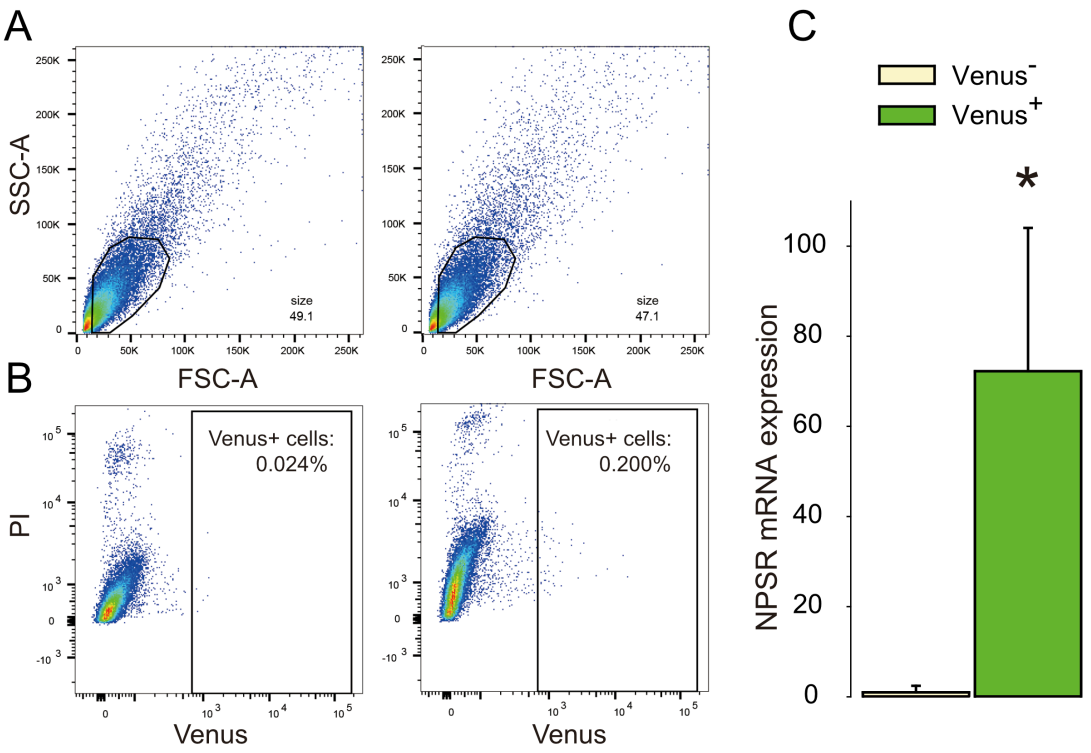

Figure 6: OXT neurons within the hypothalamic PVN express NPSR mRNA. FACS plots indicate that cells were sorted by A) size via side- (SSC) and forward-scattered light (FSC) and B) fluorescence intensity in living cells negative for propidium iodide (PI). C) qRT-PCR of reversely transcribed RNA isolated from sorted viable cells demonstrated prominent NPSR mRNA expression in Venus$^+$ neurons, whereas NPSR mRNA expression in Venus$^-$ cells was almost negligible. Data represent mean + SEM. *p<0.05.

To investigate the localization of the NPSR within the PVN at protein level, I performed an immunofluorescent staining of both NPSR and OXT. NPSR immunoreactivity using Ab2 (Leonard & Ring, 2011) was mostly somatic and punctuate, suggesting vesicular and membrane microdomain localization in OXT-immunopositive neurons (Fig. 7). Further, cellular resolution revealed few cells immunoreactive for NPSR, but not OXT, suggesting that NPSR is

not exclusively localized on PVN-OXT neurons.

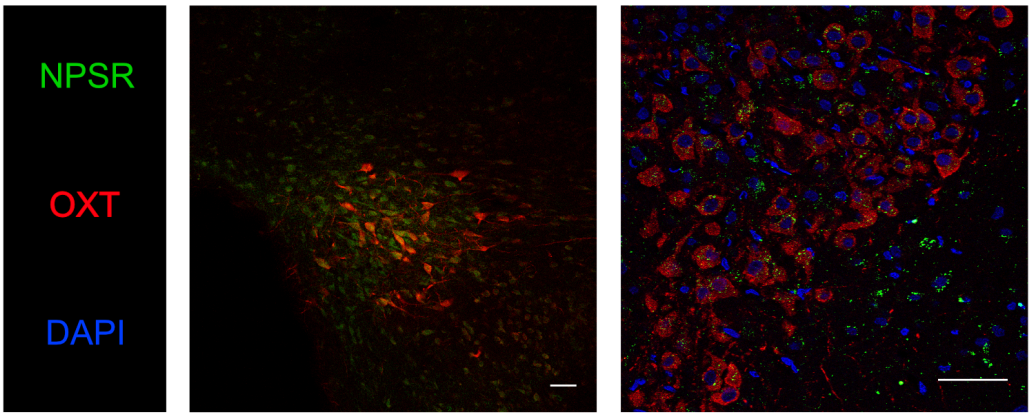

Figure 7: Immunofluorescent staining demonstrates NPSR localization on PVN-OXT neurons. Scale bar: 50 µm

Specificity of NPSR antibody Ab2 and commercially available NPSR1 antibody (ab92425) was examined using NPSR knockout and wild type hypothalamic mouse tissue micropunches. First, knockout tissue was analyzed to confirm molecular background of transgenic mice. NPSR mRNA expression was not detectable in knockout mouse tissue micropunches compared to wild type (Fig. 8). Second, genotyping of DNA indicated a PCR product of 418 bp from the homozygous wild-type mice ($NPSR^{+/+}$) and a 599-bp DNA fragment was amplified from homozygous knockout mice ($NPSR^{-/-}$) accordant to the literature (Camarda *et al.*, 2009). More importantly, I performed western blot analysis in both knockout and wild-type tissue. Herein, a band was present at predicted size in both $NPSR^{+/+}$ and $NPSR^{-/-}$ tissue micropunches suggesting that neither NPSR1 antibody (ab92425, Fig. 8C) nor Ab2 (Fig. 8D) are specific. This important finding, which has been included in a recent manuscript (Slattery *et al.*, 2015), excluded the further use of the only available NPSR1 antibody for my future studies.

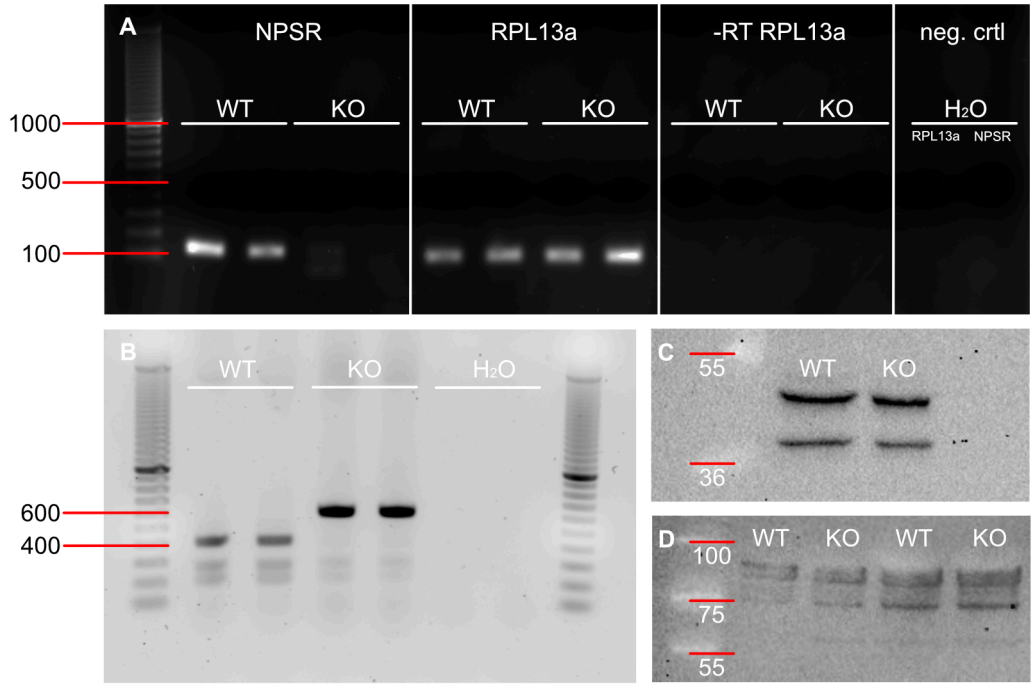

Figure 8: Unspecific binding of NPSR antibodies. A) RT-PCR demonstrates NPSR expression at mRNA (196 bp) level in $NPSR^{+/+}$ (WT), but not $NPSR^{-/-}$ (KO) hypothalamic tissue micropunches. RPL13a (182 bp) was used as reference gene. B) PCR analysis of DNA from NPSR WT and KO mice revealed a PCR product of 418 bp from the homozygous NPSR WT mice; a 599-bp DNA fragment was amplified from homozygous KO mice. Western blot analysis in NPSR WT and KO mouse hypothalamic tissue micropunches revealed bands at predicted size of NPSR protein for both C) NPSR1 antibody (abcam, ab92425) and D) Ab2 antibody.

3. NPS evokes transient Ca^{2+} influx in PVN-OXT neurons

Declaration: Ca^{2+} imaging in GCaMP6s-positive PVN-OXT neurons was performed in collaboration with Alexandre Charlet and Stephanie Goyon (University of Strasbourg, France), Valery Grinevich Grinevich and Marina Eliava (DKFZ, University of Heidelberg, Germany).

Next, I examined the hypothesis, whether NPS is capable of activating PVN-OXT neurons. To test this, I used ultrasensitive fluorescent proteins for imaging neuronal activity (Chen *et al.*, 2013). Three weeks following bilateral infusion of $AAV_{1/2}$(OXTpr-GCaMP6s) into the PVN, GCaMP6s was selectively expressed under the control of the OXT promoter fragment (Fig. 9).

Following hypothalamic slice preparation, the majority of OXT neurons were identified as constitutively silent (235/337 neurons, 69.7 %), whereas a smaller number of neurons (approximately 30 %) displayed high variability with respect to intracellular Ca^{2+} fluctuations and, thereby, were characterized as constitutively active. A subpopulation of silent OXT neurons (32/237=13.5 %) responded to NPS (2 µM for 20 s) by increased fluorescence indicative for transient rise in intracellular Ca^{2+} levels. In the presence of a selective NPSR antagonist (SHA-68, 100 µM, 30 min), NPS failed to induce any cellular response compared to baseline indicating that the NPS-induced increase in intracellular Ca^{2+} in OXT neurons is specifically mediated via the NPSR.

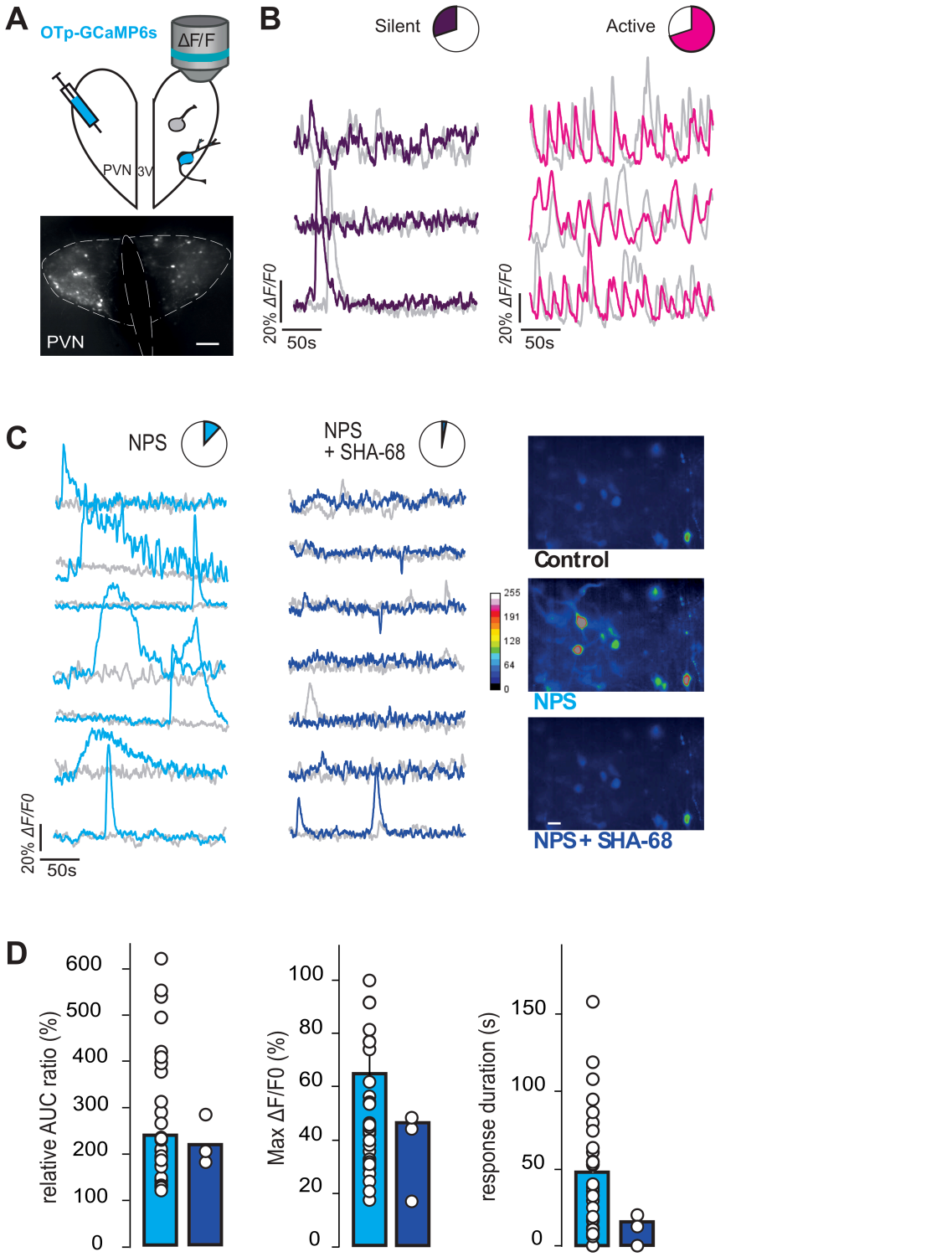

Figure 9. NPS effects on PVN-OXT neurons in hypothalamic slice preparation (A-D). A) Schematic drawing of the PVN OXTpr-GCaMP6s virus infusion and subsequent $[Ca^{2+}]_i$ imaging of OXT neurons. B) Basal activity of two distinct subpopulations of OXT neurons (silent, purple; active, pink) illustrated by typical ΔF/F traces. Pie charts show the proportion of silent (left) and active (right) OXT neurons (n slices (n_s) = 11, n OXT neurons (n_n) = 237). C) Pie charts of the proportion of responsive OXT neurons to NPS application alone (2 µM, 20s; n_s = 11, n_n = 32/237; light blue) or in presence of NPSR antagonist (SHA-68 100 µM, > 15 min; n_s = 5, n_n = 3/100; dark blue) and typical ΔF/F traces.

Pseudo-color video extract of identified OXT neurons through GCaMP6s imaging $[Ca^{2+}]_i$ either in control conditions (gray), in presence of NPS (light blue), or NPS + SHA-68 (dark blue) (stacks of 50 images/10s of recording). Scale bar: 20 µm. D) Ratio of ΔF/F AUCs, maximal peak values and response duration of OXT neurons in presence of NPS (n_s = 11, n_n = 32; light blue), or NPS + SHA-68 (n_s = 5, n_n = 3; dark blue). Only OXT neurons that responded are represented here. White circles represent individual neuron values.

4. NPS evokes release of OXT within the PVN

Declaration: Radioimmunoassay-based quantification of OXT content in microdialysates was performed by Rainer Landgraf (RIAgnosis, Sinzing, Germany).

Another indicator for a stimulated activity of OXT neurons is increased OXT release, for example within the PVN in a somato-dendritic fashion (Neumann & Landgraf, 2012), and Ca^{2+} availability, specifically an increase in intracellular Ca^{2+}, is a prerequisite for such release (Neumann *et al.*, 1993b; Fisher & Bourque, 1996; Ludwig *et al.*, 2002). Thus, I monitored OXT release within the PVN of conscious rats in response to NPS (1 nmol or 5 nmol, icv) using intracerebral microdialysis (Landgraf & Neumann, 2004). NPS dose-dependently evoked a significant rise in local OXT release (factors time x treatment; $F_{8,79}$=5.931; $p<0.001$) during the first (5 nmol, $p<0.001$ vs. vehicle (Veh)) and during the 2nd and 3rd (1 nmol, $p<0.05$ vs. Veh) 30-min dialysis period, respectively, following NPS (Fig. 10).

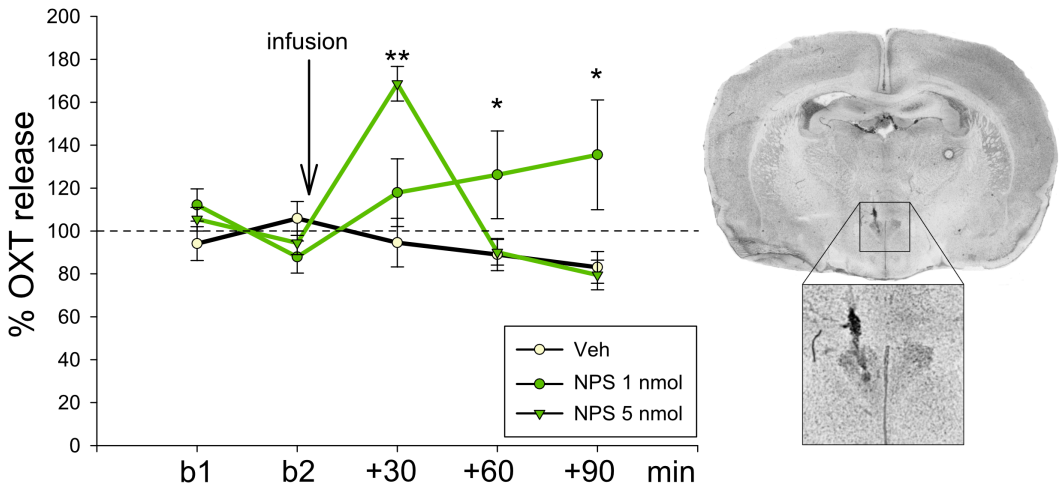

Figure 10. NPS effects on intracerebral OXT release in the PVN of conscious male rats. OXT content in 30-min microdialysates sampled within the PVN under basal conditions (b1 and b2), and after icv infusion of either Veh, or NPS (1 nmol, 5 nmol), as well as a representative microphotograph of a Nissl-stained coronal section demonstrating the placement of the microdialysis probe within the PVN. Data are expressed as percentage of baseline (mean of basal 1 and 2; =100%; dotted line) ± SEM, n=5-6. **p<0.01 vs. all; *p<0.05 vs. respective Veh.

5. Selective inhibition of OXTR and chemogenetic silencing of OXT neurons within the PVN prevent NPS-induced anxiolysis

To examine the behavioral relevance of NPS-evoked activation of OXT neurons, two strategies were employed: First, OXTRs were pharmacologically blocked by icv or intra-PVN infusion of a specific OXTR antagonist (OXTR-A, des-Gly-NH_2,d$(CH_2)_5$[Tyr(Me)^2,Thr^4]OVT) prior to icv or local infusion of NPS and behavioral testing on the light/dark box (LDB) and in the open field (OF), respectively, to assess anxiety-related behavior. Secondly, PVN-OXT neurons were chemogenetically silenced prior to icv infusion of NPS and behavioral testing on the elevated plus maze (EPM).

OXTR antagonism prevents NPS-induced anxiolysis

Pharmacological blockade of OXTR signaling by pre-infusion of a selective OXTR-A (icv: 0.75 µg, intra-PVN: 0.15 µg) 5 min prior to NPS infusion (icv: 1 nmol, intra-PVN: 0.2 nmol) prevented

NPS-induced anxiolysis in two relevant behavioral tests (Fig. 11). Specifically, comparison of the following 4 groups (Veh/Veh, Veh/NPS, OXTR-A/Veh, OXTR-A/NPS) revealed that in Veh pre-infused rats, icv NPS increased the percentage of time the rats spent in the lit compartment of the LDB ($F_{1,31}$= 4.25, p=0.049; Veh/NPS vs. Veh/Veh: p=0.006), whereas icv OXTR antagonism blocked this effect (Veh/NPS vs. OXTR-A/NPS: p=0.036). The OXTR-A alone did not affect anxiety-related behavior (OXTR-A/Veh vs. Veh/Veh: p=0.48). Neither NPS nor OXTR-A, alone or in combination, influenced the locomotor activity indicated by traveled distance ($F_{1,31}$=0.50, p=0.49). Similarly, in the OF icv NPS produced a robust anxiolytic effect as animals spent more time in the center zone ($F_{1,31}$=4.46, p=0.043; Veh/NPS vs. Veh/Veh: p=0.002). In contrast, in OXTR-A pre-infused rats, NPS failed to induce anxiolysis (OXTR-A/NPS vs. Veh/NPS: p=0.003). None of the treatments changed locomotor activity in the OF as reflected by the traveled distance ($F_{1,31}$=0.57, p=0.46).

In order to localize the effects of OXTR-A pretreatment and NPS within the PVN, local infusions were performed. In Veh-pretreated rats, local NPS exerted a robust anxiolytic effect, which was comparable to that seen after icv infusion. Pre-infusion of the OXTR-A bilaterally into the PVN prevented the anxiolytic effect of NPS infused 5 min later (Fig. 11). Specifically, in the LDB, NPS increased the time the rats spent in the lit compartment ($F_{1,41}$=6.65, p=0.014; Veh/NPS vs. Veh/Veh: p=0.003), whereas pre-infusion of OXTR-A prevented this effect (OXTR-A/Veh vs. OXTR-A/NPS: p=0.49). Neither local OXTR-A nor NPS, alone or in combination, changed the locomotor activity indicated by the distance traveled in the LDB (p=0.60). The result of local blockade of OXTR preventing the anxiolytic NPS effects within the PVN was recapitulated in the OF: in Veh-pretreated rats NPS increased the time spent in the center of the OF ($F_{1,35}$=4.17, p=0.049; Veh/NPS vs. Veh/Veh: p=0.033), whereas pre-infusion of OXTR-A prevented this anxiolytic effect (OXTR-A/Veh vs. OXTR-A/NPS: p=0.49). In the OF, NPS increased the traveled distance indicative of increased locomotor activity ($F_{1,35}$=6.82, p=0.014; Veh/NPS vs. Veh/Veh: p=0.049).

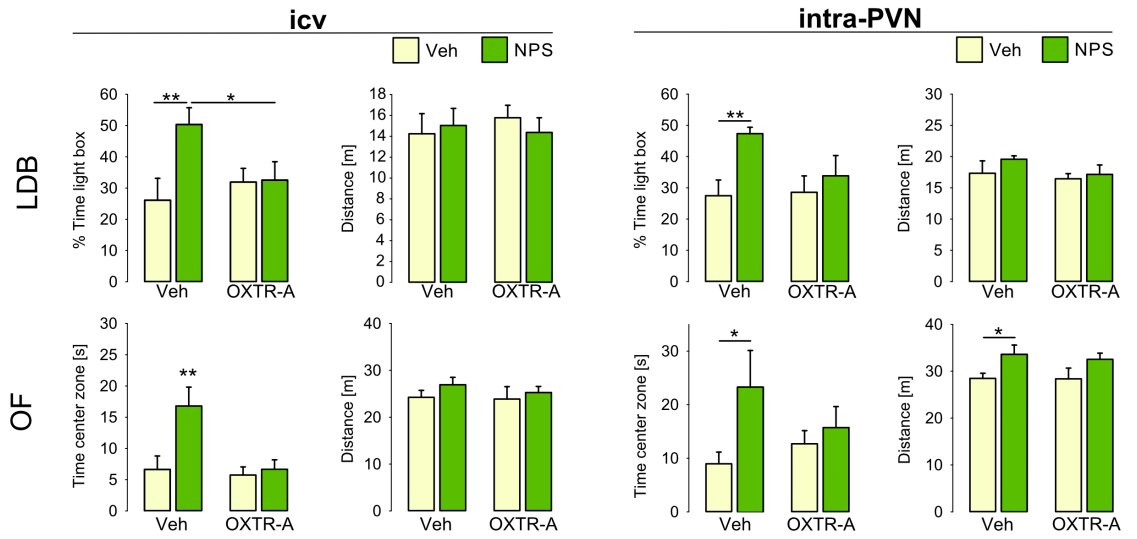

Figure 11: Icv and intra-PVN pre-infusion with an OXTR antagonist blocked NPS-induced anxiolysis. Male rats were infused with a selective OXTR antagonist (OXTR-A, icv: 0.75 µg, intra-PVN: 0.15 µg) prior to NPS infusion (icv: 1 nmol, intra-PVN: 0.2 nmol) or control (Veh). The percentage of time spent in the lit compartment of the LDB and the time spent in the center zone of the OF indicate anxiety-related behavior. Traveled distance indicates locomotor activity in each compartment. Data represent mean + SEM, group sizes: n=8-13. *p<0.05, **p<0.01 vs. all or as indicated.

Chemogenetic silencing of PVN-OXT neurons blocks NPS-evoked anxiolysis

Following intra-PVN infusion of $AAV_{1/2}$ OXTpr-hM4Di:mCherry, a G_i-coupled designer receptor (hM4Di) was expressed under the control of the OXT promoter fragment. The infusion of this rAAV into the rat PVN resulted in selective expression of hM4Di:mCherry in OXT neurons. Quantitative analysis in the PVN showed that 92.98 ± 1.35 % of mCherry-immunopositive cells (n=278) expressed OXT (94.16 ± 1.22 % of OXT-immunoreactive neurons (n=274) expressed hM4Di:mCherry), revealing an efficient and highly specific virus expression. In the presence of CNO (2 mg/kg, ip, Fig. 5), a chemically inert compound that specifically activates hM4Di, chemogenetic silencing of PVN-OXT neurons has been observed (Eliava *et al.*, 2016). Herein, in CNO-pretreated rats icv NPS (1 nmol) failed to induce anxiolysis suggesting that PVN-OXT neurons mediate NPS-induced anxiolysis. On the EPM, two-way ANOVA revealed a main effect of the first ($F_{1,31}$=6.63, p=0.016, CNO vs. PBS) and second infusion ($F_{1,31}$=7.65, p=0.010, NPS vs.

Veh). In detail, NPS increased the percentage of time spent on the open arms of the EPM in PBS-pretreated rats (PBS/NPS vs. PBS/Veh: p=0.008) indicative of an anxiolytic effect, whereas CNO-pretreatment prevented the effect of NPS (CNO/NPS vs. PBS/NPS: p=0.014; CNO/Veh vs. CNO/NPS: p=0.25). Moreover, NPS increased the percentage of open arm entries (main effect of the 1st infusion: $F_{1,35}$=11.60, p=0.002; 2nd infusion: $F_{1,31}$=10.42, p=0.003; PBS/NPS vs. PBS/Veh: p=0.048), an effect that was also blocked by chemogenetic silencing (CNO/NPS vs. PBS/NPS: p=0.042; CNO/Veh vs. CNO/NPS: p=0.019). CNO alone resulted in a partial increase in anxiety-related behaviour as seen by a reduction in the percentage of open arm entries only (p<0.05 vs. all), and this may indicate that endogenous OXT originating from PVN neurons contributes to the general anxiety level of an individual. However, icv NPS partly reversed the effect of neuronal OXT silencing possibly by acting on other limbic regions. None of the drugs altered locomotor activity expressed by the number of closed arm entries ($F_{1,31}$=1.69, p=0.21).

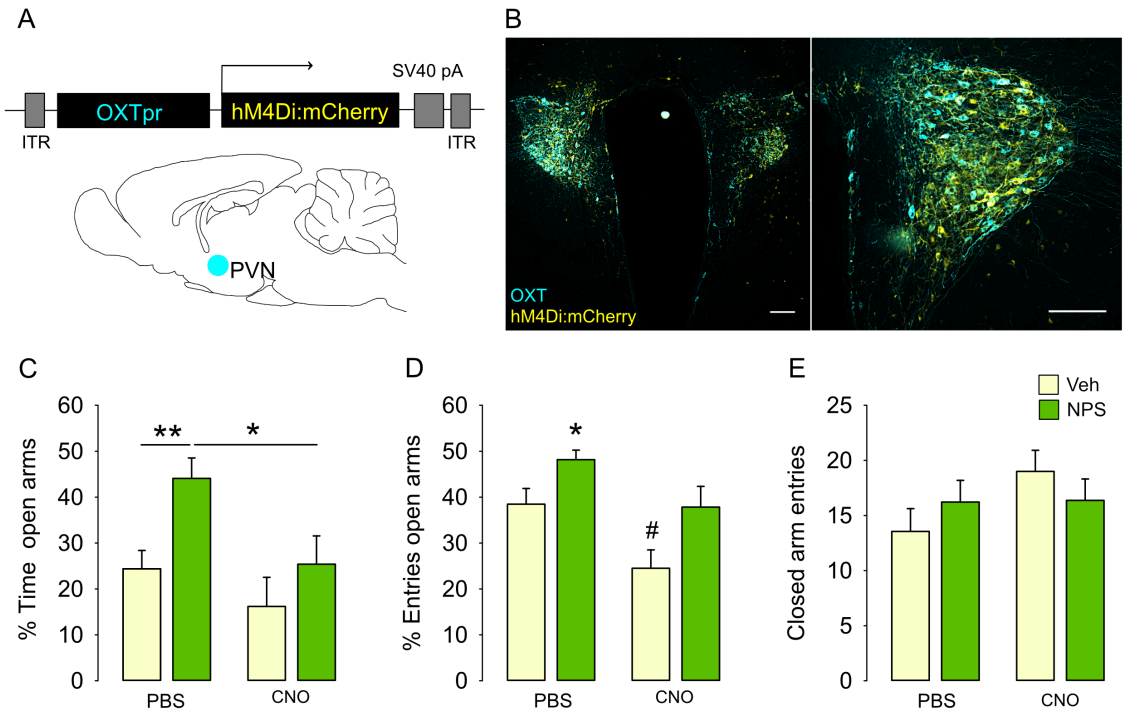

Figure 12: Chemogenetic silencing of PVN-OXT neurons prevented the anxiolytic effect of a subsequent NPS infusion. A) Schematic drawing of rAAV used to transfect PVN neurons. B) Expression of G_i-coupled DREADD (hM4Di:mCherry) in OXT neurons on tissue-wide and cellular level (scale bar: 100 µm). Rats were pretreated either

with PBS or CNO (2 mg/kg; ip), followed by icv infusion of either Ringer's solution (Veh, 5 µl) or NPS (1 nmol). C) Percentage of time spent on the open arms of the EPM and D) percentage of open arm entries indicates anxiety-related behavior. E) Number of closed arm entries reflects locomotor activity during the 5-min test period. Data represent mean + SEM, group sizes: n=8-9, except CNO/Veh: n=6. *$p<0.05$ and **$p<0.01$ vs. all or as indicated; # $p<0.05$ vs. all.

Chapter II – NPSR activation is anxiolytic in a G_q pathway-dependent manner

The results of Chapter 2 have been submitted to *Neuropsychopharmacology* on 10th of March 2017:

Grund, T., Neumann, I.D. (in revision) Neuropeptide S induces acute anxiolysis by phospholipase C-dependent signaling within the medial amygdala. *Neuropsychopharmacology*

1. Effect of bilateral infusion of NPS into the MeA on anxiety-related behavior

Bilateral infusion of NPS (0.2 nmol) into the MeA significantly reduced anxiety-related behavior of male rats both on the EPM and in the OF compared with Veh-infusion (Fig. 14). NPS-treated rats spent a higher percentage of time on the open arms (t_{15}= -2.46, p=0.027) without effects on the percentage of entries into the open arms (t_{15}= -0.37, p=0.72) and on the number of closed arm entries (t_{15}= -0.32, p=0.75). Notably, the anxiolytic effect of NPS in the MeA was confirmed in the OF test two days later, as NPS increased the time the animals spent in the center zone (U=11.00, p=0.034) and almost doubled the number of center zone entries (t_{14}= -2.58, p=0.022), when compared with Veh-treated rats. Moreover, NPS increased the distance rats travelled in the OF (t_{14}= -3.44, p=0.004) indicative of hyperlocomotion effect.

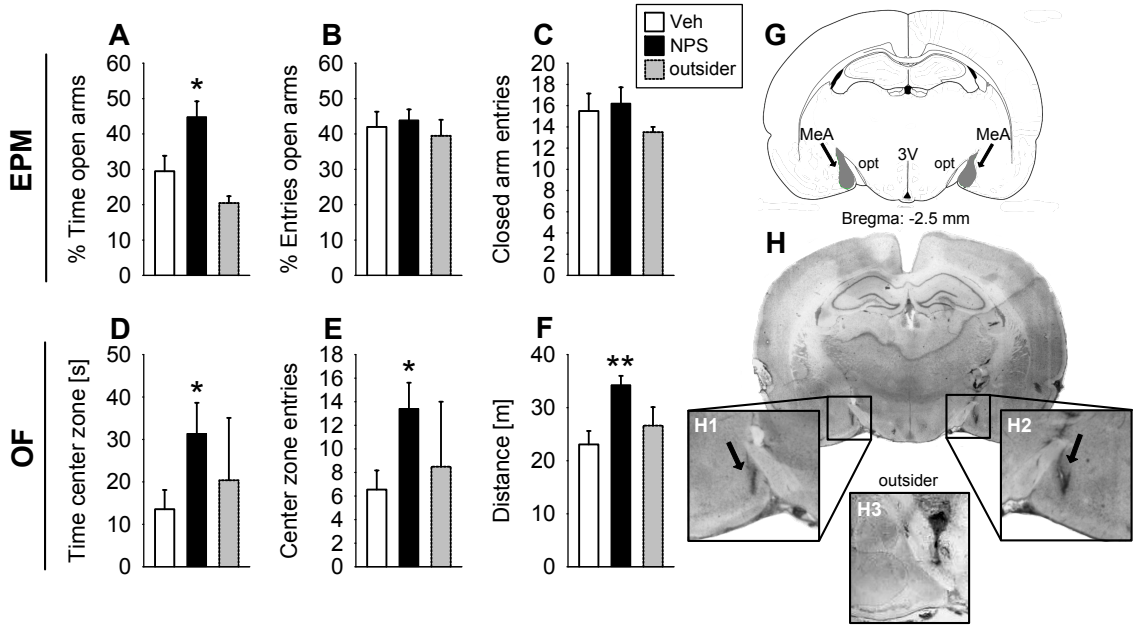

Figure 14: Anxiolytic effect of NPS infusion bilaterally into the MeA of male rats as assessed on the EPM (A-C) and the OF (D-F). During the 5-min testing on the EPM A) the percentage of time spent on, B) the percentage of entries into the open arms, and C) number of closed arm entries were monitored. During the 5-min testing in the OF D) the time spent in, E) the entries into the center zone, and F) travelled distance were analyzed. Data represent mean + SEM, *p<0.05, **p<0.01 vs. Veh (Ringer's solution); group sizes: n=7-9, outsider: n=2. G) Schematic drawing of the MeA in grey (opt: optic tract, 3V: third ventricle) and H) representative microphotographs of bilateral MeA infusion sites in a coronal brain slice (H1 and H2). H3 represents an infusion site considered as outsider.

2. Effects of icv NPS on Ca^{2+}/calmodulin-dependent kinase IIα and ERK1/2 in the amygdala

Western blot analysis of amygdala tissue micropunches revealed increased amounts of both phospho-Ca^{2+}/calmodulin-dependent kinase (CaMK) IIα (t_{20}= -2.480, p=0.022, Fig. 15B) and total CaMKIIα (t_{20}= -2.097, p=0.049, Fig. 15C) relative to *beta*-tubulin following icv infusion of NPS (1 nmol). phospho-CaMKIIα levels compared to total CaMKIIα were not altered (U=57, p=0.84, Fig. 15A).

Moreover, NPS increased cytoplasmic pERK1/2 levels. This applied to both the pERK1/2 / ERK1/2 (pERK1/ERK1: U=23, p=0.027; pERK2/ERK2: U=21, p=0.018, Fig. 15D) and the pERK1/2 / *beta*-tubulin ratios (pERK1/*beta*-tubulin: t_{18}= -2.12, p=0.048; pERK2/*beta*-tubulin: t_{18}= -2.18,

p=0.043, Fig. 15E). Total ERK1/2 levels were not altered by icv NPS (ERK1/*beta*-tubulin: t_{19}= 0.93, p=0.37; ERK2/*beta*-tubulin: t_{18}= -0.11, p=0.92, Fig. 15F).

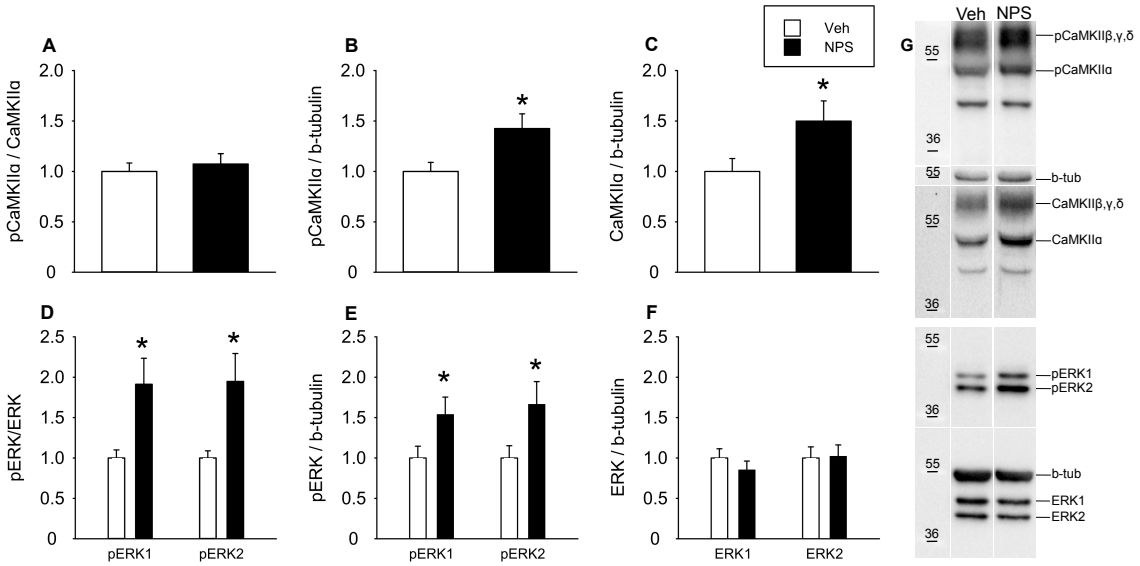

Figure 15: Effects of icv NPS (1 nmol/5 µl) on relative amount of phosphorylated CaMKIIα (pCaMKIIα) compared to A) total CaMKIIα and B) *beta*-tubulin in the cytosolic fraction of amygdala tissue micropunches of male rats. NPS evoked synthesis of C) CaMKIIα in relation to *beta*-tubulin. Relative amount of phosphorylated ERK1/2 (pERK1/2) compared to D) total ERK1/2 and E) *beta*-tubulin without affecting F) total ERK1/2 levels relative to *beta*-tubulin following NPS infusion. Data represent mean + SEM, *p<0.05 versus Veh; group sizes: n=9-12. G) Representative Western blots of (p)CaMKIIα, (p)ERK1/2, and *beta*-tubulin.

3. Effects of simultaneous blockade of both PLC and AC on NPS-induced anxiolysis

Pre-infusion of an inhibitor-cocktail consisting of both, the phospholipase C (PLC) blocker U73122 and the adenylyl cyclase (AC) inhibitor DDA bilaterally into the MeA prevented the anxiolytic effect of subsequent locally infused NPS demonstrating that PLC and/or AC mediate the anxiolytic effect (Fig. 16). On the EPM, we found an interaction between the first and second infusion on the percentage of time the rats spent on the open arms ($F_{(1,46)}$=4.23, p=0.046), whereas the percentage of entries into the open arms was not altered ($F_{(1,46)}$=1.13, p=0.29). Post hoc analysis revealed that NPS increased the percentage of time on the open

arms in Veh_1-pre-treated (p=0.003), but not in rats pre-treated with U73122/DDA (p=0.004). In Veh_2-infused rats, U73122/DDA-pre-infusion did not influence anxiety on the EPM. Local NPS did not affect locomotor activity, as measured by the number of closed arm entries ($F_{(1,46)}$=2.856, p=0.098) in both Veh_1- as well as U73122/DDA-pre-treated rats.

In the OF, the anxiolytic effect of intra-MeA NPS was likewise prevented by pre-infusion of U73122/DDA, as assessed by the time the rats spent in the center zone ($F_{(1,50)}$=3.37, p=0.073, 1st infusion: $F_{(1,50)}$=13.72, p<0.001, 2nd infusion: $F_{(1,50)}$=4.12, p=0.048) and the number of center zone entries (interaction: $F_{(1,50)}$=7.99, p=0.007). Moreover, statistical analysis revealed increased locomotion (interaction: $F_{(1,50)}$=8.28, p=0.006), an effect caused by NPS in Veh_1-pre-infused rats (p<0.001). In the OF, pre-infusion of the inhibitor-cocktail also blocked NPS-induced hyperlocomotion (p<0.001).

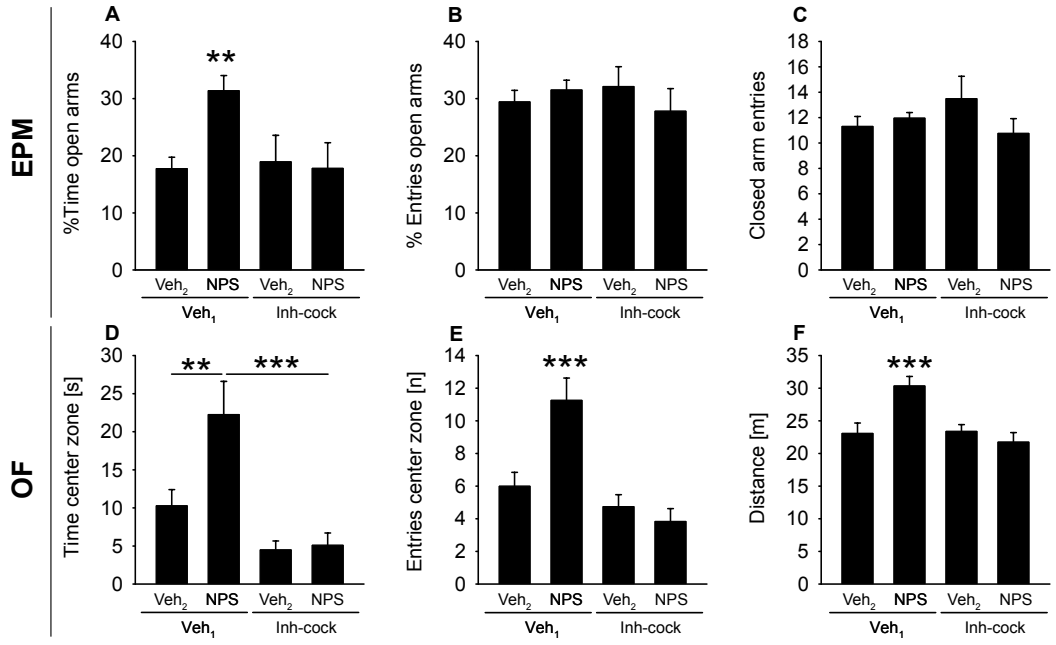

Figure 16: Effects of pre-infusion of an inhibitor-cocktail (Inh-cock) consisting of U73122 (PLC inhibitor, 0.5 nmol) and DDA (AC inhibitor, 12.5 nmol) on the anxiolytic effect of NPS bilaterally infused into the MeA (0.2 nmol/0.5 µl) on the EPM (A-C) and OF (D-F). A) Percentage of time spent on, B) percentage of entries performed into the open arms, C) closed arm entries, and D) time spent in, E) entries performed into the center zone, and F) distance travelled. As Veh_1, 0.5 µl of Ringer's solution supplemented with DMSO, and as Veh_2, 0.5 µl of Ringer's solution

were used. Data represent mean + SEM, **p<0.01, ***p<0.001 versus all other groups (A, E, F) or as indicated; group sizes: n=13-15, except Inh-cock/Veh_2: n=6-8.

4. Effects of specific blockade of either PLC or AC on NPSR-mediated anxiolysis in the MeA

To assess whether the anxiolytic activity of NPS is mediated via NPSR-evoked activation of either PLC or AC, or via both pathways within the MeA, we next pre-infused U73122 (PLC inhibitor), DDA (AC inhibitor) or Veh_1 bilaterally into the MeA prior to local NPS or Veh_2 infusion. Selective inhibition of PLC signaling by pre-infusion of U73122 prevented NPS-induced anxiolysis, whereas specific blockade of the AC by DDA pre-infusion failed to inhibit the anxiolytic properties of NPS (Fig. 17).

In detail, specific inhibition of the PLC signaling affected the percentage of time spent on the open arms (1^{st} infusion: $F_{(1,44)}$=1.75, p=0.19; 2^{nd} infusion: $F_{(1,44)}$=4.72, p=0.036; interaction: $F_{(1,44)}$=3.01, p=0.09) and the percentage of open arm entries (1^{st} infusion: $F_{(1,44)}$=7.47, p=0.009; 2^{nd} infusion: $F_{(1,44)}$=3.42, p=0.072; interaction: $F_{(1,44)}$=0.87, p=0.36) on the EPM. Post hoc analysis revealed that NPS-infused rats spent more percentaged time on the open arms (p=0.003 vs. Veh_1/Veh_2 rats) when pre-infused with Veh_1. This anxiolytic effect of NPS was prevented in the presence of U73122 (p=0.024 vs. Veh_1/NPS). Likewise, pre-infusion of U73122 reduced the percentaged entries into the open arms compared to Veh_1 (p=0.009 vs. Veh_1/NPS). Also, U73122 exerted a biologically slight, but significant stimulatory effect on locomotor activity (p=0.015 vs. Veh_1/NPS), as U73122/NPS animals showed an increased number of closed arm entries.

Separate inhibition of the AC signaling by pre-infusion of DDA revealed an effect for the second infusion on the percentage of time spent on the open arms (1^{st} infusion: $F_{(1,44)}$=0.09, p=0.76; 2^{nd} infusion: $F_{(1,44)}$=9.32, p=0.004; interaction: $F_{(1,44)}$=0.68, p=0.42) and on the percentaged open arm entries (1^{st} infusion: $F_{(1,44)}$=0.76, p=0.39; 2^{nd} infusion: $F_{(1,44)}$=8.78, p=0.005;

interaction: $F_{(1,44)}$=0.16, p=0.69). Post hoc analysis indicated that NPS almost doubled the percentage of time the animals spent on the open arms (p=0.004) and increased the percentage of open arm entries (p=0.005) in comparison to Veh_2-infused rats. More importantly, pre-infusion of DDA failed to block this anxiolytic effect of NPS (percentage of time spent on open arms: p=0.41 vs. Veh_1/NPS; percentaged open arm entries: p=0.73) suggesting that the NPS-induced anxiolysis is independent of AC signaling. None of the drug-infused rats of this experiment showed any signs of hyperlocomotion as the number of closed arm entries was not altered ($F_{(1,45)}$=0.02, p=0.90).

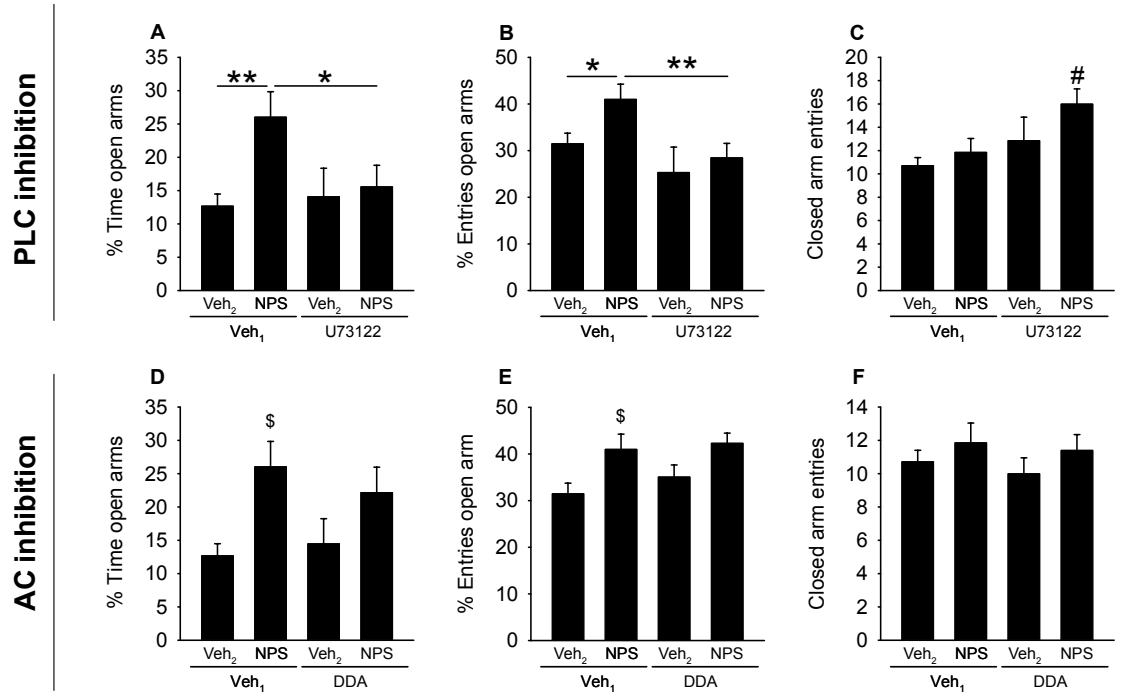

Figure 17: Effects of pre-infusion of either U73122 (PLC inhibitor, 0.5 nmol), DDA (AC inhibitor, 12.5 nmol) or Veh1 (0.5 µl of Ringer's solution supplemented with DMSO) on the anxiolytic effect of NPS bilaterally infused into the MeA (0.2 nmol/0.5 µl) on the EPM A/D) Percentage of time spent on, B/E) percentage of entries performed into the open arms, and C/F) closed arm entries. As Veh_2, 0.5 µl of Ringer's solution were used. Data represent mean + SEM, *p<0.05, **p<0.01 as indicated, $^{\#}$p<0.05 vs. Veh1/NPS, $^{\$}$p<0.05 vs. Veh_1/Veh_2; group sizes: n=13-15, except Inh-cock/Veh_2: n=6-8.

Chapter III – Characterization of DREADD-induced activation of OXT neurons in the PVN

1. Monitoring of central and peripheral OXT release following chemogenetic OXT neuron activation within the hypothalamus

DREADDs allow selective activation (or inhibition) of specific neuronal populations in order to dissect their contribution to complex behaviors and brain circuitries (Whissell *et al.*, 2016). To examine the spatiotemporal dynamics of DREADD actions with respect to OXT neurons, the cell type-specific recombinant $AAV_{1/2}$ OXTpr-hM3Dq:mCherry was infused bilaterally into the PVN or PVN, SON and AN of male rats, respectively. Within three weeks, an excitatory DREADD (hM3Dq) was selectively expressed under the control of an OXT promoter fragment indicated by prominent expression of the reporter protein mCherry in OXT neurons (Fig. 18).

Stimulated activity of OXT neurons is characterized by increased OXT release, for example within the PVN in a somato-dendritic fashion (Neumann & Landgraf, 2012). Ca^{2+} availability, specifically an increase in intracellular Ca^{2+}, is a prerequisite for such release (Neumann *et al.*, 1993b; Fisher & Bourque, 1996; Ludwig *et al.*, 2002). Since excitatory DREADDs have been described to increase intracellular Ca^{2+} levels (Armbruster *et al.*, 2007), I monitored the dynamics of OXT release within PVN, lateral septum, and peripheral blood following chemogenetic stimulation of OXT neurons initiated by CNO (2 mg/kg, ip) using microdialysis technique and via jugular vein catheter, respectively.

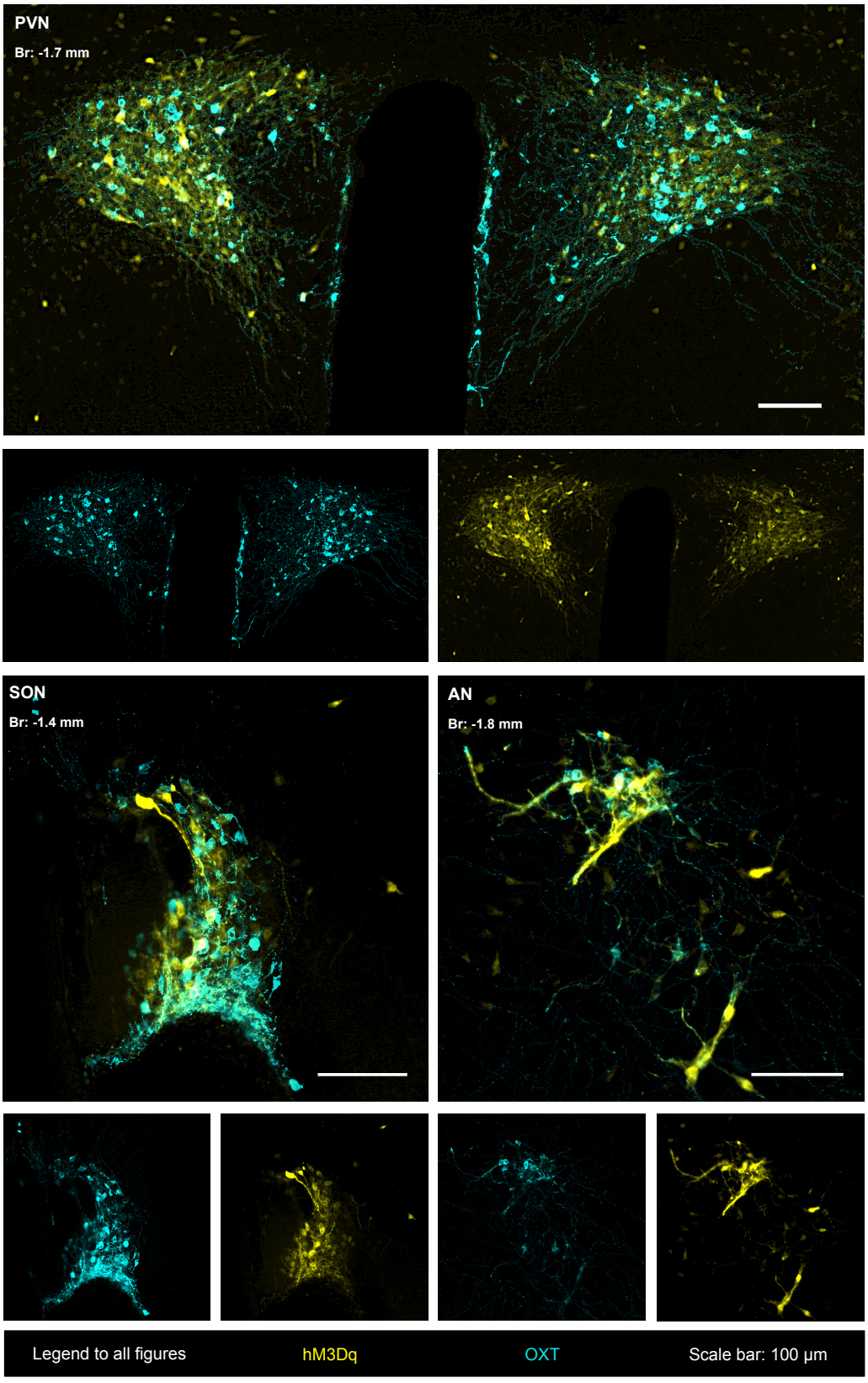

Figure 18: Expression of excitatory DREADD (hM3Dq:mCherry, yellow) in OXT neurons (cyan) within the rat hypothalamic PVN, SON and AN (scale bar: 100 µm) three weeks after stereotaxic rAAV infusion.

1.1 Chemogenetic OXT neuron activation evokes OXT release within the PVN

Herein, I monitored the dynamics of OXT release within PVN of conscious rats in response to ip administration of CNO or Veh, respectively. Microdialysis was performed on two consecutive days either under basal, unstressed conditions (day 1) or before and after exposure to forced swim (day 2) in order to examine CNO-induced basal or stimulated OXT release in hM3Dq-transfected PVN-OXT neurons. In rats bilaterally expressing an excitatory DREADD under the control of the OXT promoter fragment, CNO induced a rise in the OXT content in microdialysates indicative for intra-PVN release of OXT (Fig. 19).

In detail, OXT baseline levels in microdialysates prior to ip injection of either CNO or Veh (samples *b1+b2* Fig 19A and sample *b* Fig 19B) did not differ between rats, which were previously infused with either intra-PVN $AAV_{1/2}$-OXTpr-hM3Dq-mCherry (AAV^+) or Veh (AAV^-) indicating that expression of DREADD without specific CNO stimulation in OXT neurons does not change the activity of these cells. Specifically, comparison of the existing 4 groups (AAV^+/Veh, AAV^+/CNO, AAV^-/Veh, AAV^-/CNO) revealed that in microdialysates sampled before any stimulation, OXT content in microdialysates was not changed (two way ANOVA; day 1: basal 1 $F_{1,17}$=2.32, p=0.15; basal 2 $F_{1,17}$=0.15, p=0.71; day 2: basal $F_{1,18}$=0.14, p=0.71), demonstrating that basal OXT release is not influenced by the expression of DREADD. Moreover, OXT content in AAV^+/Veh, AAV^-/Veh and AAV^-/CNO did not change over time (two way ANOVA for repeated measures; day 1: $F_{8,58}$=0.30, p=0.96; day 2: $F_{8,54}$=0.19, p=0.99) further revealing the biologically inert nature of CNO. Therefore these three groups were combined and below defined as Veh-control.

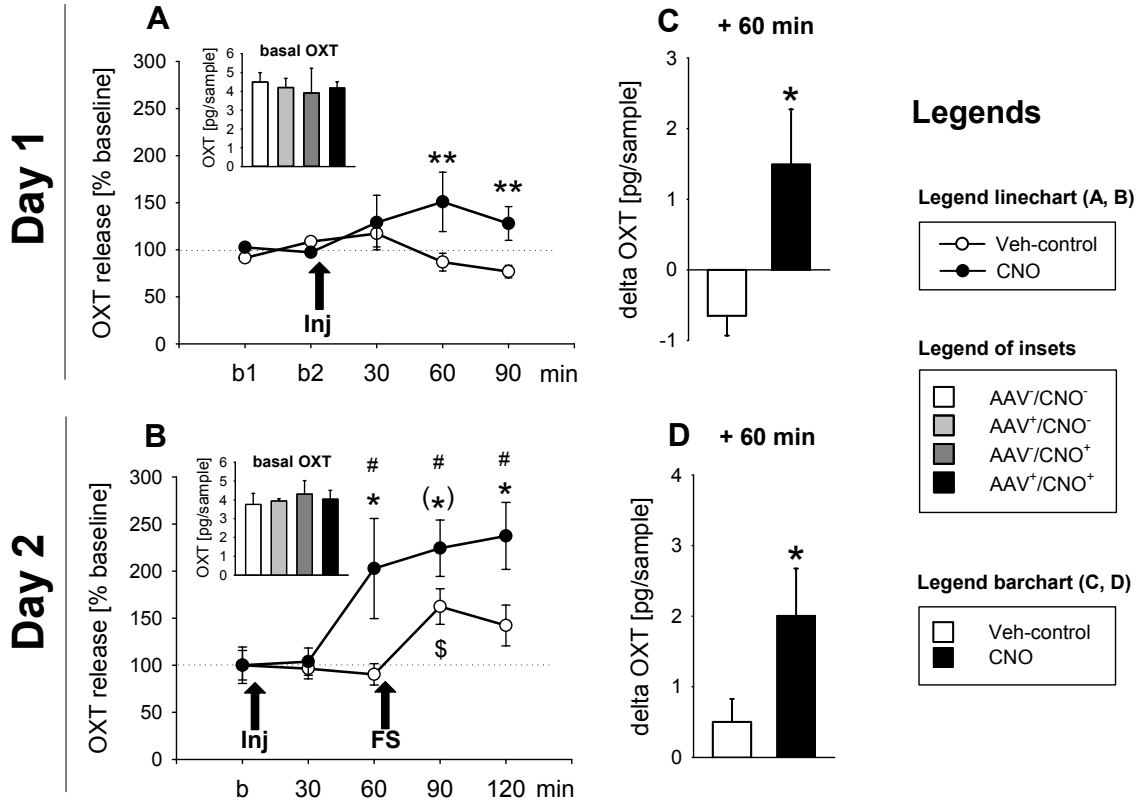

Figure 19: Chemogenetically evoked OXT release within the hypothalamic PVN in male Wistar rats expressing an excitatory DREADD in the PVN-OXT neurons. A) On day 1, 30-min dialysates were sampled before (b1 and b2) and after ip injection (Inj) of either vehicle (Veh; PBS, pH 7.4) or CNO (2 mg/kg), n=8-11. B) On day 2, one 30-min dialysate was sampled before (basal (b)) and four after ip CNO (samples 30, 60, 90 and 120 min). Samples 4 (90 min) and 5 (120 min) were collected following a 5 min forced swim stress (FS), n=7-12. Data are expressed as percentage of baseline (=100%; dotted line) ± SEM; *p<0.05, **p<0.01 and $^{(*)}$p=0.068 vs. respective Veh-control, $^{\#}$p<0.05 vs. CNO basal (sample 1), $^{\$}$p<0.05 vs. Veh-control basal (sample 1). Delta change in absolute OXT content in microdialysates in comparison to mean baseline on C) day 1 and D) day 2. Data are expressed as mean + SEM; *p<0.05.

For day 1, two-way ANOVA for repeated measures including AAV^{+}/CNO and Veh-control revealed a significant interaction of treatment x time ($F_{4,90}$=3.49, p=0.012). Specifically, post-hoc analysis revealed a more pronounced relative elevation in OXT release in the AAV^{+}/CNO group at both 60 min (p=0.002) and 90 min (p=0.005) vs. respective Veh-control (Fig. 19A). This

was also reflected by higher delta values in absolute OXT content (sample 60 min – $basal_{mean}$; t_{16}= -3.21, p=0.005; Fig. 19C).

On day 2, two way ANOVA for repeated measures showed a significant interaction of time x treatment ($F_{4,89}$=2.703, p=0.038). Post-hoc analysis revealed a more pronounced rise in OXT release under basal, unstimulated conditions 60 min after CNO injection in comparison to both the respective Veh-control (Fig. 19B, p=0.002, between subjects) and AAV^+/CNO basal levels (p=0.030, within subjects). Likewise, as depicted in Fig. 19D, the effect of an increased OXT release following CNO injection in AAV^+ rats is reproduced by increased delta levels in absolute OXT release 60 min after ip injection (t_{16}= -2.27, p=0.037) further demonstrating increased OXT release following chemogenetic OXT neuron stimulation. In response to forced swimming following basal sampling, I found in CNO-injected G_q-DREADD-expressing rats, I found an increased OXT content in both groups. In detail, separate one-way ANOVA for repeated measures (within Veh-control: $F_{4,55}$=6.12, p<0.001; within AAV^+/CNO: $F_{4,33}$=3.81, p=0.016) indicated reliably increased percentaged OXT release in both groups. More specifically, two way ANOVA for repeated measures followed by post hoc corrections showed that AAV^+/CNO rats responded with a distinct increased percentaged OXT release vs. Veh-control (sample 4: Trend with p=0.068, sample 5: p=0.006, Fig. 19B) suggesting the hypothesis of a more sustained OXT release once the system is activated.

1.2 Chemogenetic activation of hypothalamic OXT neurons failed to increase measurable OXT release within lateral septal nuclei

In a separate cohort, the effect of chemogenetically evoked OXT neuron stimulation within the hypothalamic PVN, SON and AN was assessed by intracerebral microdialysis within the lateral septum in urethane-anesthetized rats. As the lateral septum is innervated by OXT fibers (Stoop, 2012), I postulated increased OXT release within the lateral septal nuclei while chemogenetic activation of hypothalamic OXT neurons. In contrast to my hypothesis, two-way

ANOVA for repeated measures revealed neither an interaction of treatment x time ($F_{4,84}$=0.41, p=0.80, Fig. 20A) nor main effects of time ($F_{4,84}$=2.19, p=0.08) or treatment ($F_{1,84}$=0.00, p=0.99). This result was also reflected by unchanged delta values in absolute OXT content (sample 60 min – $basal_{mean}$; t_{15}= -0.15, p=0.88; Fig. 20B).

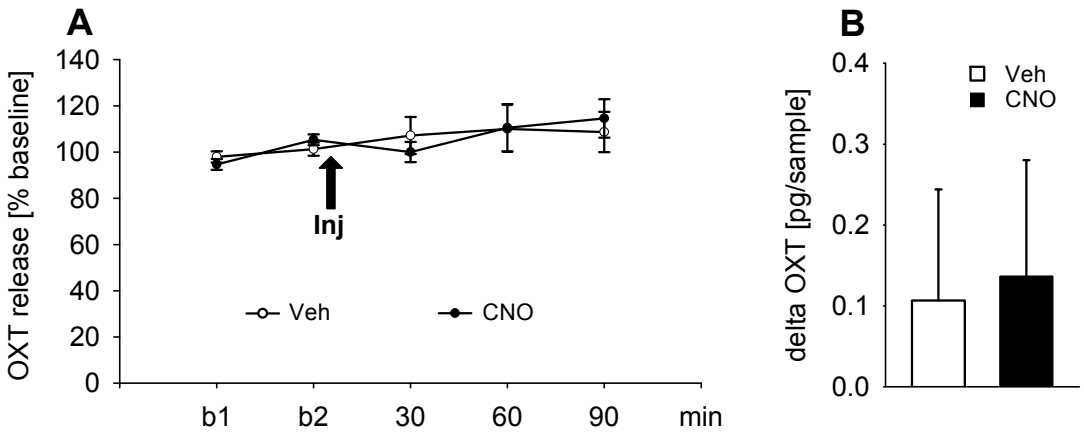

Figure 20: Chemogenetic activation of hypothalamic OXT neurons failed to increase measurable OXT release within the lateral septal nuclei. A) 30-min dialysates were sampled before (b1 and b2) and after ip injection (Inj) of either vehicle (Veh; PBS, pH 7.4) or CNO (2 mg/kg), n=8-9. Data are expressed as percentage of baseline (=100%) ± SEM. B) Delta change in absolute OXT content in microdialysates in comparison to mean baseline. Data are expressed as mean + SEM, n=8-9.

1.3 Chemogenetically evoked activation of hypothalamic OXT neurons increases peripheral OXT release

OXT is released from magnocellular neurons into the periphery via axons forming neurohemal contacts within the neurohypophysis (Gimpl & Fahrenholz, 2001; Meyer-Lindenberg *et al.*, 2011). Herein, the effect of chemogenetically evoked OXT neuron stimulation within the hypothalamic PVN, SON and AN on peripheral OXT release was analyzed in plasma sampled before and after stimulation. In rats bilaterally expressing an excitatory DREADD under the control of the OXT promoter fragment, CNO induced a rise in plasma OXT concentration indicative for peripheral release of OXT from neurohypophysial terminals (Fig. 21).

In detail, two-way ANOVA for repeated measures revealed a significant interaction of treatment x time ($F_{1,29}$=11.60, p=0.005; Fig. 21A). While basal plasma OXT levels did not differ between treatment groups (p=0.61), post-hoc analysis revealed reliably increased plasma OXT concentration (CNO^{+45min} vs. $Veh^{+45\ min}$: p<0.001) when OXT neurons were chemogenetically activated. Within-group comparison demonstrated that chemogenetic activation of OXT neurons by CNO evokes peripheral OXT release as OXT content in plasma samples was increased (within CNO group: p<0.001). In contrast, rats receiving an ip injection of sterile PBS failed to alter OXT content in plasma (within Veh group: p=0.84). These findings are also reflected by higher delta values in absolute OXT content ($sample^{+45min}$ – $sample^{-45\ min}$; U= 81.0, p=0.002; Fig. 21B).

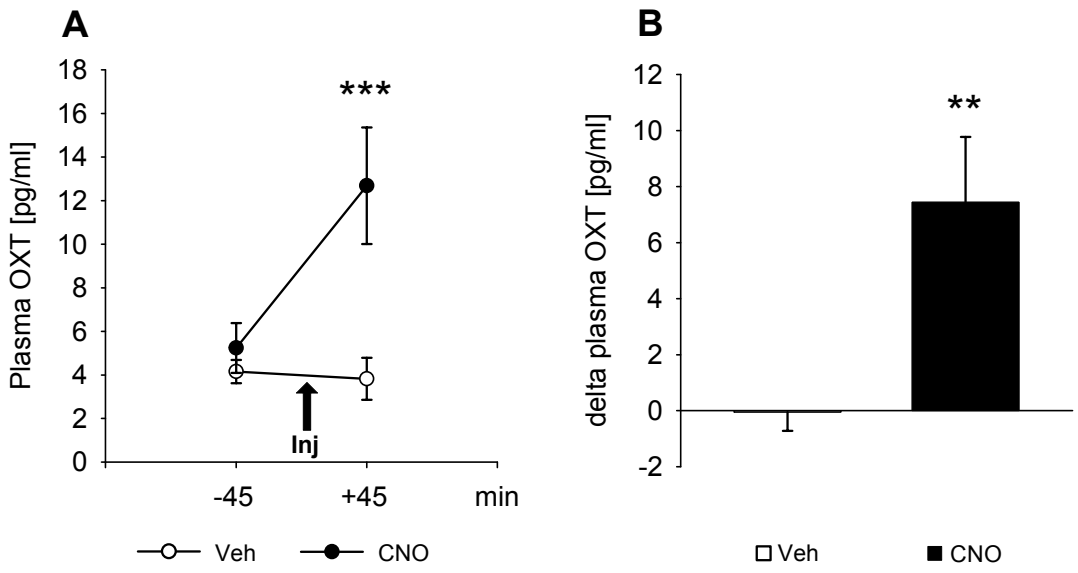

Figure 21: Chemogenetic activation of hypothalamic OXT neurons evokes peripheral OXT release. A) Absolute plasma OXT concentration sampled before (-45 min) and after (+45 min) ip injection (Inj) of either vehicle (Veh; PBS, pH 7.4) or CNO (2 mg/kg), n=8-9. Data are expressed as mean ± SEM, n=7-9. B) Delta change in absolute OXT content in plasma samples ($cOXT^{+45\ min}$ – $cOXT^{-45min}$). Data are expressed as mean + SEM, n=7-9.

2. Chemogenetically activation of OXT neurons induces anxiolysis and self-grooming behavior

In order to test the hypothesis that chemogenetic activation of PVN-OXT neurons reduces anxiety-related behavior as a consequence of increased intracerebral OXT release, animals were tested in the LDB 55 min after ip injection of CNO or Veh (PBS). Chemogenetic activation of PVN-OXT neurons resulted in an anxiolytic effect, since CNO-treated animals spent more time in the light box (t_{13}= -2.25, p=0.042 Fig. 22A), and tended to perform more entries into the light box (t_{13}= -1.29, p=0.22, Fig. 20B). CNO did not alter the locomotor activity of the animals (t_{13}= -1.50, p=0.16, Fig. 22C).

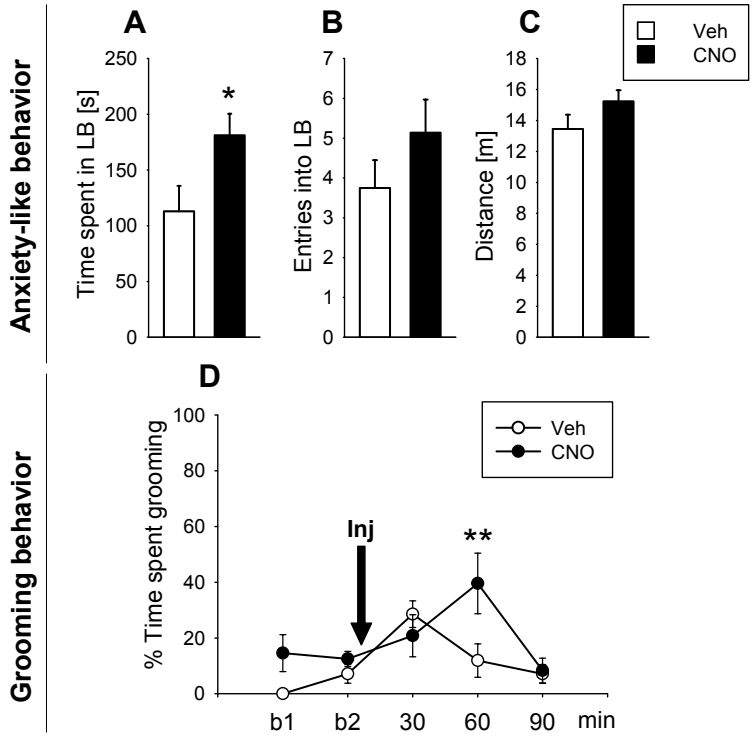

Figure 22: Behavioral responses following chemogenetic activation of PVN-OXT neurons. Anxiety-related behavior was tested using the LDB. Data show A) time spent in light box, B) entries into the light compartment and C) locomotor activity of rats treated with CNO (2 mg/kg, ip) or Veh (PBS, 1 ml/kg, ip). Data are represented as mean + SEM; *p<0.05. D) During ongoing microdialysis within the hypothalamic PVN, behavioral assessment revealed increased self-grooming, when OXT neurons were activated chemogenetically. Data represent mean ± SEM, **p<0.01 vs. respective Veh. Group sizes: n=7-8.

Behavioral analysis during ongoing intra-PVN microdialysis on day 1 revealed a significant interaction of time x treatment with regard to self-grooming ($F_{4,74}$=2.56, p=0.049; Fig. 22D). Specifically, CNO treatment resulted in increased grooming behavior, which peaked 60 min after ip injection in comparison to Veh-control ($CNO^{+60\ min}$ vs. $Veh^{+60\ min}$: p=0.002). Moreover, within group analysis revealed that control rats spend significantly more time on grooming behavior during the first 30-min period after ip injection of Veh compared to baseline 1 ($Veh^{+30\ min}$ vs. Veh^{b1}: p=0.016). Other behaviors such as sleep ($F_{4,74}$=0.74, p=0.57), exploration ($F_{4,74}$=0.31, p=0.87) or food/water-intake ($F_{4,74}$=0.06, p=0.99) did not differ between groups (data not shown).

3. Effect of chemogenetic PVN-OXT neuron activation on EtOH-induced locomotor impairments

Icv infusion of synthetic OXT was found to selectively attenuate ethanol-induced motor impairments in rats (Bowen *et al.*, 2015). In order to test whether DREADD-induced excitation of OXT neurons in the PVN attenuates ethanol-induced locomotor impairments, PVN-OXT neurons have been transfected with an excitatory DREADD (Fig. 23).

In contrast to my hypothesis, I did not see any effect of PVN-OXT neuron activation on the wire-hanging test performance (+5 min: U(67.0), p=0.383, +35 min: U(78.0) p=0.758). The attenuation of acute ethanol effects by CNO-evoked excitation of OXT neurons was only seen in a decreased duration of the rightning reflex test during second execution of the test (+35 min: U(30.0), p=0.009), but not during the first performance (+5 min: U(64.5), p=0.479).

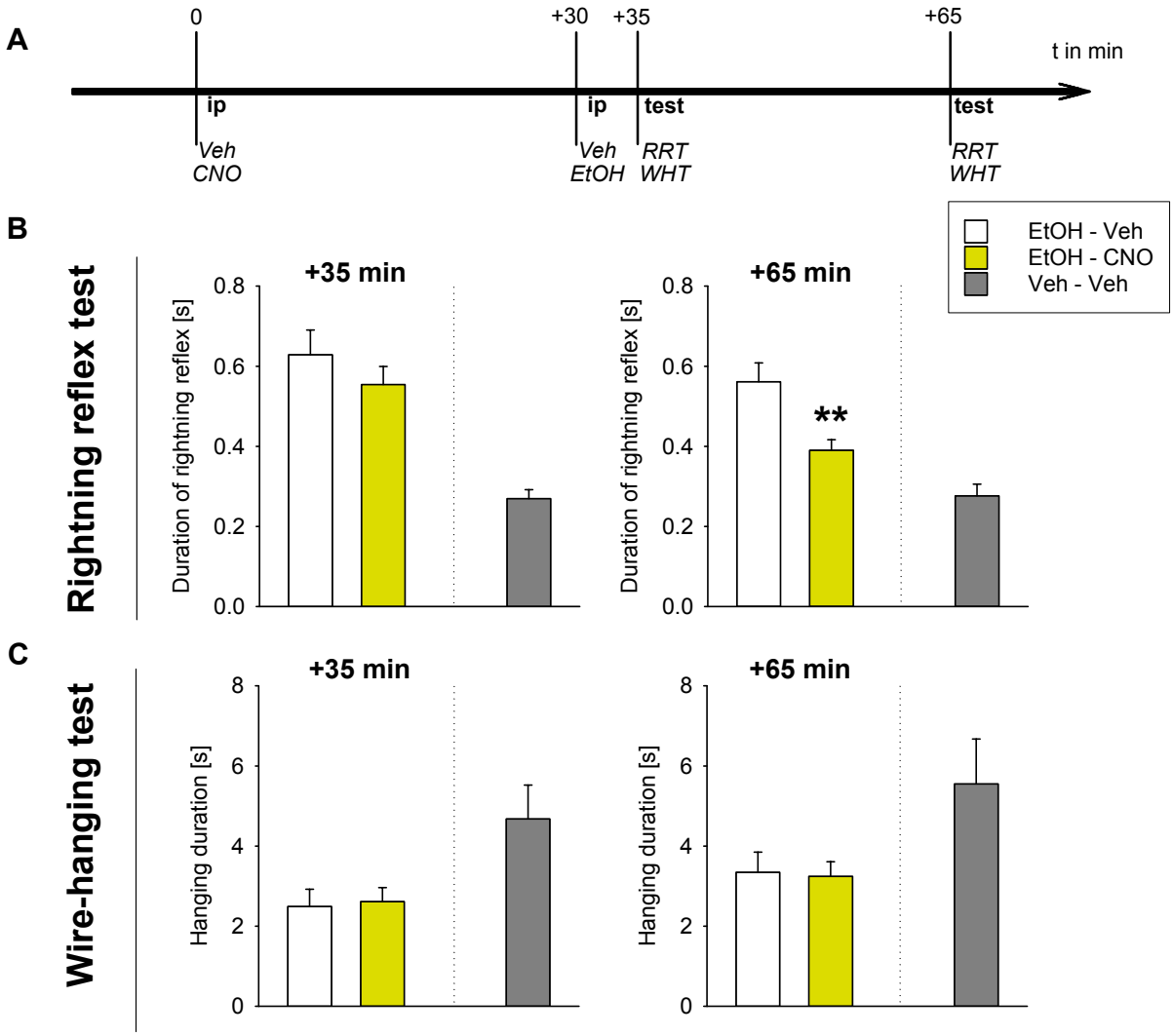

Figure 21: Chemogenetic activation of PVN-OXT neurons partly attenuates ethanol-induced locomotor impairments. A) Experimental timeline of rightning reflex test (RRT) and wire-hanging test (WHT) after injection of ethanol (EtOH, 1.5 g/kg, 15% wt/vol), CNO (2 mg/kg, ip), or Veh (sterile PBS). Effect of chemogenetic activation of PVN-OXT neurons on ethanol-induced locomotor impairments in B) the rightning reflex test and C) the wire-hanging test and. Data are expressed as mean + SEM, group sizes: n=8-13.

4 General discussion

Brain OXT and NPS have been described for their anxiolytic profile over the last decades. In the present study, I advanced our understanding of the regulation of anxiety-like behavior by brain NPS and OXT in male Wistar rats. First, I described a novel intra-hypothalamic circuit through which NPS activates a subpopulation of PVN-OXT neurons to promote anxiolysis. Furthermore, I found that intra-MeA infusion of NPS reduces anxiety-related behavior, an effect that strictly depends on NPSR-mediated PLC signaling. Moreover, I examined the spatiotemporal processes following chemogenetic activation of the endogenous PVN-OXT system. These findings come at a time of growing interest in the therapeutic potential of brain neuropeptides to treat psychopathologies, such as anxiety disorders (Mathew *et al.*, 2008). The results presented in this thesis reflect the importance of brain NPS and OXT specifically within the PVN as part of the limbic system as a regulator of anxiety-related behavior, highlight these systems as potential targets to understand the development of anxiety disorders, and emphasize the importance of the PVN and the MeA as key brain regions in the regulation of anxiety. Below I will discuss the major findings revealed in each of the three chapters, individually.

Chapter I: NPS-induced anxiolysis is mediated via the OXT system within the hypothalamic PVN

Based on the behavioral similarities of the NPS and OXT system (Neumann, 2008; Pape *et al.*, 2010), and the overlap in NPS(R) and OXT(R) expression described before, I hypothesized that NPS effects are mediated via the OXT system by acting on OXT neurons within the PVN. The present study describes a novel intra-hypothalamic circuit through which NPS activates a subpopulation of PVN-OXT neurons to promote anxiolysis. Herein, retrograde tracing demonstrated NPS afferents originating in the LC innervating the PVN. Moreover, FACS analysis revealed abundant NPSR expression in OXT neurons. Measuring Ca^{2+} influx in OXT neurons and OXT release within the PVN demonstrated an NPS-induced activation of the PVN-OXT system. Both, chemogenetic silencing of PVN-OXT neurons and pharmacological OXTR antagonism blocked NPS-induced anxiolysis demonstrating that NPS promotes anxiolysis by acting on PVN-OXT neurons.

Antero- and retrograde tracing demonstrated prominent LC-neurons innervating limbic brain regions such as the PVN, the amygdala, the septum, bed nucleus of the stria terminalis, and thalamus (Jones & Yang, 1985). Besides arousal-promoting catecholamines such as noradrenaline (Loughlin *et al.*, 1986), the LC harbors a cluster of predominantly glutamatergic neurons synthetizing NPS (Xu *et al.*, 2007). In order to verify neuroanatomical target structures receiving input from NPS neurons located in the LC, I performed a retrograde tracing study. By intra-PVN infusion of CTB-488, a powerful retrograde tracer, I identified NPS-immunoreactive neurons in the LC projecting towards the PVN. The correct intra-PVN infusion of CTB-488 was verified by co-staining of OXT in coronal brain slices containing the PVN. Prominent NPS-immunopositive afferents innervating the PVN have also been described in C57Bl/6 mice (Clark *et al.*, 2011). Altogether, NPS afferents from the LC innervate the PVN in both rats and mice.

In line, *in situ* hybridization revealed abundant NPSR expression in the PVN of rats (Xu *et al.*, 2007). In order to determine whether PVN-OXT neurons express the NPSR, I applied a more

sensitive and highly specific technique – FACS analysis of Venus-labelled PVN and SON OXT neurons - and demonstrated prominent NPSR expression in OXT neurons, whereas NPSR mRNA in Venus-negative cells, likely to be vasopressin or corticotrophin-releasing hormone (CRH) neurons, was almost negligible. Earlier experiments revealed selective expression of Venus in OXT neurons with more than 97 % colocalization of OXT supporting the significance of our results in terms of cell-type specific Venus-labeling (Knobloch *et al.*, 2012).

My attempt to validate the finding of NPSR mRNA in OXT neurons at protein level generally failed due to lack of a specific antibody for NPSR. My first attempt to fluorescently label the NPSR using Ab2 (Leonard & Ring, 2011) in the PVN showed mostly somatic and punctuate staining, suggesting vesicular and membrane microdomain localization in OXT-immunoreactive neurons. The antibody Ab2 was generated in rabbits injected with keyhole limpet hemocyanin-conjugated peptide encoding a portion of the second extracellular loop (GKRTLSNGEVQCWALWPD) of the NPSR (Leonard & Ring, 2011). However, I could reveal that Ab2 is not specific to reliably detect NPSR protein. Koller and colleagues generated the $NPSR^{-/-}$ mouse line by homologous recombination with a targeting plasmid and, thus, a 744-bp region in the NPSR gene is replaced, which includes the majority of exon 4 (Allen *et al.*, 2006b). This deletion removes the third transmembrane domain and the second extracellular loop (predicted binding site of Ab2) of the NPSR resulting in a non-functional GPCR (Allen *et al.*, 2006b). Thus, Ab2 cannot longer bind to its predicted target protein. Specifically, I could show that homozygous $NPSR^{-/-}$ mice do not express NPSR mRNA. Moreover, PCR analysis of DNA from $NPSR^{+/+}$ and KO mice revealed a PCR product of 418 bp from the homozygous $NPSR^{+/+}$ mice and a 599-bp DNA fragment was amplified from homozygous $NPSR^{-/-}$ mice accordant to the literature (Camarda *et al.*, 2009). Having characterized tissue micropunches at DNA and mRNA level, I performed Western blot analysis using PVN tissue micropunches from $NPSR^{-/-}$ and $NPSR^{+/+}$ mice, which revealed a non-specific binding of Ab2. Thus, this antibody is not suitable to analyze NPSR localization.

Moreover, I verified the specificity of the commercially available NPSR1 antibody (abcam, ab92425), which targets residues 350 to the C-terminus of the human NPSR1. Western blot analysis demonstrated bands in both $NPSR^{+/+}$ and $NPSR^{-/-}$ mouse samples suggesting aspecific binding of this antibody. Although this antibody targets the C-terminal domain, it is very unlikely that the NPSR is expressed in $NPSR^{-/-}$ mice. When the sequence of NPSR transcript from $NPSR^{-/-}$ mice was transfected into COS-1 cells, a fibroblast-like cell line, analysis of these transfected cells showed that the transcript failed to properly integrate into the membrane (Allen *et al.*, 2006a). Moreover, Girolamo Calo and colleagues demonstrated that NPS failed to induce any behavioral changes following NPS infusion in $NPSR^{-/-}$ mice (Camarda *et al.*, 2009). In conclusion, although I could find NPSR mRNA in PVN-OXT neurons, NPSR localization at protein level cannot be determined due to non-specific binding of currently available NPSR antibodies.

Having evidenced NPSR mRNA expression in PVN-OXT neurons by FACS analysis, I sought to determine whether NPS activates OXT neurons. Ultrasensitive fluorescent proteins represent a powerful tool to monitor changes in intracellular Ca^{2+} levels, which is based on rapid deprotonation of green fluorescent protein following conformational change of calmodulin upon Ca^{2+} binding (Chen *et al.*, 2013). In hypothalamic slice preparations, a subpopulation of constitutively silent OXT neurons expressing a genetically encoded Ca^{2+} indicator (GCaMP6s) responded to synthetic NPS with transient Ca^{2+} influx, which reflects neuronal activation. The recorded Ca^{2+} response was heterogeneous, but massive, with a slow rise time and relative long-lasting responses of several seconds. This observation is compatible with a previous study in hippocampal mouse neurons (Erdmann *et al.*, 2015). The NPS effects on intracellular Ca^{2+} also studied in NPSR1-transfected HEK293T and CHO cells are most likely mediated by NPSR-induced G_q-signaling (Reinscheid *et al.*, 2005; Liao *et al.*, 2016; Clark *et al.*, 2017).

It is important to note that repeated NPS application failed to induce a repeated Ca^{2+} response in the same OXT neurons, as already reported by previous studies (Jungling *et al.*, 2008; Meis *et al.*, 2008). While the mechanism involved is yet to be determined, one can hypothesize a

high desensitization of NPSR. However, the specific involvement of NPSR on NPS-induced activation of OXT neurons was successfully demonstrated, since NPS failed to increase intracellular Ca^{2+} levels in the presence of the selective NPSR antagonist SHA-68 (Okamura *et al.*, 2008; Ruzza *et al.*, 2010).

Thus, from these experiments I concluded that NPS originating from the LC acts at NPSR in the PVN, specifically in OXT neurons causing their activation. This conclusion has further been substantiated by the finding of increased OXT release. Ca^{2+} influx in OXT neurons is a prerequisite for OXT release (Ludwig *et al.*, 2002; Ludwig & Leng, 2006). Central OXT is released from OXT neurons of the PVN and SON (Ludwig, 1998; Bergquist & Ludwig, 2008). Like the release of OXT from axonal terminals in the neurohypophysis (Fisher & Bourque, 1996), dendritic release of OXT depends on local increase in intracellular Ca^{2+} concentration (Neumann *et al.*, 1993b; de Kock *et al.*, 2003). Herein, microdialysis in combination with a highly sensitive radioimmunoassay demonstrated NPS-evoked OXT release within the PVN, dose-dependently. When NPS was infused at 1 nmol while ongoing microdialysis, a moderate, but long lasting increase in OXT content in microdialysates was monitored. This might be explained by an autocrine mechanism through which dendritic OXT release, once triggered, can become self-sustaining and thus long-lasting (Ludwig *et al.*, 2002). In contrast, 5 nmol of NPS induced a prominent increase in relative OXT content in microdialysates, which declined to baseline in the next sample. Since the rise in intracellular Ca^{2+} levels induced by NPS is reported to have different sources (Erdmann *et al.*, 2015), it is unclear which mechanism(s) of NPS-induced intracellular Ca^{2+} rise predominates in PVN-OXT neurons and whether these mechanisms are dose-dependent.

The stimulatory effects of NPS on the activity of OXT neurons within the PVN, which are NPSR-mediated, highlight an intra-hypothalamic mechanism at cellular level. Moreover, I can show that NPS exerts a behavioral effect directly within the PVN, and this anxiolytic effect required the activation of local OXT neurons. Based on pharmacological and chemogenetic inhibition of

the OXT system, my results indicate an important role for OXT to mediate the anxiolytic effect of NPS in the hypothalamic PVN.

Specifically, pre-infusion of a selective OXTR-A (Manning *et al.*, 2012) into the cerebral ventricular system was able to prevent the NPS-induced reduction in anxiety levels as seen in two separate and well established tests for anxiety-related behavior, namely the LDB and the OF. The OXTR-A alone did not alter general anxiety in comparison to control; an effect that has been observed earlier in male rats (Waldherr & Neumann, 2007). Importantly, also local pre-infusion of OXTR-A bilaterally into the PVN reduced the robust NPS-induced anxiolysis seen in rats pre-infused with vehicle, although to a lower degree. Thus, I hypothesize that NPS infused into the PVN activates local OXT neurons and local somato-dendritic OXT release; endogenous as well synthetic OXT within the PVN have been repeatedly shown to exert anxiolytic effects (Neumann *et al.*, 2000; Blume *et al.*, 2008; Jurek *et al.*, 2012; van den Burg *et al.*, 2015). Moreover, local NPS may activate those OXT neurons in the PVN, which project to other limbic brain regions, such as the amygdala (Knobloch *et al.*, 2012), where OXT was also found to exert anxiolytic effects (Neumann *et al.*, 2000; Bale *et al.*, 2001).

In order to specifically prove for the involvement of PVN-OXT neurons in the behavioral effects of NPS, I chemogenetically silenced OXT neurons of the PVN using a G_i-coupled designer receptor selectively expressed under the control of the OXT promoter fragment. DREADD-evoked silencing of OXT neurons by ip CNO reliably prevented the anxiolytic effect of a subsequent central NPS infusion as seen on the EPM. At cellular level, CNO-induced hM4Di stimulation has been shown to result in reduced mean frequency of spikes induced by application of currents, increased inward currents, and decreased input resistance of OXT neurons (Eliava *et al.*, 2016). Thus, chemogenetically silenced OXT neurons can no longer be activated by NPS. In my experiment, I found a loss of the anxiolytic profile of NPS after CNO injection, which provides final evidence for the essential role of stimulated PVN-OXT neurons in mediating this behavioral effect of NPS. Importantly, injection of CNO alone, which should

result in a general inhibition of OXT neurons of the PVN, slightly increased anxiety-related behavior. Although this has only be seen from a reduced percentage of entries performed into the open arms of the EPM, chemogenetic silencing of OXT neurons might abolish intracerebral OXT release under basal conditions within the PVN or in other relevant limbic brain regions, important for the individual level of state anxiety. Also, dysregulation/disinhibition of the CRH system after silencing of OXT neurons, especially during exposure to an emotional stressor such as the EPM, cannot be ruled out, the more as OXT was found to attenuate the stress-induced expression of CRH in a CREB-dependent manner (Jurek *et al.*, 2015).

Based on my results I postulate the following scenario under physiological conditions: In response to a challenging and stressful situation, pericoerulear CRH-sensitive NPS neurons become activated (Jungling *et al.*, 2012), resulting in NPS release from NPS axonal projections as shown in the basolateral amygdala during forced swimming (Ebner *et al.*, 2011). However, NPS neurons also project to the PVN as described in mice (Clark *et al.*, 2011), and in rats using a powerful retrograde tracer infused into the PVN. Thus, NPS released within the PVN from terminals of pericoerulear NPS neurons activate OXT neurons, as indicated by increased intracellular Ca^{2+} levels, which results in local OXT release or stimulation of centrally projecting OXT neurons as described above. Finally, the rise in OXT availability in the regional extracellular fluid results in the modulation of an appropriate anxiety response of an individual to cope with the environmental challenge.

In summary, my findings demonstrate a novel intra-hypothalamic neurophysiological mechanism involving NPSR-expressing OXT neurons of the PVN, which are activated by NPS and respond with transient increase in intracellular Ca^{2+} and local somato-dendritic OXT release. The stimulation of local OXT neurons is essential for NPS-induced anxiolysis, as this effect was blocked by specific pharmacological and chemogenetic inhibition of the OXT system. These findings provide important evidence for interactions of NPS with another neuropeptidergic system, but obviously warrant further research into how these circuits

orchestrate specific physiological effects resulting in distinct behavioral outputs, i.e. such as the regulation of stress or anxiety-related behavior. Based on a growing interest in the development of therapeutic strategies for anxiety- and stress-related disorders, a wide-ranging knowledge about the neuronal and behavioral consequences of brain neuropeptide signaling modulating emotional responses is required for efficient development of new therapeutic strategies.

Chapter II: NPS induces acute anxiolysis by PLC-dependent signaling within the MeA

The present study describes the MeA as an important brain target of NPS to induce an anxiolytic effect in male rats and the G_q pathway as the essential intracellular signaling cascade underlying this local anxiolytic effect. More specifically, the PLC inhibitor U73122 prevented NPS-induced anxiolysis in NPS-sensitive amygdalar neurons.

The MeA pointed out as an important relay station and regulator of emotional responses including anxiety-related behaviors (LeDoux, 2007; Keshavarzi *et al.*, 2014). It receives input from various brain regions involved in sensory processing, neuroendocrine and autonomic regulation including the pericoerulear region and the parabrachial nucleus (Moore & Bloom, 1979; Saper & Loewy, 1980). In the latter brain regions, a cluster of predominantly glutamatergic NPS-immunoreactive neurons has been identified (Xu *et al.*, 2007). This suggested that NPS neurons project towards the MeA thereby regulating behavioral responses. In rats, in-situ hybridization revealed that the MeA and the intercalated nucleus of the amygdala prominently express NPSR, whereas NPSR expression in other amygdala nuclei is almost negligible (Xu *et al.*, 2007). This was recently confirmed by immunohistochemical localization of NPSR at protein level (Leonard & Ring, 2011), although the specificity of the available NPSR antibodies has been questioned (Slattery *et al.*, 2015).

Our data demonstrating that NPS infusion into the MeA reduced the anxiety-related behavior both on the EPM and in the OF of male rats, confirm the robust anxiolytic profile of NPS described following icv infusion (Xu *et al.*, 2004; Leonard *et al.*, 2008; Rizzi *et al.*, 2008; Vitale *et al.*, 2008; Wegener *et al.*, 2011; Slattery *et al.*, 2015; Zoicas *et al.*, 2016) and intranasal application (Ionescu *et al.*, 2012; Lukas & Neumann, 2012; Dine *et al.*, 2015) in both rats and mice, and infusion into the lateral and basolateral amygdala in mice (Jungling *et al.*, 2008). Specifically, intra-MeA infusion of NPS increased the percentage of time the animals spent on

the open arms of the EPM and in the exposed center zone of the OF indicating reduced anxiety levels.

In-vitro activation of the NPSR has been described to increase intracellular Ca^{2+} levels and to phosphorylate ERK1/2 in NPSR-transfected HEK293T cells (Reinscheid *et al.*, 2005). Further, NPS-induced mobilization of intracellular Ca^{2+} has been reported in NPSR-transfected hippocampal mouse neurons *in vitro*, an effect that was strictly dependent on PLC activity (Erdmann *et al.*, 2015). As activation of intracellular signaling cascades is cell-type specific and depends on the cellular micro-environment, the NPS-induced increase in intracellular Ca^{2+} levels and activation of ERK1/2 found *in vitro* may not necessarily reflect intracellular signaling upon NPS binding to its receptor within the brain. My in-vivo results are the first to show NPSR-induced activation of intracellular signaling cascades within the brain. Specifically, quantification of pCaMKIIα as a biological marker of NPSR-mediated Ca^{2+} influx after icv NPS revealed increased relative quantities of pCaMKIIα reflecting NPS-induced rise in intracellular Ca^{2+} levels. My results also demonstrate NPS-induced activation of the MAPK pathway in amygdala punches as reflected by increased pERK1/2 levels in relation to both, total ERK1/2 and *beta*-tubulin. Thus, NPSR-evoked phosphorylation and synthesis of CaMKIIα and the phosphorylation of ERK1/2 provide important confirmation of intracellular actions of NPS in the amygdala. However, my results are based on amygdala micropunches. Therefore, it remains elusive, whether the described NPSR-mediated pathway activation is restricted to NPSR-positive neurons. Thus, future studies should address signal amplification at cellular level by fluorescent labeling of neurons using NPSR promoter-based expression of reporter proteins.

As in-vitro studies demonstrated that NPSR can couple to intracellular Ca^{2+} as well as cAMP pathways, indicating interaction with both G_q and G_s types of G proteins (Reinscheid *et al.*, 2005), I aimed to reveal the specific involvement of PLC and/or AC signaling in NPS-induced anxiolysis. As an initial approach, I infused a cocktail composed of both, the aminosteroidic PLC inhibitor U73122 and the non-competitive AC inhibitor DDA prior to NPS infusion into the

MeA. NPS failed to induce anxiolysis in rats pre-treated with an inhibitor cocktail composed of U73122 and DDA indicating that either both or one of these intracellular pathways in the MeA are critically involved in NPS-induced behavioral changes. Next, each of the inhibitors was separately applied prior to local infusion of NPS. Separate pre-infusion of U73122 prevented the anxiolytic effect of locally infused NPS both on the EPM and in the OF, suggesting that activation of PLC is crucial to orchestrate acute NPS-induced anxiolysis. In contrast, separate pre-infusion of DDA failed to block NPS-induced anxiolysis suggesting that the behavioral effect is independent of AC activation. Although NPS was already found to induce cAMP accumulation in HEK293T cells *in vitro* (Reinscheid *et al.*, 2005), a cAMP-independent mechanism seems to be involved in the anxiolytic effect of NPS in the MeA. My observation that U73122 and DDA, when infused alone, did not significantly alter anxiety-like behavior compared to control, excluded the possibility that the inhibitors changed baseline anxiety.

Based on their chemical structure both, U73122 and DDA, are cell membrane-permeable. Thus, inhibitor infusion 20 min prior local NPS treatment should be sufficient to locally block the respective effector proteins. The different doses of U73122 and DDA used need some considerations: U73122 is reported to reliably inhibit PLC (MacMillan & McCarron, 2010), and usually used at a concentration of 10 µM *in vitro* (Erdmann *et al.*, 2015). As the binding domain of PLC isoforms is highly conserved (Rhee *et al.*, 1989; Rhee & Bae, 1997), U73122 should inhibit all isoforms of PLC (Carvou *et al.*, 2007). Moreover, U73122 reduces Ca^{2+} release, when evoked by direct activation of inositol-1,4,5-triphosphate receptors or ryanodine receptors independent of G_q or PLC activity (MacMillan & McCarron, 2010). Here, we used a dose of 0.5 nmol of U73122 for local infusion into each MeA.

In mammals, nine isoforms of AC are expressed catalyzing the production of the second messenger cAMP (Hanoune & Defer, 2001). A Ca^{2+}/Calmodulin-dependent mechanism was demonstrated to activate the AC isoforms 1, 3 and 8 (MacNeil *et al.*, 1985; Halls & Cooper, 2011). Hence, this demonstrates that intracellular pathways do not necessarily act in a linear

fashion, but can be integrated to bring about the appropriate physiological and behavioral responses. However, whether NPS-evoked cAMP accumulation depends on local rise in intracellular Ca^{2+} levels needs further investigation. For example, the analysis of NPSR / G protein interactions using fluorescence resonance energy transfer might demonstrate, whether NPSR stimulation recruits both G_q and G_s proteins or whether cAMP accumulation is maintained by a Ca^{2+}-dependent activation of AC. Herein, I used DDA to block the membrane-bound AC. The half-maximal inhibitory concentration of DDA is described with 250 µM *in vitro* (Holgate *et al.*, 1980; Ogawa *et al.*, 1995). Therefore, I infused DDA at a 25-fold higher concentration in order to exert a potentially similar effective inhibition compared to U73122. The total amount of U73122 (0.5 nmol) and DDA (12.5 nmol) applied was selected following diffusion-based calculations in order to maintain at least half-maximal inhibition of the effector proteins within the MeA.

In summary, the *in vivo* data identified another brain region in rats, the MeA, where NPS reliably exerts anxiolytic properties, and demonstrated that this behavioral effect is strictly dependent upon local NPSR-mediated PLC activation. I could further show that icv NPS infusion induced phosphorylation and synthesis of CaMKIIα in amygdala punches, thereby promoting the activation of the MAPK pathway as another NPSR-mediated intracellular signaling cascade. These findings contribute to a broader knowledge about the molecular, cellular, and behavioral consequences of NPSR activation in the context of its profound anxiolytic profile.

Chapter III: Efficiency of DREADD system in PVN-OXT neurons

Chemogenetics is based on genetically engineered GPCRs that are activated by biologically inert drugs (Boyden *et al.*, 2005; Armbruster *et al.*, 2007). During the last decade, DREADDs have evolved as a new technique to regulate the activity of a particular neuronal population. As the hypothalamic PVN consists of a heterogeneous group of neurons expressing amongst others OXT, vasopressin and CRH, pharmacological approaches are limited in a way, since icv or even local infusions to inhibit or activate neurons act more generally rather than specifically on a subpopulation of PVN-OXT neurons. In a myriad of neurophysiological and translational settings, DREADD technology has been used in different species to specifically modulate the activity of various cell types, for example serotonergic neurons demonstrating that acute enhancement of serotonergic activity in the hindbrain, but not inhibition, is anxiogenic (Teissier *et al.*, 2015). Other DREADD studies have revealed an important contribution of inhibitory circuitry in the medial prefrontal cortex to mood regulation (Perova *et al.*, 2015; Whissell *et al.*, 2016). With respect to OXT neurons, there is still a lack of precise temporal control that causes complications when attempting to dissect complex circuitries involved in anxiety-, depressive- and aggressive-like behavior, fear responses, or empathy. Thus, it is essential to validate DREADD as a specific tool to modulate OXT neuronal activity. In this context it was also the aim to characterize the specific temporal dynamics of DREADD-evoked OXT neuron activation. OXT is released within the brain, both from soma and dendrites within the PVN and SON, as well as from axon terminals in distant brain and spinal cord areas (Landgraf & Neumann, 2004; Ludwig & Leng, 2006; Knobloch *et al.*, 2012; Eliava *et al.*, 2016) and, moreover, OXT can be released from the neurohypophysis into the circulation in response to various stimuli (Neumann & Landgraf, 2012). For instance forced swim stress has been demonstrated to result in both, increased central and peripheral OXT release (Wotjak *et al.*, 1998). However, it has repeatedly been shown that central OXT release does not necessarily coincide with peripheral OXT secretion (Engelmann *et al.*, 2004; Torner *et al.*, 2017). Herein, I

demonstrated that chemogenetic activation of OXT neurons resulted in increased OXT content in plasma samples and PVN microdialysates indicative for evoked axonal and somato-dendritic OXT release in the periphery and the PVN, respectively, whereas local OXT release within the lateral septum was not altered. Moreover, chemogenetic stimulation of OXT neurons reduced anxiety-related behavior, increased self-grooming, and partly attenuated ethanol-induced locomotor impairments.

In order to monitor local OXT release within the PVN as a consequence of chemogenetic OXT neuron activation, I infused $AAV_{1/2}$OXTpr-hM3Dq-mCherry bilaterally into the PVN. Here, hM3Dq was expressed selectively under the control of an OXT promoter fragment in PVN-OXT neurons and, hence, DREADD expression was confined to PVN-OXT neurons as illustrated in Fig. 18. In human pulmonary artery smooth muscle cells, stimulation of hM3Dq by CNO has been shown to activate PLC and thereby increases intracellular Ca^{2+} levels in an IP_3-dependent manner (Armbruster *et al.*, 2007). A rise in intracellular Ca^{2+} concentration is a prerequisite for neuronal OXT release (Ludwig *et al.*, 2002; Ludwig & Leng, 2006; Ludwig *et al.*, 2016). On experimental day 1, OXT content in microdialysates sampled under otherwise basal conditions from conscious rats was not increased during the 1st (0-30 min), but peaked within the 2nd 30-min dialysate (30-60 min) after CNO administration indicative for increased local OXT release in comparison to Veh-control injected with sterile PBS. This effect was reliably recapitulated on experimental day 2, as OXT content in microdialysates was doubled within the 2nd 30-min sampling period following CNO administration, further demonstrating maximal OXT release between 30-60 min after chemogenetic activation of OXT neurons. In accordance with these findings, analysis of plasma concentrations of CNO demonstrated a prominent peak 30 min following ip injection of CNO (Guettier *et al.*, 2009). Thus, bioavailable CNO binds to designer receptors at around 30 min following ip injection, which explains the increased OXT content in the 2nd 30-min dialysate following CNO administration. Various reports controversially describe the intensity and duration of CNO-induced activation of DREADD-expressing cell types

(Alexander *et al.*, 2009). Here, OXT content in microdialysates was still increased within the 3rd 30-min dialysate following CNO injection compared to ip Veh-control suggesting a longer-lasting stimulation of the OXT neurons within the PVN.

Forced swim stress has been demonstrated to trigger OXT release within the PVN (Wigger & Neumann, 2002). In line with this, 5-min forced swim stress at the beginning of the 3rd sampling period reliably increased OXT content in microdialysates in the control group compared to baseline levels. In rats, transfected with hM3Dq under the control of the OXT promoter fragment, forced swim stress failed to further enhance OXT release in AAV^+/CNO^+ group suggesting the incidence of a ceiling effect. As the release of Ca^{2+} from intracellular stores triggers dendritic OXT release, which can become self-sustaining and thus long-lasting due to autocrine mechanisms (Lambert *et al.*, 1994; Ludwig *et al.*, 2002), it might explain the increased OXT content in microdialysates indicative for increased brain OXT release over a larger timescale. In conclusion, the monitoring of local somato-dendritic OXT release within the PVN as a consequence of chemogenetic activation of PVN-OXT neurons demonstrates a reliable chemogenetic activation of PVN-OXT neurons and describes the spatiotemporal release patterns of OXT.

Moreover, I postulated an increase in local OXT release within the lateral septum as a consequence of chemogenetic activation of OXT neurons located in the PVN, SON and AN. Although OXT neurons were successfully transfected with an OXTpr-hM3Dq-mCherry construct bilaterally in all three hypothalamic nuclei expressing OXT, monitoring of septal OXT revealed no measurable differences in local OXT release during the 30-min sampling periods. This finding is in contrast to my hypothesis and need some elucidation with respect to microdialysis procedure: First, the microdialysis procedure is limited to a 30-min dialysis period, as shorter sampling periods result in lower sampling volumes and OXT concentrations near the detection limit, thus making it difficult to monitor short bursts of OXT release. Second, due to the low number of septal OXT fibers, it is problematic to adequately place the microdialysis probe

resulting in inter-individual differences in OXT content in dialysates that might explain the high standard error of the mean when delta OXT levels were analyzed.

In order to analyze the consequence of chemogenetic OXT neuron activation in PVN, SON and AN on peripheral OXT release, I examined OXT content in plasma samples collected via jugular vein catheter 45 min before and after chemogenetic stimulation, respectively. Here, my results indicate that basal OXT concentration in plasma did not differ between treatment groups, demonstrating that rAAV infusion and expression of an excitatory DREADD does not alter basal OXT release into the periphery. Following chemogenetic activation of OXT neurons within the hypothalamic PVN, SON and AN, plasma OXT concentration was more than doubled when animals were treated with CNO, whereas plasma OXT in the control group was not altered. This result is indicative for increased axonal OXT release via the neurohypophysis into the blood stream after chemogenetic activation of hypothalamic OXT neurons. My findings are in line with increased local OXT release within the PVN during the 2nd 30-min sampling period post treatment, demonstrating DREADD technique as a powerful tool to reliably increase the activity of hypothalamic OXT neurons.

In order to analyze behavioral consequences of CNO-evoked activation of OXT neurons within the PVN, I focused on three independent behavioral readout parameters described to be reliably influenced by OXT. OXT applied icv is known to increase self-grooming in rats (Drago *et al.*, 1986), a behavior blocked by pre-infusion of an OXTR-A into the nucleus accumbens (Drago *et al.*, 1991). Here, I monitored grooming behavior during ongoing microdialysis on experimental day 1 and found that self-grooming behavior peaked during the 2nd 30-min sampling period (+60 min) of microdialysis after CNO administration, at a time of highest OXT release following chemogenetic activation of PVN-OXT neurons. However, self-grooming behavior was restored to control level during the 3rd 30-min sampling period (+90 min) even in the presence of increased OXT-release, which might be an effect of OXTR desensitization following stimulation within a 20-min period (Conti *et al.*, 2009). This limits the time window

when behaviors are analyzed that depend on intracellular OXTR signaling. As self-grooming is unlikely due to local OXT release within the PVN, it is quite plausible that chemogenetic activation of PVN-OXT neurons evokes OXT release in other brain regions, too, i.e. the nucleus accumbens. Since I monitored central OXT release exclusively within the PVN and lateral septum, I cannot rule out intracerebral OXT release as a consequence of chemogenetic stimulation of OXT neurons in other brain regions. To draw a clear picture with respect to locally increased OXT release in various brain regions, a receptor-autoradiography is needed in order to quantify relative amount of OXT binding to its GPCR following chemogenetic activation of hypothalamic OXT neurons.

Besides OXT-evoked increase in self-grooming, intra-PVN infusion of synthetic OXT has repeatedly been shown to reliably reduce general anxiety-related behavior in male rats (Blume *et al.*, 2008; Neumann, 2008; van den Burg & Neumann, 2011; van den Burg *et al.*, 2015). Moreover, mating-induced release of OXT within the PVN has been associated with reduced anxiety-related behavior in male rats (Waldherr & Neumann, 2007). Therefore, in a separate cohort of hM3Dq-expressing rats, I assessed anxiety-like behavior in the LDB 55 min after CNO injection. Rats bilaterally expressing hM3Dq in PVN-OXT neurons spent more time in the lit compartment and tended to increase the number of entries into the light box in the presence of CNO, indicative for being less anxious.

The third behavioral effect of OXT I have tested in the context of chemogenetic stimulation of OXT neurons in the PVN was the prevention of ethanol-induced locomotor impairment shown in rats (Pucilowski *et al.*, 1985; Bowen *et al.*, 2015). Specifically, McGregor and colleagues demonstrated that OXT prevents the potentiating actions of ethanol on $GABA_A$ receptor signaling. Although these OXT effects were found to be independent of OXTR signaling, I examined the consequence of chemogenetic activation of PVN-OXT neurons on ethanol-induced locomotor impairments in two locomotor tests. CNO administration in rats expressing an excitatory DREADD in PVN-OXT neurons failed to attenuate the ataxic effects in the wire-

hanging test, but improved the performance in the rightning reflex 65 min after ip CNO or 35 min after ip ethanol injection, respectively. In detail, CNO administration reduced the duration of the rightning reflex in ethanol-pretreated rats suggesting that activation of brain OXT neurons beneficially counteracts ethanol-induced prolongation of the rightning reflex. The differences in the behavioral outcome of these two studies need further critical discussion: In the experiments of McGregor and colleagues, a relatively high dose of 1 µg of OXT was applied icv (Bowen *et al.*, 2015) thus reaching all relevant brain regions. After CNO administration, only a specific population of OXT neurons in the PVN was targeted and activated, and it is unknown where these neurons project to and to which extent they also release OXT.

Altogether, DREADD represents a powerful tool to manipulate the activity of hypothalamic OXT neurons. Herein, I demonstrated a reliable increase in both central and peripheral OXT release as a consequence of chemogenetic activation of OXT neurons. Moreover, my results indicate that stimulation of an excitatory DREADD selectively expressed in OXT neurons increases self-grooming, reduces anxiety-related behavior, and partly attenuates ethanol-induced locomotor impairments. Although experiments in the presence of an OXTR-A are necessary to provide a final causal link, my results validate DREADD as a specific tool to modulate OXT neuronal activity. In this context, my data also characterize the specific temporal dynamics of DREADD-evoked OXT neuron activation and, thus, proves the DREADD technology as a reliable tool in order to dissect complex circuitries involved in emotional behaviors, such as anxiety and fear.

Perspectives and future directions

The findings described in this thesis open up a number of additional research questions, which will lead to a better understanding of the etiology of anxiety disorders and of the underlying mechanisms responsible for the anxiolytic profile of NPS. These future studies can be divided into the following sections:

OXTR expression in NPS neurons and OXT projections to the locus coeruleus

My findings demonstrate a novel intra-hypothalamic mechanism involving NPSR-expressing OXT neurons of the PVN that are activated by NPS. Here, OXT neurons treated with NPS respond with transient increase in intracellular Ca^{2+} and local somato-dendritic OXT release. I demonstrated that stimulation of local OXT neurons is essential for NPS-induced anxiolysis, as this effect was blocked by specific pharmacological and chemogenetic inhibition of the OXT system. These findings provide important evidence for interactions of NPS with another neuropeptidergic system, but obviously warrant further research into how these circuits orchestrate specific physiological effects resulting in distinct behavioral outputs, i.e. such as the regulation of stress or anxiety-related behavior. Based on a growing interest in the development of therapeutic strategies for anxiety- and stress-related disorders, a wide-ranging knowledge about the neuronal and behavioral consequences of brain neuropeptide signaling modulating emotional responses is required for efficient development of new therapeutic strategies.

It has been demonstrated that NPS-synthesizing neurons originating in the pericoerulear region innervate the PVN (Xu *et al.*, 2004; Xu *et al.*, 2007). Interestingly, in situ hybridization revealed OXTR expression in the pericoerulear region and parabrachial nucleus (Vaccari *et al.*, 1998; Yoshida *et al.*, 2009). Thus, an interesting hypothesis is that NPS and OXT neurons form a

bilateral functional circuitry to modulate behavioral and physiological parameters. However, whether NPS-synthesizing neurons express the OXTR or whether these neurons are innervated by OXT fibers remains elusive. To answer these questions, NPS-immunoreactive neurons have to be labeled in transgenic rats expressing Venus selectively under the control of the OXTR promoter fragment. Future antero- and retrograde tracing studies in combination with an immunofluorescent staining of both, OXT and NPS, will unravel potential OXT afferents within the NPS-synthesizing brain clusters.

Examination of the intracellular signaling mechanisms of NPSR-positive neurons

I demonstrated that pharmacological blockade of the membrane-bound PLC inhibited NPS-induced anxiolysis suggesting G_q protein activation, whereas infusion of an AC inhibitor failed to block NPS-induced anxiolysis. Whether NPS activates AC by a G_s-dependent mechanism is currently not known, as increased Ca^{2+} levels have been demonstrated to activate Ca^{2+}/calmodulin-dependent AC isoforms 1, 3 and 8 (MacNeil *et al.*, 1985; Halls & Cooper, 2011). Thus, fluorescence resonance energy transfer approach is necessary to analyze possible NPSR interaction with G_s protein. Moreover, the route of extracellular Ca^{2+} entry in NPSR-positive cells needs to be investigated. In most cells, Ca^{2+} release from the endoplasmic reticulum (ER) and the according fall in ER-luminal Ca^{2+} concentration subsequently activates Ca^{2+} channels in the cell membrane in a process called store-operated Ca^{2+} entry (SOCE). Pape and colleagues demonstrated a reduced amplitude and duration of the slow Ca^{2+} entry in the presence of two SOCE inhibitors called ML-9 and SKF96365 (Erdmann *et al.*, 2015). Both blockers inhibit the stromal interaction molecule 1 (which activates Ca^{2+} release-activated Ca^{2+} channel 1 upon Ca^{2+} decrease to a critical level in the ER), but they also block voltage-gated Ca^{2+} channels and transient receptor potential cation channels (Merritt *et al.*, 1990; Varnai *et al.*, 2009; Singh *et al.*, 2010). Therefore, further studies should address the underlying mechanism of extracellular Ca^{2+} entry and the related cellular activation.

NPSR-transfected cell cultures represent a limited model to study intracellular signaling

pathways as intracellular signaling depends on the cellular microenvironment. Therefore, evaluation of a microarray or next generation sequencing in RNA samples extracted from brain tissue micropunches are necessary to reveal NPS-induced gene expression. Analysis of the target genes and the knowledge about the putative transcription factor binding sites to the respective promoter will confine the number of signaling pathways activated upon NPSR activation.

Projections of NPS(R)-positive neurons and their involvement in stress- and fear circuitries

I have found that NPS stimulates the activity of OXT neurons within the PVN, which, as a consequence of activation, exert anxiolytic activity. Besides anxiolysis, OXT is well described for its stress-coping actions (Neumann & Landgraf, 2012). In this context, it would be of interest to evaluate possible stress-protective effects of NPS. Stress is a critical factor that induces an anxiogenic phenotype (Roozendaal *et al.*, 2009). Following acute stress exposure, an increased number of cFos-positive NPS neurons indicative of an activation of the endogenous NPS system due to CRH-R1 stimulation on NPS-immunoreactive neurons in mice have been demonstrated (Jungling *et al.*, 2012). In addition, Singewald and colleagues showed increased NPS release in the amygdala following forced swim stress (Ebner *et al.*, 2011). These data clearly identify the NPS system to play a major role in stress responsiveness. Whether NPS exerts stress-protective effects is currently not known. Thus, it is suitable to analyze the effect of a chemogenetic as well as pharmacological stimulation or inhibition, respectively, of the NPS/NPSR system and its effect on hypothalamo-pituitary adrenal axis activity, plasma adrenocorticotropic hormone and corticosterone levels in rodents in response to a stressor. Specifically, this could be achieved by infusion of $AAV_{1/2}$NPSpr-hM3Dq-mCherry or $AAV_{1/2}$-NPSpr-hM4Di-mCherry or by icv infusion of either NPS or SHA-68 prior to 5-min exposure to stressors such as forced swimming or a novel environment.

In rats selectively bred for high anxiety-related behavior, icv NPS reliably reduced freezing

during cued fear extinction in the cued fear-conditioning model (Slattery *et al.*, 2015). However, within the central nucleus of the amygdala, NPSR expression is almost negligible (Xu *et al.*, 2007). Whether fear-on/off neurons are innervated by afferents deriving from NPSR-positive neurons located in the MeA remains elusive. At cellular and tissue-wide levels, fluorescent labeling of NPSR-positive neurons using adenoviral promoter-based reporter protein expression provides the basis to successfully trace projections of NPSR-positive neurons and their potential effects on other neuronal populations such as fear-on/off neurons in the central nucleus of the amygdala.

Spatiotemporal activation patterns of OXT neurons expressing an excitatory DREADD

The DREADD technique represents a powerful tool to unravel neuronal circuits, and contributes to the experimental regulation of the behavioral phenotype of an individual. Here, my findings demonstrate increased OXT release locally within the PVN and in the periphery as a consequence of DREADD-evoked activation of OXT neurons. Sampling of microdialysates is limited to a 30-min dialysis period, as shorter sampling periods may result in lower sampling volumes and OXT concentrations near the detection limit, thus making it difficult to monitor short bursts of OXT release especially in brain regions innervated by few OXT fibers. Therefore, my findings would benefit from three experimental approaches in order to draw a clear conclusion regarding the spatiotemporal resolution of DREADD-induced neuronal activation of OXT neurons: First, a receptor-autoradiography will give rise to increased relative OXT release and binding to its receptor once the hypothalamic OXT neurons are activated by DREADD technique. Second, in vivo electrophysiological recordings of OXT neurons in anesthetized rats before and after administration of CNO ip will illuminate the exact time points for first and maximal stimulatory effects of chemogenetic activation of OXT neurons. Finally, Ca^{2+} imaging using genetically encoded Ca^{2+} sensors (e.g. GCaMP6s) selectively co-expressed with an excitatory DREADD in OXT neurons will demonstrate the intensity of CNO-evoked Ca^{2+} influx as a consequence of neuronal activation. Moreover, in the presence of Ca^{2+} channel blockers, the

source of Ca^{2+} can be identified, which might be indicative for the type of OXT release since the source of Ca^{2+} impacts on somato-dendritic as well as axonal release and even priming effects as previously described (Ludwig et al., 2016).

With the help of these approaches it should be possible to expand the findings presented in this thesis and to understand the neuronal circuits underlying the potent anxiolytic and fear-attenuating effects of NPS and OXT. These factors could potentially serve as a basis for the development of novel pharmacological treatments of anxiety disorders.

Acknowledgement

First of all, I thank Prof. Dr. Inga Neumann for the opportunity to perform my research in her group, for the permanent support and scientific guidance that contributed not only to the quality of this thesis, but also to my personal and scientific development. Many thanks for the excellent expertise, shared knowledge, and fruitful discussions.

Special thanks goes to Prof. Dr. Oliver Bosch, Prof. Dr. David Slattery, and the senior scientists Dr. Ben Jurek and Dr. Trynke de Jong for their kind advice during the initial steps in the lab that modeled my practical skills and experimental planning, for the helpful scientific discussions, and for introducing me to the scientific field of neuroscience at international conferences.

Warm acknowledgement goes to our collaborators Dr. Valery Grinevich and Dr. Marina Eliava. Many thanks for fruitful discussions, the constant support, and the warm welcome in your lab in Heidelberg during my visit. Special thanks goes to Dr. Alexandre Charlet and Stephanie Goyon for advancing my PhD project with a latest-state-of-the-art technique.

I thank Rodrigue Maloumby, Gabriele Schindler, Andrea Havasi, and Martina Fuchs for the great help with surgery, brain cutting, ordering, and the special task forces whenever I needed something unique for surgeries.

A great thanks goes to my Master students Anna Schmidtner, Sandra Tillmann, Valentina Rodigari, Sanchita Pasi, Lena Oppenländer, and Sophia Probst for excellent experimental assistance.

I thank Rohit Menon, Dr. Doris Bayerl, Anna Bludau, Vinicius Oliveira, Anna Schmidtner, and all former and new members of the group for the friendly atmosphere in the lab, lively discussions and helpful hands.

Finally, warm acknowledgements go to my family and my life partner Roland Sintic, my friends for the mental support, love, positive thinking, helpful advice, and permanent encouragement.

Curriculum vitae

Personal information

Name:	Thomas Grund
Date of birth:	26th of October 1988
Place of birth:	Arnstadt, Thuringia, Germany
Nationality:	German

Education

Since 2013	PhD student in Neurobiology at the University of Regensburg, Department of Behavioural and Molecular Neurobiology, Prof. Dr. Inga D. Neumann
2010-2013	Master of Science in Biology, University of Regensburg, Regensburg
2007-2010	Bachelor of Science in Biology, University of Regensburg, Regensburg
1999-2007	Johann-Gottfried-Herder Gymnasium, Arnstadt
1995-1999	Ludwig-Bechstein Grundschule, Arnstadt

Working life

Since 2016	DanceImperial GmbH, Regensburg
2009-2011	GeneArt/Lifetechnologies: Oligosynthesis, Regensburg

List of publications

Grund, T., Goyon, S., Charlet, A., Grinevich, V., Neumann, I.D. (under review) At the core of neuropeptidergic modulation of anxiety: Activation of oxytocin neurons by neuropeptide S. *Journal of Physiology*

Grund, T., Neumann, I.D. (in revision) Neuropeptide S induces acute anxiolysis by phospholipase C-dependent signaling within the medial amygdala. *Neuropsychopharmacology*

Grund, T., Grinevich, V., Neumann, I.D. (2016) Interaction of neuropeptide S with the endogenous oxytocin system within the hypothalamic PVN. *Psychoneuroendocrinology,* **71S**, 61-62, IPSNE Conference, Miami, 2016

De Jong, T.R., Menon, R., Bludau, A., **Grund, T.**, Biermeier, V., Klampfl, S.M. Jurek, B., Bosch, O.J., Hellhammer, J., Neumann, I.D. (2015) Salivary oxytocin concentrations in response to running, sexual self-stimulation, breastfeeding and the TSST: The Regensburg Oxytocin Challenge (ROC) study. *Psychoneuroendocrinology*, **62**, 381-388.

Slattery, D.A., Naik, R.R., **Grund, T.**, Yen, Y.C., Sartori, S.B., Fuchsl, A., Finger, B.C., Elfving, B., Nordemann, U., Guerrini, R., Calo, G., Wegener, G., Mathe, A.A., Singewald, N., Czibere, L., Landgraf, R. & Neumann, I.D. (2015) Selective breeding for high anxiety introduces a synonymous SNP that increases neuropeptide s receptor activity. *J Neurosci*, **35**, 4599-4613.

van den Burg, E.H., Stindl, J., **Grund, T.**, Neumann, I.D. & Strauss, O. (2015) Oxytocin Stimulates Extracellular Ca(2+) Influx Through TRPV2 Channels in Hypothalamic Neurons to Exert Its Anxiolytic Effects. *Neuropsychopharmacology*, **40**, 2938-2947.

References

Adori, C., Barde, S., Vas, S., Ebner, K., Su, J., Svensson, C., Mathe, A.A., Singewald, N., Reinscheid, R.R., Uhlen, M., Kultima, K., Bagdy, G. & Hokfelt, T. (2015) Exploring the role of neuropeptide S in the regulation of arousal: a functional anatomical study. *Brain Struct Funct*.

Akerboom, J., Rivera, J.D., Guilbe, M.M., Malave, E.C., Hernandez, H.H., Tian, L., Hires, S.A., Marvin, J.S., Looger, L.L. & Schreiter, E.R. (2009) Crystal structures of the GCaMP calcium sensor reveal the mechanism of fluorescence signal change and aid rational design. *J Biol Chem*, **284**, 6455-6464.

Alexander, G.M., Rogan, S.C., Abbas, A.I., Armbruster, B.N., Pei, Y., Allen, J.A., Nonneman, R.J., Hartmann, J., Moy, S.S., Nicolelis, M.A., McNamara, J.O. & Roth, B.L. (2009) Remote control of neuronal activity in transgenic mice expressing evolved G protein-coupled receptors. *Neuron*, **63**, 27-39.

Allen, I.C., Pace, A.J., Jania, L.A., Ledford, J.G., Latour, A.M., Snouwaert, J.N., Bernier, V., Stocco, R., Therien, A.G. & Koller, B.H. (2006a) Expression and function of NPSR1/GPRA in the lung before and after induction of asthma-like disease. *Am J Physiol-Lung Cell Mol Physiol*, **291**, L1005-L1017.

Allen, I.C., Pace, A.J., Jania, L.A., Ledford, J.G., Latour, A.M., Snouwaert, J.N., Bernier, V., Stocco, R., Therien, A.G. & Koller, B.H. (2006b) Expression and function of NPSR1/GPRA in the lung before and after induction of asthma-like disease. *Am J Physiol-Lung Cell Mol Physiol*, **291**, L1005-1017.

Allgulander, C., Florea, I. & Huusom, A.K. (2006) Prevention of relapse in generalized anxiety disorder by escitalopram treatment. *Int J Neuropsychopharmacol*, **9**, 495-505.

Argiolas, A. & Melis, M.R. (2004) The role of oxytocin and the paraventricular nucleus in the sexual behaviour of male mammals. *Physiol Behav*, **83**, 309-317.

Armbruster, B.N., Li, X., Pausch, M.H., Herlitze, S. & Roth, B.L. (2007) Evolving the lock to fit the key to create a family of G protein-coupled receptors potently activated by an inert ligand. *PNAS*, **104**, 5163-5168.

Armstrong, W.E. (1995) Morphological and electrophysiological classification of hypothalamic supraoptic neurons. *Prog Neurobiol*, **47**, 291-339.

Arun, K.H., Kaul, C.L. & Ramarao, P. (2005) Green fluorescent proteins in receptor research: an emerging tool for drug discovery. *J Pharmacol Toxicol Methods*, **51**, 1-23.

Atasoy, D., Betley, J.N., Su, H.H. & Sternson, S.M. (2012) Deconstruction of a neural circuit for hunger. *Nature*, **488**, 172-177.

Bale, T.L., Davis, A.M., Auger, A.P., Dorsa, D.M. & McCarthy, M.M. (2001) CNS region-specific oxytocin receptor expression: importance in regulation of anxiety and sex behavior. *J Neurosci*, **21**, 2546-2552.

Ban, T.A. (2007) Fifty years chlorpromazine: a historical perspective. *Neuropsychiatr Dis Treat*, **3**, 495-500.

Beck, B., Fernette, B. & Stricker-Krongrad, A. (2005) Peptide S is a novel potent inhibitor of voluntary and fast-induced food intake in rats. *Biochem Biophys Res Comm*, **332**, 859-865.

Beiderbeck, D.I., Lukas, M. & Neumann, I.D. (2014) Anti-aggressive effects of neuropeptide S independent of anxiolysis in male rats. *Front Behav Neurosci*, **8**, 185.

Ben-Barak, Y., Russell, J.T., Whitnall, M.H., Ozato, K. & Gainer, H. (1985) Neurophysin in the hypothalamo-neurohypophysial system. I. Production and characterization of monoclonal antibodies. *J Neurosci*, **5**, 81-97.

Bergquist, F. & Ludwig, M. (2008) Dendritic transmitter release: a comparison of two model systems. *J Neuroendocrinol*, **20**, 677-686.

Bernier, V., Stocco, R., Bogusky, M.J., Joyce, J.G., Parachoniak, C., Grenier, K., Arget, M., Mathieu, M.C., O'Neill, G.P., Slipetz, D., Crackower, M.A., Tan, C.M. & Therien, A.G. (2006) Structure-function relationships in the neuropeptide S receptor: molecular consequences of the asthma-associated mutation N107I. *J Biol Chem*, **281**, 24704-24712.

Berridge, M.J., Lipp, P. & Bootman, M.D. (2000) The versatility and universality of calcium signalling. *Nat Rev Mol Cell Biol*, **1**, 11-21.

Blume, A., Bosch, O.J., Miklos, S., Torner, L., Wales, L., Waldherr, M. & Neumann, I.D. (2008) Oxytocin reduces anxiety via ERK1/2 activation: local effect within the rat hypothalamic paraventricular nucleus. *Eur J Neurosci*, **27**, 1947-1956.

Boender, A.J., de Jong, J.W., Boekhoudt, L., Luijendijk, M.C.M., van der Plasse, G. & Adan, R.A.H. (2014) Combined Use of the Canine Adenovirus-2 and DREADD-Technology to Activate Specific Neural Pathways In Vivo. *PloS one*, **9**.

Bosch, O.J., Kromer, S.A., Brunton, P.J. & Neumann, I.D. (2004) Release of oxytocin in the hypothalamic paraventricular nucleus, but not central amygdala or lateral septum in lactating residents and virgin intruders during maternal defence. *Neuroscience*, **124**, 439-448.

Bosch, O.J., Meddle, S.L., Beiderbeck, D.I., Douglas, A.J. & Neumann, I.D. (2005) Brain oxytocin correlates with maternal aggression: link to anxiety. *J Neurosci*, **25**, 6807-6815.

Bouras, N. & Holt, G. (2007) *Psychiatric and Behavioural Disorders in Intellectual and Developmental Disabilities.* .

Bowen, M.T., Peters, S.T., Absalom, N., Chebib, M., Neumann, I.D. & McGregor, I.S. (2015) Oxytocin prevents ethanol actions at delta subunit-containing GABAA receptors and attenuates ethanol-induced motor impairment in rats. *PNAS*, **112**, 3104-3109.

Boyce-Rustay, J.M. & Holmes, A. (2006) Ethanol-related behaviors in mice lacking the NMDA receptor NR2A subunit. *Psychopharmacology*, **187**, 455-466.

Boyden, E.S., Zhang, F., Bamberg, E., Nagel, G. & Deisseroth, K. (2005) Millisecond-timescale, genetically targeted optical control of neural activity. *Nat Neurosci*, **8**, 1263-1268.

Burnett, C.J. & Krashes, M.J. (2016) Resolving Behavioral Output via Chemogenetic Designer Receptors Exclusively Activated by Designer Drugs. *J Neurosci*, **36**, 9268-9282.

Camarda, V., Rizzi, A., Ruzza, C., Zucchini, S., Marzola, G., Marzola, E., Guerrini, R., Salvadori, S., Reinscheid, R.K., Regoli, D. & Calo, G. (2009) In vitro and in vivo pharmacological characterization of the neuropeptide s receptor antagonist [D-Cys(tBu)5]neuropeptide S. *J Pharm Exp Ther*, **328**, 549-555.

Carter, C.S., DeVries, A.C. & Getz, L.L. (1995) Physiological substrates of mammalian monogamy: the prairie vole model. *Neurosci Biobehav Rev*, **19**, 303-314.

Carvou, N., Norden, A.G.W., Unwin, R.J. & Cockcroft, S. (2007) Signalling through phospholipase C interferes with clathrin-mediated endocytosis. *Cellular signalling*, **19**, 42-51.

Chen, T.W., Wardill, T.J., Sun, Y., Pulver, S.R., Renninger, S.L., Baohan, A., Schreiter, E.R., Kerr, R.A., Orger, M.B., Jayaraman, V., Looger, L.L., Svoboda, K. & Kim, D.S. (2013) Ultrasensitive fluorescent proteins for imaging neuronal activity. *Nature*, **499**, 295-300.

Cheung, W.Y. (1980) Calmodulin plays a pivotal role in cellular regulation. *Science*, **207**, 19-27.

Cho, M.M., DeVries, A.C., Williams, J.R. & Carter, C.S. (1999) The effects of oxytocin and vasopressin on partner preferences in male and female prairie voles (Microtus ochrogaster). *Behav Neurosci*, **113**, 1071-1079.

Chung, S. & Civelli, O. (2006) Orphan neuropeptides. Novel neuropeptides modulating sleep or feeding. *Neuropeptides*, **40**, 233-243.

Civelli, O. (2012) Orphan GPCRs and neuromodulation. *Neuron*, **76**, 12-21.

Civelli, O., Saito, Y., Wang, Z., Nothacker, H.P. & Reinscheid, R.K. (2006) Orphan GPCRs and their ligands. *Pharmacol Therapeutics*, **110**, 525-532.

Clapham, D.E. (2007) Calcium signaling. *Cell*, **131**, 1047-1058.

Clark, S.D., Duangdao, D.M., Schulz, S., Zhang, L., Liu, X., Xu, Y.L. & Reinscheid, R.K. (2011) Anatomical characterization of the neuropeptide S system in the mouse brain by in situ hybridization and immunohistochemistry. *J Comp Neurol*, **519**, 1867-1893.

Clark, S.D., Kenakin, T.P., Gertz, S., Hassler, C., Gay, E.A., Langston, T.L., Reinscheid, R.K. & Runyon, S.P. (2017) Identification of the first biased NPS receptor agonist that retains anxiolytic and memory promoting effects with reduced levels of locomotor stimulation. *Neuropharmacology*, **118**, 69-78.

Conti, F., Sertic, S., Reversi, A. & Chini, B. (2009) Intracellular trafficking of the human oxytocin receptor: evidence of receptor recycling via a Rab4/Rab5 "short cycle". *Am J Physiol Endocrinol Metab*, **296**, E532-542.

Crabbe, J.C., Cotnam, C.J., Cameron, A.J., Schlumbohm, J.P., Rhodes, J.S., Metten, P. & Wahlsten, D. (2003) Strain differences in three measures of ethanol intoxication in mice: the screen, dowel and grip strength tests. *Genes, brain, and behavior*, **2**, 201-213.

Crick, F.H.C. (1979) Thinking About the Brain. *Scientific American*, **241**, 219-&.

Dannlowski, U., Kugel, H., Franke, F., Stuhrmann, A., Hohoff, C., Zwanzger, P., Lenzen, T., Grotegerd, D., Suslow, T., Arolt, V., Heindel, W. & Domschke, K. (2011) Neuropeptide-S (NPS) receptor genotype modulates basolateral amygdala responsiveness to aversive stimuli. *Neuropsychopharmacology*, **36**, 1879-1885.

Davidson, J.R., Foa, E.B., Huppert, J.D., Keefe, F.J., Franklin, M.E., Compton, J.S., Zhao, N., Connor, K.M., Lynch, T.R. & Gadde, K.M. (2004) Fluoxetine, comprehensive cognitive behavioral therapy, and placebo in generalized social phobia. *Arch Gen Psychiatry*, **61**, 1005-1013.

de Jong, T.R., Beiderbeck, D.I. & Neumann, I.D. (2014) Measuring virgin female aggression in the female intruder test (FIT): effects of oxytocin, estrous cycle, and anxiety. *PloS one*, **9**, e91701.

de Jong, T.R., Menon, R., Bludau, A., Grund, T., Biermeier, V., Klampfl, S.M., Jurek, B., Bosch, O.J., Hellhammer, J. & Neumann, I.D. (2015) Salivary oxytocin concentrations in response to running, sexual self-stimulation, breastfeeding and the TSST: The Regensburg Oxytocin Challenge (ROC) study. *Psychoneuroendocrinology*, **62**, 381-388.

de Kock, C.P.J., Wierda, K.D.B., Bosman, L.W.J., Min, R., Koksma, J.J., Mansvelder, H.D., Verhage, M. & Brussaard, A.B. (2003) Somatodendritic secretion in oxytocin neurons is upregulated during the female reproductive cycle. *J Neurosci*, **23**, 2726-2734.

Dine, J., Ionescu, I.A., Avrabos, C., Yen, Y.C., Holsboer, F., Landgraf, R., Schmidt, U. & Eder, M. (2015) Intranasally applied neuropeptide S shifts a high-anxiety electrophysiological endophenotype in the ventral hippocampus towards a "normal"-anxiety one. *PloS one*, **10**, e0120272.

Dolen, G., Darvishzadeh, A., Huang, K.W. & Malenka, R.C. (2013) Social reward requires coordinated activity of nucleus accumbens oxytocin and serotonin. *Nature*, **501**, 179-184.

Domschke, K., Reif, A., Weber, H., Richter, J., Hohoff, C., Ohrmann, P., Pedersen, A., Bauer, J., Suslow, T., Kugel, H., Heindel, W., Baumann, C., Klauke, B., Jacob, C., Maier, W., Fritze, J., Bandelow, B., Krakowitzky, P., Rothermundt, M., Erhardt, A., Binder, E.B., Holsboer, F., Gerlach, A.L., Kircher, T., Lang, T., Alpers, G.W., Strohle, A., Fehm, L., Gloster, A.T., Wittchen, H.U., Arolt, V., Pauli, P., Hamm, A. & Deckert, J. (2011) Neuropeptide S receptor gene -- converging evidence for a role in panic disorder. *Molecular psychiatry*, **16**, 938-948.

Dong, S., Rogan, S.C. & Roth, B.L. (2010) Directed molecular evolution of DREADDs: a generic approach to creating next-generation RASSLs. *Nature protocols*, **5**, 561-573.

Donner, J., Haapakoski, R., Ezer, S., Melen, E., Pirkola, S., Gratacos, M., Zucchelli, M., Anedda, F., Johansson, L.E., Soderhall, C., Orsmark-Pietras, C., Suvisaari, J., Martin-Santos, R.,

Torrens, M., Silander, K., Terwilliger, J.D., Wickman, M., Pershagen, G., Lonnqvist, J., Peltonen, L., Estivill, X., D'Amato, M., Kere, J., Alenius, H. & Hovatta, I. (2010) Assessment of the neuropeptide S system in anxiety disorders. *Biological psychiatry*, **68**, 474-483.

Drago, F., Pedersen, C.A., Caldwell, J.D. & Prange, A.J., Jr. (1986) Oxytocin potently enhances novelty-induced grooming behavior in the rat. *Brain research*, **368**, 287-295.

Drago, F., Sarnyai, Z. & D'Agata, V. (1991) The inhibition of oxytocin-induced grooming by a specific receptor antagonist. *Physiol Behav*, **50**, 533-536.

Ebner, K., Rjabokon, A., Pape, H.C. & Singewald, N. (2011) Increased in vivo release of neuropeptide S in the amygdala of freely moving rats after local depolarisation and emotional stress. *Amino acids*, **41**, 991-996.

Eliava, M., Melchior, M., Knobloch-Bollmann, H.S., Wahis, J., da Silva Gouveia, M., Tang, Y., Ciobanu, A.C., Triana Del Rio, R., Roth, L.C., Althammer, F., Chavant, V., Goumon, Y., Gruber, T., Petit-Demouliere, N., Busnelli, M., Chini, B., Tan, L.L., Mitre, M., Froemke, R.C., Chao, M.V., Giese, G., Sprengel, R., Kuner, R., Poisbeau, P., Seeburg, P.H., Stoop, R., Charlet, A. & Grinevich, V. (2016) A New Population of Parvocellular Oxytocin Neurons Controlling Magnocellular Neuron Activity and Inflammatory Pain Processing. *Neuron*, **89**, 1291-1304.

Engelmann, M., Landgraf, R. & Wotjak, C.T. (2004) The hypothalamic-neurohypophysial system regulates the hypothalamic-pituitary-adrenal axis under stress: an old concept revisited. *Front Neuroendocrinol*, **25**, 132-149.

Erdmann, F., Kugler, S., Blaesse, P., Lange, M.D., Skryabin, B.V., Pape, H.C. & Jungling, K. (2015) Neuronal expression of the human neuropeptide S receptor NPSR1 identifies NPS-induced calcium signaling pathways. *PloS one*, **10**, e0117319.

Fedeli, A., Braconi, S., Economidou, D., Cannella, N., Kallupi, M., Guerrini, R., Calo, G., Cifani, C., Massi, M. & Ciccocioppo, R. (2009) The paraventricular nucleus of the hypothalamus is a neuroanatomical substrate for the inhibition of palatable food intake by neuropeptide S. *Eur J Neurosci*, **30**, 1594-1602.

Feighner, J.P. (1999) Overview of antidepressants currently used to treat anxiety disorders. *J Clin Psychiatry*, **60**, 18-22.

Feisst, C., Albert, D., Steinhilber, D. & Werz, O. (2005) The aminosteroid phospholipase C antagonist U-73122 (1-[6-[[17-beta-3-methoxyestra-1,3,5(10)-trien-17-yl]amino]hexyl]-1H-pyrrole-2,5- dione) potently inhibits human 5-lipoxygenase in vivo and in vitro. *Mol Pharmacol*, **67**, 1751-1757.

Fendt, M., Imobersteg, S., Burki, H., McAllister, K.H. & Sailer, A.W. (2010) Intra-amygdala injections of neuropeptide S block fear-potentiated startle. *Neuroscience letters*, **474**, 154-157.

Ferguson, J.M., Khan, A., Mangano, R., Entsuah, R. & Tzanis, E. (2007) Relapse prevention of panic disorder in adult outpatient responders to treatment with venlafaxine extended release. *J Clin Psychiatry*, **68**, 58-68.

Fields, H.L., Heinricher, M.M. & Mason, P. (1991) Neurotransmitters in nociceptive modulatory circuits. *Annu Rev Neurosci*, **14**, 219-245.

Fisher, T.E. & Bourque, C.W. (1996) Calcium-channel subtypes in the somata and axon terminals of magnocellular neurosecretory cells. *Trends Neurosciences*, **19**, 440-444.

Frank, J.B., Kosten, T.R., Giller, E.L., Jr. & Dan, E. (1988) A randomized clinical trial of phenelzine and imipramine for posttraumatic stress disorder. *Am J Psychiatry*, **145**, 1289-1291.

Fuchs, A.R. & Poblete, V.F., Jr. (1970) Oxytocin and uterine function in pregnant and parturient rats. *Biol Reprod*, **2**, 387-400.

Gauriau, C. & Bernard, J.F. (2002) Pain pathways and parabrachial circuits in the rat. *Exp Physiol*, **87**, 251-258.

Gimpl, G. & Fahrenholz, F. (2001) The oxytocin receptor system: structure, function, and regulation. *Physiological reviews*, **81**, 629-683.

Goodman, W.K., Bose, A. & Wang, Q. (2005) Treatment of generalized anxiety disorder with escitalopram: pooled results from double-blind, placebo-controlled trials. *J Affect Disorders*, **87**, 161-167.

Grant, B.F., Stinson, F.S., Dawson, D.A., Chou, S.P., Dufour, M.C., Compton, W., Pickering, R.P. & Kaplan, K. (2004) Prevalence and co-occurrence of substance use disorders and independent mood and anxiety disorders - Results from the national epidemiologic survey on alcohol and related conditions. *Arch Gen Psychiatry*, **61**, 807-816.

Grayson, D.S., Bliss-Moreau, E., Machado, C.J., Bennett, J., Shen, K., Grant, K.A., Fair, D.A. & Amaral, D.G. (2016) The Rhesus Monkey Connectome Predicts Disrupted Functional Networks Resulting from Pharmacogenetic Inactivation of the Amygdala. *Neuron*, **91**, 453-466.

Gross, C. & Hen, R. (2004) The developmental origins of anxiety. *Nature reviews. Neuroscience*, **5**, 545-552.

Guettier, J.M., Gautam, D., Scarselli, M., Ruiz de Azua, I., Li, J.H., Rosemond, E., Ma, X., Gonzalez, F.J., Armbruster, B.N., Lu, H., Roth, B.L. & Wess, J. (2009) A chemical-genetic approach to study G protein regulation of beta cell function in vivo. *PNAS*, **106**, 19197-19202.

Guez-Barber, D., Fanous, S., Harvey, B.K., Zhang, Y., Lehrmann, E., Becker, K.G., Picciotto, M.R. & Hope, B.T. (2012) FACS purification of immunolabeled cell types from adult rat brain. *J Neurosci Methods*, **203**, 10-18.

Gustavsson, A., Svensson, M., Jacobi, F., Allgulander, C., Alonso, J., Beghi, E., Dodel, R., Ekman, M., Faravelli, C., Fratiglioni, L., Gannon, B., Jones, D.H., Jennum, P., Jordanova, A., Jonsson, L., Karampampa, K., Knapp, M., Kobelt, G., Kurth, T., Lieb, R., Linde, M., Ljungcrantz, C., Maercker, A., Melin, B., Moscarelli, M., Musayev, A., Norwood, F., Preisig, M., Pugliatti, M., Rehm, J., Salvador-Carulla, L., Schlehofer, B., Simon, R., Steinhausen, H.C., Stovner, L.J., Vallat, J.M., Van den Bergh, P., van Os, J., Vos, P., Xu, W., Wittchen, H.U., Jonsson, B., Olesen, J. & Group, C.D. (2011) Cost of disorders of the brain in Europe 2010. *Eur Neuropsychopharmacol*, **21**, 718-779.

Halls, M.L. & Cooper, D.M. (2011) Regulation by Ca2+-signaling pathways of adenylyl cyclases. *Cold Spring Harb Perspect Biol*, **3**, a004143.

Hanoune, J. & Defer, N. (2001) Regulation and role of adenylyl cyclase isoforms. *Annu Rev Pharmacol Toxicol*, **41**, 145-174.

Hasnie, F.S., Breuer, J., Parker, S., Wallace, V., Blackbeard, J., Lever, I., Kinchington, P.R., Dickenson, A.H., Pheby, T. & Rice, A.S.C. (2007) Further characterization of a rat model of varicella zoster virus-associated pain: Relationship between mechanical hypersensitivity and anxiety-related behavior, and the influence of analgesic drugs. *Neuroscience*, **144**, 1495-1508.

Higuchi, T., Tadokoro, Y., Honda, K. & Negoro, H. (1986) Detailed analysis of blood oxytocin levels during suckling and parturition in the rat. *J Endocrinol*, **110**, 251-256.

Hoeflich, K.P. & Ikura, M. (2002) Calmodulin in action: diversity in target recognition and activation mechanisms. *Cell*, **108**, 739-742.

Hokfelt, T. (1991) Neuropeptides in perspective: the last ten years. *Neuron*, **7**, 867-879.

Hokfelt, T., Bartfai, T. & Bloom, F. (2003) Neuropeptides: opportunities for drug discovery. *Lancet Neurol*, **2**, 463-472.

Holgate, S.T., Lewis, R.A. & Austen, K.F. (1980) Role of adenylate cyclase in immunologic release of mediators from rat mast cells: agonist and antagonist effects of purine- and ribose-modified adenosine analogs. *PNAS*, **77**, 6800-6804.

Horn, T.F. & Engelmann, M. (2001) In vivo microdialysis for nonapeptides in rat brain--a practical guide. *Methods*, **23**, 41-53.

Hu, B. & Bourque, C.W. (1992) NMDA receptor-mediated rhythmic bursting activity in rat supraoptic nucleus neurones in vitro. *J Physiol*, **458**, 667-687.

Insel, T.R. & Hulihan, T.J. (1995) A gender-specific mechanism for pair bonding: oxytocin and partner preference formation in monogamous voles. *Behav Neurosci*, **109**, 782-789.

Insel, T.R. & Shapiro, L.E. (1992) Oxytocin receptor distribution reflects social organization in monogamous and polygamous voles. *PNAS*, **89**, 5981-5985.

Ionescu, I.A., Dine, J., Yen, Y.C., Buell, D.R., Herrmann, L., Holsboer, F., Eder, M., Landgraf, R. & Schmidt, U. (2012) Intranasally administered neuropeptide S (NPS) exerts anxiolytic effects following internalization into NPS receptor-expressing neurons. *Neuropsychopharmacology*, **37**, 1323-1337.

Ji, G., Feldman, M.E., Deng, K.Y., Greene, K.S., Wilson, J., Lee, J.C., Johnston, R.C., Rishniw, M., Tallini, Y., Zhang, J., Wier, W.G., Blaustein, M.P., Xin, H.B., Nakai, J. & Kotlikoff, M.I. (2004) Ca2+-sensing transgenic mice: postsynaptic signaling in smooth muscle. *J Biol Chem*, **279**, 21461-21468.

Jones, B.E. & Yang, T.Z. (1985) The efferent projections from the reticular formation and the locus coeruleus studied by anterograde and retrograde axonal transport in the rat. *J Comp Neurol*, **242**, 56-92.

Juif, P.E., Breton, J.D., Rajalu, M., Charlet, A., Goumon, Y. & Poisbeau, P. (2013) Long-Lasting Spinal Oxytocin Analgesia Is Ensured by the Stimulation of Allopregnanolone Synthesis Which Potentiates GABA(A) Receptor-Mediated Synaptic Inhibition. *Journal of Neuroscience*, **33**, 16617-16626.

Juif, P.E. & Poisbeau, P. (2013) Neurohormonal effects of oxytocin and vasopressin receptor agonists on spinal pain processing in male rats. *Pain*, **154**, 1449-1456.

Jungling, K., Liu, X., Lesting, J., Coulon, P., Sosulina, L., Reinscheid, R.K. & Pape, H.C. (2012) Activation of neuropeptide S-expressing neurons in the locus coeruleus by corticotropin-releasing factor. *J Physiol*, **590**, 3701-3717.

Jungling, K., Seidenbecher, T., Sosulina, L., Lesting, J., Sangha, S., Clark, S.D., Okamura, N., Duangdao, D.M., Xu, Y.L., Reinscheid, R.K. & Pape, H.C. (2008) Neuropeptide S-mediated control of fear expression and extinction: role of intercalated GABAergic neurons in the amygdala. *Neuron*, **59**, 298-310.

Jurek, B., Slattery, D.A., Hiraoka, Y., Liu, Y., Nishimori, K., Aguilera, G., Neumann, I.D. & van den Burg, E.H. (2015) Oxytocin Regulates Stress-Induced Crf Gene Transcription through CREB-Regulated Transcription Coactivator 3. *J Neurosci*, **35**, 12248-12260.

Jurek, B., Slattery, D.A., Maloumby, R., Hillerer, K., Koszinowski, S., Neumann, I.D. & van den Burg, E.H. (2012) Differential contribution of hypothalamic MAPK activity to anxiety-like behaviour in virgin and lactating rats. *PloS one*, **7**, e37060.

Kerr, R., Lev-Ram, V., Baird, G., Vincent, P., Tsien, R.Y. & Schafer, W.R. (2000) Optical imaging of calcium transients in neurons and pharyngeal muscle of C. elegans. *Neuron*, **26**, 583-594.

Keshavarzi, S., Sullivan, R.K., Ianno, D.J. & Sah, P. (2014) Functional properties and projections of neurons in the medial amygdala. *J Neurosci*, **34**, 8699-8715.

Kessler, R.C., Brandenburg, N., Lane, M., Roy-Byrne, P., Stang, P.D., Stein, D.J. & Wittchen, H.U. (2005) Rethinking the duration requirement for generalized anxiety disorder: evidence from the National Comorbidity Survey Replication. *Psychol Med*, **35**, 1073-1082.

Kessler, R.C. & Wang, P.S. (2008) The descriptive epidemiology of commonly occurring mental disorders in the United States. *Annu Rev Pub Health*, **29**, 115-129.

Knobloch, H.S., Charlet, A., Hoffmann, L.C., Eliava, M., Khrulev, S., Cetin, A.H., Osten, P., Schwarz, M.K., Seeburg, P.H., Stoop, R. & Grinevich, V. (2012) Evoked axonal oxytocin release in the central amygdala attenuates fear response. *Neuron*, **73**, 553-566.

Knowles, J.A., Fyer, A.J., Vieland, V.J., Weissman, M.M., Hodge, S.E., Heiman, G.A., Haghighi, F., de Jesus, G.M., Rassnick, H., Preud'homme-Rivelli, X., Austin, T., Cunjak, J., Mick, S., Fine, L.D., Woodley, K.A., Das, K., Maier, W., Adams, P.B., Freimer, N.B., Klein, D.F. & Gilliam, T.C. (1998) Results of a genome-wide genetic screen for panic disorder. *Am J Med Genet*, **81**, 139-147.

Kosten, T.R., Frank, J.B., Dan, E., Mcdougle, C.J. & Giller, E.L. (1991) Pharmacotherapy for Posttraumatic-Stress-Disorder Using Phenelzine or Imipramine. *J Nerv Mental Disease*, **179**, 366-370.

Krebs, J. (1998) Calmodulin-dependent protein kinase IV: regulation of function and expression. *Biochim Biophys Acta*, **1448**, 183-189.

Kroenke, K., Krebs, E.E. & Bair, M.J. (2009) Pharmacotherapy of chronic pain: a synthesis of recommendations from systematic reviews. *Gen Hosp Psychiatry*, **31**, 206-219.

Laitinen, T., Polvi, A., Rydman, P., Vendelin, J., Pulkkinen, V., Salmikangas, P., Makela, S., Rehn, M., Pirskanen, A., Rautanen, A., Zucchelli, M., Gullsten, H., Leino, M., Alenius, H., Petays, T., Haahtela, T., Laitinen, A., Laprise, C., Hudson, T.J., Laitinen, L.A. & Kere, J. (2004) Characterization of a common susceptibility locus for asthma-related traits. *Science*, **304**, 300-304.

Lambert, R.C., Dayanithi, G., Moos, F.C. & Richard, P. (1994) A rise in the intracellular Ca2+ concentration of isolated rat supraoptic cells in response to oxytocin. *J Physiol*, **478 (Pt 2)**, 275-287.

Landgraf, R., Neumann, I., Holsboer, F. & Pittman, Q.J. (1995) Interleukin-1-Beta Stimulates Both Central and Peripheral Release of Vasopressin and Oxytocin in the Rat. *Eur J Neurosci*, **7**, 592-598.

Landgraf, R. & Neumann, I.D. (2004) Vasopressin and oxytocin release within the brain: a dynamic concept of multiple and variable modes of neuropeptide communication. *Front Neuroendocrinol*, **25**, 150-176.

LeDoux, J. (2007) The amygdala. *Curr Biol*, **17**, R868-874.

Lee, H.J., Macbeth, A.H., Pagani, J.H. & Young, W.S., 3rd (2009) Oxytocin: the great facilitator of life. *Prog Neurobiol*, **88**, 127-151.

Leonard, S.K., Dwyer, J.M., Sukoff Rizzo, S.J., Platt, B., Logue, S.F., Neal, S.J., Malberg, J.E., Beyer, C.E., Schechter, L.E., Rosenzweig-Lipson, S. & Ring, R.H. (2008) Pharmacology of neuropeptide S in mice: therapeutic relevance to anxiety disorders. *Psychopharmacology*, **197**, 601-611.

Leonard, S.K. & Ring, R.H. (2011) Immunohistochemical localization of the neuropeptide S receptor in the rat central nervous system. *Neuroscience*, **172**, 153-163.

Lewis, M., Haviland-Jones, J.M. & Barrett, L.F. (2010) *Handbook of Emotions*.

Li, W., Chang, M., Peng, Y.L., Gao, Y.H., Zhang, J.N., Han, R.W. & Wang, R. (2009) Neuropeptide S produces antinociceptive effects at the supraspinal level in mice. *Regulatory Peptides*, **156**, 90-95.

Li, Y., Schmidt-Edelkraut, U., Poetz, F., Oliva, I., Mandl, C., Holzl-Wenig, G., Schonig, K., Bartsch, D. & Ciccolini, F. (2015) gamma-Aminobutyric A receptor (GABA(A)R) regulates aquaporin 4 expression in the subependymal zone: relevance to neural precursors and water exchange. *J Biol Chem*, **290**, 4343-4355.

Liao, Y., Lu, B., Ma, Q., Wu, G., Lai, X., Zang, J., Shi, Y., Liu, D., Han, F. & Zhou, N. (2016) Human Neuropeptide S Receptor Is Activated via a Galphaq Protein-biased Signaling Cascade by a Human Neuropeptide S Analog Lacking the C-terminal 10 Residues. *J Biol Chem*, **291**, 7505-7516.

Little, P.J., Kuhn, C.M., Wilson, W.A. & Swartzwelder, H.S. (1996) Differential effects of ethanol in adolescent and adult rats. *Alcohol Clin Exp Res*, **20**, 1346-1351.

Liu, X., Zeng, J., Zhou, A., Theodorsson, E., Fahrenkrug, J. & Reinscheid, R.K. (2011) Molecular fingerprint of neuropeptide S-producing neurons in the mouse brain. *J Comp Neurol*, **519**, 1847-1866.

Lobo, M.K., Karsten, S.L., Gray, M., Geschwind, D.H. & Yang, X.W. (2006) FACS-array profiling of striatal projection neuron subtypes in juvenile and adult mouse brains. *Nat Neurosci*, **9**, 443-452.

Logue, M.W., Vieland, V.J., Goedken, R.J. & Crowe, R.R. (2003) Bayesian analysis of a previously published genome screen for panic disorder reveals new and compelling evidence for linkage to chromosome 7. *Am J Med Genet B Neuropsychiatr Genet*, **121B**, 95-99.

Loughlin, S.E., Foote, S.L. & Grzanna, R. (1986) Efferent projections of nucleus locus coeruleus: morphologic subpopulations have different efferent targets. *Neuroscience*.

Ludwig, M. (1998) Dendritic release of vasopressin and oxytocin. *J Neuroendocrinol*, **10**, 881-895.

Ludwig, M., Apps, D., Menzies, J., Patel, J.C. & Rice, M.E. (2016) Dendritic Release of Neurotransmitters. *Compr Physiol*, **7**, 235-252.

Ludwig, M. & Leng, G. (2006) Dendritic peptide release and peptide-dependent behaviours. *Nature reviews. Neuroscience*, **7**, 126-136.

Ludwig, M., Sabatier, N., Bull, P.M., Landgraf, R., Dayanithi, G. & Leng, G. (2002) Intracellular calcium stores regulate activity-dependent neuropeptide release from dendrites. *Nature*, **418**, 85-89.

Lukas, M. & Neumann, I.D. (2012) Nasal application of neuropeptide S reduces anxiety and prolongs memory in rats: social versus non-social effects. *Neuropharmacology*, **62**, 398-405.

Lukas, M. & Neumann, I.D. (2013) Oxytocin and vasopressin in rodent behaviors related to social dysfunctions in autism spectrum disorders. *Behav Brain Res*, **251**, 85-94.

Lukas, M., Toth, L., Veenema, A.H. & Neumann, I.D. (2013) Oxytocin mediates rodent social memory within the lateral septum and the medial amygdala depending on the relevance of the social stimulus: Male juvenile versus female adult conspecifics. *Psychoneuroendocrinology*, **38**, 916-926.

Luthi, A. & Luscher, C. (2014) Pathological circuit function underlying addiction and anxiety disorders. *Nat Neurosci*, **17**, 1635-1643.

Mack, S.O., Kc, P., Wu, M., Coleman, B.R., Tolentino-Silva, F.P. & Haxhiu, M.A. (2002) Paraventricular oxytocin neurons are involved in neural modulation of breathing. *J Appl Physiol (1985)*, **92**, 826-834.

MacMillan, D. & McCarron, J.G. (2010) The phospholipase C inhibitor U-73122 inhibits Ca2+release from the intracellular sarcoplasmic reticulum Ca2+store by inhibiting Ca2+pumps in smooth muscle. *Br J Pharmacol*, **160**, 1295-1301.

MacNeil, S., Lakey, T. & Tomlinson, S. (1985) Calmodulin regulation of adenylate cyclase activity. *Cell calcium*, **6**, 213-216.

Manning, M., Misicka, A., Olma, A., Bankowski, K., Stoev, S., Chini, B., Durroux, T., Mouillac, B., Corbani, M. & Guillon, G. (2012) Oxytocin and vasopressin agonists and antagonists as research tools and potential therapeutics. *j Neuroendocrinol*, **24**, 609-628.

Mathew, S.J., Price, R.B. & Charney, D.S. (2008) Recent advances in the neurobiology of anxiety disorders: implications for novel therapeutics. *Am J Med Genet C Semin Med Genet*, **148C**, 89-98.

Mavissakalian, M.R. & Perel, J.M. (1999) Long-term maintenance and discontinuation of imipramine therapy in panic disorder with agoraphobia. *Arch Gen Psychiatry*, **56**, 821-827.

McCarthy, M.M., Kleopoulos, S.P., Mobbs, C.V. & Pfaff, D.W. (1994) Infusion of antisense oligodeoxynucleotides to the oxytocin receptor in the ventromedial hypothalamus reduces estrogen-induced sexual receptivity and oxytocin receptor binding in the female rat. *Neuroendocrinology*, **59**, 432-440.

McCombs, J.E. & Palmer, A.E. (2008) Measuring calcium dynamics in living cells with genetically encodable calcium indicators. *Methods*, **46**, 152-159.

Meis, S., Bergado-Acosta, J.R., Yanagawa, Y., Obata, K., Stork, O. & Munsch, T. (2008) Identification of a neuropeptide S responsive circuitry shaping amygdala activity via the endopiriform nucleus. *PloS one*, **3**, e2695.

Merikangas, K.R., Mehta, R.L., Molnar, B.E., Walters, E.E., Swendsen, J.D., Aguilar-Gaziola, S., Bijl, R., Borges, G., Caraveo-Anduaga, J.J., Dewit, D.J., Kolody, B., Vega, W.A., Wittchen, H.U. & Kessler, R.C. (1998) Comorbidity of substance use disorders with mood and

anxiety disorders: Results of the International Consortium in Psychiatric Epidemiology. *Addictive Behaviors*, **23**, 893-907.

Merritt, J.E., Armstrong, W.P., Benham, C.D., Hallam, T.J., Jacob, R., Jaxa-Chamiec, A., Leigh, B.K., McCarthy, S.A., Moores, K.E. & Rink, T.J. (1990) SK&F 96365, a novel inhibitor of receptor-mediated calcium entry. *Biochemical journal*, **271**, 515-522.

Meyer-Lindenberg, A., Domes, G., Kirsch, P. & Heinrichs, M. (2011) Oxytocin and vasopressin in the human brain: social neuropeptides for translational medicine. *Nat Rev Neurosci*, **12**, 524-538.

Miyawaki, A., Llopis, J., Heim, R., McCaffery, J.M., Adams, J.A., Ikura, M. & Tsien, R.Y. (1997) Fluorescent indicators for Ca2+ based on green fluorescent proteins and calmodulin. *Nature*, **388**, 882-887.

Moore, R.Y. & Bloom, F.E. (1979) Central catecholamine neuron systems: anatomy and physiology of the norepinephrine and epinephrine systems. *Annu Rev Neurosci*, **2**, 113-168.

Neumann, I., Ludwig, M., Engelmann, M., Pittman, Q.J. & Landgraf, R. (1993a) Simultaneous microdialysis in blood and brain: oxytocin and vasopressin release in response to central and peripheral osmotic stimulation and suckling in the rat. *Neuroendocrinology*, **58**, 637-645.

Neumann, I., Russell, J.A. & Landgraf, R. (1993b) Oxytocin and Vasopressin Release within the Supraoptic and Paraventricular Nuclei of Pregnant, Parturient and Lactating Rats - a Microdialysis Study. *Neuroscience*, **53**, 65-75.

Neumann, I.D. (2008) Brain oxytocin: a key regulator of emotional and social behaviours in both females and males. *J Neuroendocrinol*, **20**, 858-865.

Neumann, I.D. & Landgraf, R. (2012) Balance of brain oxytocin and vasopressin: implications for anxiety, depression, and social behaviors. *Trends Neurosciences*, **35**, 649-659.

Neumann, I.D. & Slattery, D.A. (2016) Oxytocin in General Anxiety and Social Fear: A Translational Approach. *Biological psychiatry*, **79**, 213-221.

Neumann, I.D., Torner, L. & Wigger, A. (2000) Brain oxytocin: differential inhibition of neuroendocrine stress responses and anxiety-related behaviour in virgin, pregnant and lactating rats. *Neuroscience*, **95**, 567-575.

Neumann, I.D., Wigger, A., Liebsch, G., Holsboer, F. & Landgraf, R. (1998) Increased basal activity of the hypothalamo-pituitary-adrenal axis during pregnancy in rats bred for high anxiety-related behaviour. *Psychoneuroendocrinology*, **23**, 449-463.

Newcomer, K.L., Shelerud, R.A., Douglas, K.S.V., Larson, D.R. & Crawford, B.J. (2010) Anxiety Levels, Fear-avoidance Beliefs, and Disability Levels at Baseline and at 1 Year among Subjects With Acute and Chronic Low Back Pain. *Pm&R*, **2**, 514-520.

Nutt, D. & Ballenger, J. (2003) *Anxiety Disorders*.

Nyuyki, K.D., Maloumby, R., Reber, S.O. & Neumann, I.D. (2012) Comparison of corticosterone responses to acute stressors: chronic jugular vein versus trunk blood samples in mice. *Stress*, **15**, 618-626.

Oettl, L.L., Ravi, N., Schneider, M., Scheller, M.F., Schneider, P., Mitre, M., da Silva Gouveia, M., Froemke, R.C., Chao, M.V., Young, W.S., Meyer-Lindenberg, A., Grinevich, V., Shusterman, R. & Kelsch, W. (2016) Oxytocin Enhances Social Recognition by Modulating Cortical Control of Early Olfactory Processing. *Neuron*, **90**, 609-621.

Ogawa, K., Tashima, M., Takeda, Y., Sawai, H., Toi, T., Sawada, H., Maruyama, Y. & Okuma, M. (1995) Erythroid differentiation and growth inhibition of K562 cells by 2',5'-dideoxyadenosine: synergism with interferon-alpha. *Leuk Res*, **19**, 749-755.

Okamura, N., Garau, C., Duangdao, D.M., Clark, S.D., Jungling, K., Pape, H.C. & Reinscheid, R.K. (2011) Neuropeptide S enhances memory during the consolidation phase and interacts with noradrenergic systems in the brain. *Neuropsychopharmacology*, **36**, 744-752.

Okamura, N., Habay, S.A., Zeng, J., Chamberlin, A.R. & Reinscheid, R.K. (2008) Synthesis and pharmacological in vitro and in vivo profile of 3-oxo-1,1-diphenyl-tetrahydro-oxazolo[3,4-a]pyrazine-7-carboxylic acid 4-fluoro-benzylamide (SHA 68), a selective antagonist of the neuropeptide S receptor. *J Pharm Exp Ther*, **325**, 893-901.

Okamura, N., Hashimoto, K., Iyo, M., Shimizu, E., Dempfle, A., Friedel, S. & Reinscheid, R.K. (2007) Gender-specific association of a functional coding polymorphism in the Neuropeptide S receptor gene with panic disorder but not with schizophrenia or attention-deficit/hyperactivity disorder. *Progress in neuro-psychopharmacology & biological psychiatry*, **31**, 1444-1448.

Olson, B.R., Drutarosky, M.D., Chow, M.S., Hruby, V.J., Stricker, E.M. & Verbalis, J.G. (1991a) Oxytocin and an oxytocin agonist administered centrally decrease food intake in rats. *Peptides*, **12**, 113-118.

Olson, B.R., Drutarosky, M.D., Stricker, E.M. & Verbalis, J.G. (1991b) Brain oxytocin receptor antagonism blunts the effects of anorexigenic treatments in rats: evidence for central oxytocin inhibition of food intake. *Endocrinology*, **129**, 785-791.

Paneda, C., Huitron-Resendiz, S., Frago, L.M., Chowen, J.A., Picetti, R., de Lecea, L. & Roberts, A.J. (2009) Neuropeptide S reinstates cocaine-seeking behavior and increases locomotor activity through corticotropin-releasing factor receptor 1 in mice. *J Neurosci*, **29**, 4155-4161.

Pape, H.C., Jungling, K., Seidenbecher, T., Lesting, J. & Reinscheid, R.K. (2010) Neuropeptide S: a transmitter system in the brain regulating fear and anxiety. *Neuropharmacology*, **58**, 29-34.

Pausch, M.H. (1997) G-protein-coupled receptors in Saccharomyces cerevisiae: high-throughput screening assays for drug discovery. *Trends Biotechnol*, **15**, 487-494.

Paxinos, G. & Watson, C. (1998) *The Rat Brain in Stereotaxic Coordinates*. Academic Press, San Diego.

Pedersen, C.A. & Prange, A.J., Jr. (1979) Induction of maternal behavior in virgin rats after intracerebroventricular administration of oxytocin. *PNAS*, **76**, 6661-6665.

Pedersen, C.A., Vadlamudi, S.V., Boccia, M.L. & Amico, J.A. (2006) Maternal behavior deficits in nulliparous oxytocin knockout mice. *Genes Brain Behav*, **5**, 274-281.

Peng, Y.L., Zhang, J.N., Chang, M., Li, W., Han, R.W. & Wang, R. (2010) Effects of central neuropeptide S in the mouse formalin test. *Peptides*, **31**, 1878-1883.

Perova, Z., Delevich, K. & Li, B. (2015) Depression of excitatory synapses onto parvalbumin interneurons in the medial prefrontal cortex in susceptibility to stress. *J Neurosci*, **35**, 3201-3206.

Peters, S.T., Bowen, M.T., Bohrer, K., McGregor, I.S. & Neumann, I.D. (2016) Oxytocin inhibits ethanol consumption and ethanol-induced dopamine release in the nucleus accumbens. *Addiction biology*.

Petersson, M. (2002) Cardiovascular effects of oxytocin. *Prog Brain Res*, **139**, 281-288.

Pow, D.V. & Morris, J.F. (1989) Dendrites of hypothalamic magnocellular neurons release neurohypophysial peptides by exocytosis. *Neuroscience*, **32**, 435-439.

Price, J.S. (2003) Evolutionary aspects of anxiety disorders. *Dialogues Clin Neurosci*, **5**, 223-236.

Pucilowski, O., Kostowski, W. & Trzaskowska, E. (1985) The effect of oxytocin and fragment (MIF-I) on the development of tolerance to hypothermic and hypnotic action of ethanol in the rat. *Peptides*, **6**, 7-10.

Raczka, K.A., Gartmann, N., Mechias, M.L., Reif, A., Buchel, C., Deckert, J. & Kalisch, R. (2010) A neuropeptide S receptor variant associated with overinterpretation of fear reactions: a potential neurogenetic basis for catastrophizing. *Molecular psychiatry*, **15**, 1045, 1067-1074.

Ravindran, L.N. & Stein, M.B. (2009) Pharmacotherapy of PTSD: premises, principles, and priorities. *Brain research*, **1293**, 24-39.

Reinscheid, R.K. (2007) Phylogenetic appearance of neuropeptide S precursor proteins in tetrapods. *Peptides*, **28**, 830-837.

Reinscheid, R.K. & Xu, Y.L. (2005a) Neuropeptide S and its receptor: a newly deorphanized G protein-coupled receptor system. *Neuroscientist*, **11**, 532-538.

Reinscheid, R.K. & Xu, Y.L. (2005b) Neuropeptide S as a novel arousal promoting peptide transmitter. *FEBS journal*, **272**, 5689-5693.

Reinscheid, R.K., Xu, Y.L., Okamura, N., Zeng, J., Chung, S., Pai, R., Wang, Z. & Civelli, O. (2005) Pharmacological characterization of human and murine neuropeptide s receptor variants. *J Pharm Exp Ther*, **315**, 1338-1345.

Reme, S.E., Tangen, T., Moe, T. & Eriksen, H.R. (2011) Prevalence of psychiatric disorders in sick listed chronic low back pain patients. *Eur J Pain*, **15**, 1075-1080.

Rhee, S.G. & Bae, Y.S. (1997) Regulation of phosphoinositide-specific phospholipase C isozymes. *J Biol Chem*, **272**, 15045-15048.

Rhee, S.G., Suh, P.G., Ryu, S.H. & Lee, S.Y. (1989) Studies of inositol phospholipid-specific phospholipase C. *Science*, **244**, 546-550.

Rhodes, C.H., Morrell, J.I. & Pfaff, D.W. (1981) Immunohistochemical analysis of magnocellular elements in rat hypothalamus: distribution and numbers of cells containing neurophysin, oxytocin, and vasopressin. *J Comp Neurol*, **198**, 45-64.

Rickels, K., Downing, R., Schweizer, E. & Hassman, H. (1993) Antidepressants for the treatment of generalized anxiety disorder. A placebo-controlled comparison of imipramine, trazodone, and diazepam. *Arch Gen Psychiatry*, **50**, 884-895.

Rizzi, A., Vergura, R., Marzola, G., Ruzza, C., Guerrini, R., Salvadori, S., Regoli, D. & Calo, G. (2008) Neuropeptide S is a stimulatory anxiolytic agent: a behavioural study in mice. *Br J Pharmacol*, **154**, 471-479.

Rogan, S.C. & Roth, B.L. (2011) Remote control of neuronal signaling. *Pharmacol Rev*, **63**, 291-315.

Roozendaal, B., McEwen, B.S. & Chattarji, S. (2009) Stress, memory and the amygdala. *Nature reviews. Neuroscience*, **10**, 423-433.

Ruzza, C., Asth, L., Guerrini, R., Trapella, C. & Gavioli, E.C. (2015) Neuropeptide S reduces mouse aggressiveness in the resident/intruder test through selective activation of the neuropeptide S receptor. *Neuropharmacology*, **97**, 1-6.

Ruzza, C., Rizzi, A., Trapella, C., Pela, M., Camarda, V., Ruggieri, V., Filaferro, M., Cifani, C., Reinscheid, R.K., Vitale, G., Ciccocioppo, R., Salvadori, S., Guerrini, R. & Calo, G. (2010) Further studies on the pharmacological profile of the neuropeptide S receptor antagonist SHA 68. *Peptides*, **31**, 915-925.

Sabatini, B.L., Oertner, T.G. & Svoboda, K. (2002) The life cycle of Ca(2+) ions in dendritic spines. *Neuron*, **33**, 439-452.

Saper, C.B. & Loewy, A.D. (1980) Efferent connections of the parabrachial nucleus in the rat. *Brain research*, **197**, 291-317.

Sato, S., Shintani, Y., Miyajima, N. & Yoshimura, K. (2002) Novel G protein-coupled receptor protein and DNA thereof. *World Patent Application*.

Scott, K.M., Bruffaerts, R., Tsang, A., Ormel, J., Alonso, J., Angermeyer, M.C., Benjet, C., Bromet, E., de Girolamo, G., de Graaf, R., Gasquet, I., Gureje, O., Haro, J.M., He, Y., Kessler, R.C., Levinson, D., Mneimneh, Z.N., Oakley Browne, M.A., Posada-Villa, J., Stein, D.J., Takeshima, T. & Von Korff, M. (2007) Depression-anxiety relationships with chronic physical conditions: results from the World Mental Health Surveys. *J Affect Disorders*, **103**, 113-120.

Seligman, M., Walker, E.F. & Rosenhan, D.l. (2000) *Abnormal Psychology*. W. W. Norton & Company.

Shestatzky, M., Greenberg, D. & Lerer, B. (1988) A controlled trial of phenelzine in posttraumatic stress disorder. *Psychiatry Res*, **24**, 149-155.

Shimomura, Y., Harada, M., Goto, M., Sugo, T., Matsumoto, Y., Abe, M., Watanabe, T., Asami, T., Kitada, C., Mori, M., Onda, H. & Fujino, M. (2002) Identification of neuropeptide W as the endogenous ligand for orphan G-protein-coupled receptors GPR7 and GPR8. *J Biol Chem*, **277**, 35826-35832.

Shukitt-Hale, B., Mouzakis, G. & Joseph, J.A. (1998) Psychomotor and spatial memory performance in aging male Fischer 344 rats. *Exp Gerontol*, **33**, 615-624.

Singh, A., Hildebrand, M.E., Garcia, E. & Snutch, T.P. (2010) The transient receptor potential channel antagonist SKF96365 is a potent blocker of low-voltage-activated T-type calcium channels. *Br J Pharmacol*, **160**, 1464-1475.

Slattery, D.A., Naik, R.R., Grund, T., Yen, Y.C., Sartori, S.B., Fuchsl, A., Finger, B.C., Elfving, B., Nordemann, U., Guerrini, R., Calo, G., Wegener, G., Mathe, A.A., Singewald, N., Czibere, L., Landgraf, R. & Neumann, I.D. (2015) Selective breeding for high anxiety introduces a synonymous SNP that increases neuropeptide s receptor activity. *J Neurosci*, **35**, 4599-4613.

Smallridge, R.C., Kiang, J.G., Gist, I.D., Fein, H.G. & Galloway, R.J. (1992) U-73122, an aminosteroid phospholipase C antagonist, noncompetitively inhibits thyrotropin-releasing hormone effects in GH3 rat pituitary cells. *Endocrinology*, **131**, 1883-1888.

Smith, K.L., Patterson, M., Dhillo, W.S., Patel, S.R., Semjonous, N.M., Gardiner, J.V., Ghatei, M.A. & Bloom, S.R. (2006) Neuropeptide S stimulates the hypothalamo-pituitary-adrenal axis and inhibits food intake. *Endocrinology*, **147**, 3510-3518.

Sokolowska, E. & Hovatta, I. (2013) Anxiety genetics - findings from cross-species genome-wide approaches. *Biol Mood Anxiety Disord*, **3**, 9.

Steimer, T. (2002) The biology of fear- and anxiety-related behaviors. *Dialogues Clin Neurosci*, **4**, 231-249.

Stoop, R. (2012) Neuromodulation by oxytocin and vasopressin. *Neuron*, **76**, 142-159.

Stoop, R., Hegoburu, C. & van den Burg, E. (2015) New opportunities in vasopressin and oxytocin research: a perspective from the amygdala. *Annu Rev Neurosci*, **38**, 369-388.

Strand, F.L. (1999) *Neuropeptides: Regulators of Physiological Processes*.

Suga, H. & Haga, T. (2007) Ligand screening system using fusion proteins of G protein-coupled receptors with G protein alpha subunits. *Neurochemistry Int*, **51**, 140-164.

Swanson, L.W. & Sawchenko, P.E. (1980) Paraventricular nucleus: a site for the integration of neuroendocrine and autonomic mechanisms. *Neuroendocrinology*, **31**, 410-417.

Swanson, L.W. & Sawchenko, P.E. (1983) Hypothalamic integration: organization of the paraventricular and supraoptic nuclei. *Annu Rev Neurosci*, **6**, 269-324.

Tang, X.L., Wang, Y., Li, D.L., Luo, J. & Liu, M.Y. (2012) Orphan G protein-coupled receptors (GPCRs): biological functions and potential drug targets. *Acta Pharmacol Sin*, **33**, 363-371.

Tank, D.W., Sugimori, M., Connor, J.A. & Llinas, R.R. (1988) Spatially resolved calcium dynamics of mammalian Purkinje cells in cerebellar slice. *Science*, **242**, 773-777.

Teissier, A., Chemiakine, A., Inbar, B., Bagchi, S., Ray, R.S., Palmiter, R.D., Dymecki, S.M., Moore, H. & Ansorge, M.S. (2015) Activity of Raphe Serotonergic Neurons Controls Emotional Behaviors. *Cell Rep*, **13**, 1965-1976.

Teo, A.R., Lerrigo, R. & Rogers, M.A. (2013) The role of social isolation in social anxiety disorder: a systematic review and meta-analysis. *J Anxiety Disord*, **27**, 353-364.

Torner, L., Plotsky, P.M., Neumann, I.D. & de Jong, T.R. (2017) Forced swimming-induced oxytocin release into blood and brain: Effects of adrenalectomy and corticosterone treatment. *Psychoneuroendocrinology*, **77**, 165-174.

Toth, I. & Neumann, I.D. (2013) Animal models of social avoidance and social fear. *Cell Tissue Res*, **354**, 107-118.

Toth, I., Neumann, I.D. & Slattery, D.A. (2012) Social fear conditioning: a novel and specific animal model to study social anxiety disorder. *Neuropsychopharmacology*, **37**, 1433-1443.

Tovote, P., Fadok, J.P. & Luthi, A. (2015) Neuronal circuits for fear and anxiety. *Nat Rev Neurosci*, **16**, 317-331.

Urban, D.J. & Roth, B.L. (2015) DREADDs (designer receptors exclusively activated by designer drugs): chemogenetic tools with therapeutic utility. *Annu Rev Pharmacol Toxicol*, **55**, 399-417.

Urban, D.J., Zhu, H., Marcinkiewcz, C.A., Michaelides, M., Oshibuchi, H., Rhea, D., Aryal, D.K., Farrell, M.S., Lowery-Gionta, E., Olsen, R.H., Wetsel, W.C., Kash, T.L., Hurd, Y.L., Tecott, L.H. & Roth, B.L. (2016) Elucidation of The Behavioral Program and Neuronal Network Encoded by Dorsal Raphe Serotonergic Neurons. *Neuropsychopharmacology*, **41**, 1404-1415.

Vaccari, C., Lolait, S.J. & Ostrowski, N.L. (1998) Comparative distribution of vasopressin V1b and oxytocin receptor messenger ribonucleic acids in brain. *Endocrinology*, **139**, 5015-5033.

van den Burg, E.H. & Neumann, I.D. (2011) Bridging the gap between GPCR activation and behaviour: oxytocin and prolactin signalling in the hypothalamus. *J Mol Neurosci*, **43**, 200-208.

van den Burg, E.H., Stindl, J., Grund, T., Neumann, I.D. & Strauss, O. (2015) Oxytocin Stimulates Extracellular Ca(2+) Influx Through TRPV2 Channels in Hypothalamic Neurons to Exert Its Anxiolytic Effects. *Neuropsychopharmacology*, **40**, 2938-2947.

Vardy, E., Robinson, J.E., Li, C., Olsen, R.H., DiBerto, J.F., Giguere, P.M., Sassano, F.M., Huang, X.P., Zhu, H., Urban, D.J., White, K.L., Rittiner, J.E., Crowley, N.A., Pleil, K.E., Mazzone, C.M., Mosier, P.D., Song, J., Kash, T.L., Malanga, C.J., Krashes, M.J. & Roth, B.L. (2015)

A New DREADD Facilitates the Multiplexed Chemogenetic Interrogation of Behavior. *Neuron*, **86**, 936-946.

Varnai, P., Hunyady, L. & Balla, T. (2009) STIM and Orai: the long-awaited constituents of store-operated calcium entry. *Trends Pharmacol Sci*, **30**, 118-128.

Vitale, G., Filaferro, M., Ruggieri, V., Pennella, S., Frigeri, C., Rizzi, A., Guerrini, R. & Calo, G. (2008) Anxiolytic-like effect of neuropeptide S in the rat defensive burying. *Peptides*, **29**, 2286-2291.

Viviani, D., Charlet, A., van den Burg, E., Robinet, C., Hurni, N., Abatis, M., Magara, F. & Stoop, R. (2011) Oxytocin Selectively Gates Fear Responses Through Distinct Outputs from the Central Amygdala. *Science*, **333**, 104-107.

Waldherr, M. & Neumann, I.D. (2007) Centrally released oxytocin mediates mating-induced anxiolysis in male rats. *PNAS*, **104**, 16681-16684.

Wang, Q., Shui, B., Kotlikoff, M.I. & Sondermann, H. (2008) Structural basis for calcium sensing by GCaMP2. *Structure*, **16**, 1817-1827.

Wegener, G., Finger, B.C., Elfving, B., Keller, K., Liebenberg, N., Fischer, C.W., Singewald, N., Slattery, D.A., Neumann, I.D. & Mathe, A.A. (2011) Neuropeptide S alters anxiety, but not depression-like behaviour in Flinders Sensitive Line rats: a genetic animal model of depression. *Int J Neuropsychopharmacol*, 1-13.

Whissell, P.D., Tohyama, S. & Martin, L.J. (2016) The Use of DREADDs to Deconstruct Behavior. *Front Genetics*, **7**, 70.

Wick, J.Y. (2013) The history of benzodiazepines. *Consult Pharm*, **28**, 538-548.

Wigger, A. & Neumann, I.D. (2002) Endogenous opioid regulation of stress-induced oxytocin release within the hypothalamic paraventricular nucleus is reversed in late pregnancy: A microdialysis study. *Neuroscience*, **112**, 121-129.

Wittchen, H.U., Jacobi, F., Rehm, J., Gustavsson, A., Svensson, M., Jonsson, B., Olesen, J., Allgulander, C., Alonso, J., Faravelli, C., Fratiglioni, L., Jennum, P., Lieb, R., Maercker, A., van Os, J., Preisig, M., Salvador-Carulla, L., Simon, R. & Steinhausen, H.C. (2011) The size and burden of mental disorders and other disorders of the brain in Europe 2010. *Eur Neuropsychopharmacol*, **21**, 655-679.

Wotjak, C.T., Ganster, J., Kohl, G., Holsboer, F., Landgraf, R. & Engelmann, M. (1998) Dissociated central and peripheral release of vasopressin, but not oxytocin, in response to repeated swim stress: New insights into the secretory capacities of peptidergic neurons. *Neuroscience*, **85**, 1209-1222.

Xu, Y.L., Gall, C.M., Jackson, V.R., Civelli, O. & Reinscheid, R.K. (2007) Distribution of neuropeptide S receptor mRNA and neurochemical characteristics of neuropeptide S-expressing neurons in the rat brain. *J Comp Neurol*, **500**, 84-102.

Xu, Y.L., Reinscheid, R.K., Huitron-Resendiz, S., Clark, S.D., Wang, Z., Lin, S.H., Brucher, F.A., Zeng, J., Ly, N.K., Henriksen, S.J., de Lecea, L. & Civelli, O. (2004) Neuropeptide S: a neuropeptide promoting arousal and anxiolytic-like effects. *Neuron*, **43**, 487-497.

Yoshida, M., Takayanagi, Y., Inoue, K., Kimura, T., Young, L.J., Onaka, T. & Nishimori, K. (2009) Evidence that oxytocin exerts anxiolytic effects via oxytocin receptor expressed in serotonergic neurons in mice. *J Neurosci*, **29**, 2259-2271.

Yoshimura, R., Kiyama, H., Kimura, T., Araki, T., Maeno, H., Tanizawa, O. & Tohyama, M. (1993) Localization of oxytocin receptor messenger ribonucleic acid in the rat brain. *Endocrinology*, **133**, 1239-1246.

Yuste, R. (2005) Fluorescence microscopy today. *Nat Methods*, **2**, 902-904.

Zhang, S., Jin, X., You, Z., Wang, S., Lim, G., Yang, J., McCabe, M., Li, N., Marota, J., Chen, L. & Mao, J. (2014) Persistent Nociception Induces Anxiety-like Behavior in Rodents: Role of Endogenous Neuropeptide S. *Pain*.

Zhong, M., Murtazina, D.A., Phillips, J., Ku, C.Y. & Sanborn, B.M. (2008) Multiple signals regulate phospholipase CBeta3 in human myometrial cells. *Biol Reprod*, **78**, 1007-1017.

Zoicas, I., Menon, R. & Neumann, I.D. (2016) Neuropeptide S reduces fear and avoidance of con-specifics induced by social fear conditioning and social defeat, respectively. *Neuropharmacology*, **108**, 284-291.

Zoicas, I., Slattery, D.A. & Neumann, I.D. (2014) Brain oxytocin in social fear conditioning and its extinction: involvement of the lateral septum. *Neuropsychopharmacology*, **39**, 3027-3035.